Modeling tauopathies *in vitro* with diverse aggregation inducing techniques

© 2021

By David J. Ingham
B.Sc., Missouri Southern State University, Joplin, MO, 2014

Submitted to the graduate degree program in the Department of Molecular Biosciences and the Graduate Faculty of the University of Kansas in partial fulfillment of the requirements for the degree of Doctor of Philosophy.

Co-Chair: Dr. T. Chris Gamblin

Co-Chair: Dr. Erik Lundquist

Dr. Berl Oakley

Dr. Yoshiaki Azuma

Dr. Michael Hageman

Date Defended: 08/09/2021

The dissertation committee for David J. Ingham certifies that this is the approved version of the following dissertation:

Modeling tauopathies *in vitro* with diverse aggregation inducing techniques

Co-Chair: Dr. T. Chris Gamblin

Co-Chair: Dr. Erik Lundquist

Date Approved: 08/10/2021

Abstract

The microtubule-associated protein tau promotes the stabilization of the axonal cytoskeleton in neurons. In several neurodegenerative diseases, such as Alzheimer's disease, Pick's disease, corticobasal degeneration, chronic traumatic encephalopathy, and progressive supranuclear palsy, tau has been found to dissociate from microtubules leading to the formation of pathological aggregates that display an amyloid fibril-like structure. Recent structural studies have shown that the tau filaments isolated from different neurodegenerative disorders have structurally distinct fibril cores that are specific to the disease, or groups of diseases. These "strains" of tau fibrils appear to propagate between neurons in a prion-like fashion that maintains their initial template structure. In addition, the strains isolated from diseased tissue appear to have structures that are different from those made by the most commonly used *in vitro* modeling inducer molecule, heparin. The structural differences among strains in different diseases and, potentially, *in vitro* induced tau fibrils may contribute to recent failures in clinical trials of compounds designed to target tau pathology. Unfortunately, isolating authentic tau filaments from diseased brain tissue is not practical due to the large amount of protein required to conduct high-throughput drug screening, and studies aimed at characterizing tau aggregation dynamics and understanding the effects of disease related mutations.

This body of work encompasses two studies that highlight the importance of developing disease relevant *in vitro* tau aggregation model systems. The first shows how different *in vitro* tau aggregation inducer molecules can have significant effects on how tau interacts with different classes of aggregation inhibitors. We identified an isoquinoline compound (ANTC-15) isolated from the fungus *Aspergillus nidulans* that is able to both inhibit filaments induced by arachidonic

acid (ARA) and also disassemble pre-formed ARA-fibrils. When compared to a phenothiazine tau aggregation inhibitor currently in clinical trials, LMTX (LMTM, or TRx0237), ANTC-15 and LMTX were found to have opposing inducer-specific activities against ARA and heparin *in vitro* induced tau filaments. These findings may help explain the disappointing results in translating potent pre-clinical inhibitor candidates to successful clinical treatments.

The second study highlights how different inducer molecules can have fundamental disparities to how disease related mutations effect the aggregation dynamics of tau. Using three different classes of tau aggregation inducer molecules we characterized disease relevant mutations in tau's PGGG motifs at positions P301S, P332S, and P364S. When comparing these mutations to wild type tau, we found that depending on the type of inducer molecule used we saw fundamental differences in total aggregation, aggregation kinetics, immunoreactivity, and filament morphology. These data support the hypothesis that different tau aggregation inducer molecules make different polymorphs and perhaps structurally distinct strains. The impact of using non-disease relevant induced filaments for research studies may lead to significant set-backs to research of tau-based pathology. Moving forward, we must prioritize identifying disease relevant aggregation inducer molecules, methods for propagating tau fibril folds from authentic filaments with high fidelity and reproducibility, or co-factor free systems that convert monomeric tau to disease relevant structures. Chapter 4 discusses some preliminary data, techniques, and protocols for A) comparing synthetic filaments using a range of different inducer molecules, B) *in vitro* seeding assays using authentic filaments isolated from Alzheimer's disease and progressive supranuclear palsy brain tissue, C) a technique for mechanically inducing co-factor free aggregates of a 3R tau isoform. The importance of furthering our fundamental understanding of how tau aggregates in disease and how we can best

reproduce disease relevant structures *in vitro* is not to be underestimated. It is likely to have a critical impact on the future of treatment discovery and development of this devastating set of neurological disorders.

Acknowledgments

First and foremost, I would like to thank my wife, Amanda, for her continued love and support. She always inspires me to be a better learner, husband, and person. She has stood by me throughout this journey and is always ready to bring me back down to earth and remind me of the important things in life. I admire her love, care, and empathy. She motivates me to work toward improving the world we live in. Together we are raising three beautiful children, Dylan, Lucas, and Lilliah, who have not only provided a well needed distraction at times, but are also been a daily reminder as to why education and research is so important for future generations.

I would also like to thank my parents who have always supported my decisions, even when it means moving to a different continent. The work ethic and moral foundation they instilled in me as a child continues to serve me throughout my higher education and adulthood. They are both excellent role models, not only in parenting, scholarship, and professionalism, but also in how to build and develop a loving relationship and treat others in the world around me. In addition to my own parents, this would not have been possible without the love and support from my mother in-law, Phyllis Painter. Sadly, we lost my father in-law, Steve Painter, in 2019 after suffering with Alzheimer's disease, but his lessons in honesty and integrity have guided me throughout my studies. The love Phyllis showed Steve throughout his illness was a reminder of the importance of investing in research efforts of this devastating disease.

I would also like to thank former members of the Gamblin Lab for their support, guidance, and friendship. Dr. Yamini Mutreja and Bryce Blankenfeld provided a friendly, welcoming, and thorough rotation and are the reason I chose to join the lab. Both completed excellent research

while in the lab that has been extremely useful for me in developing my own projects. I would also like to thank the three undergraduate research assistants that I have mentored while working in the Gamblin Lab: Kelsey Hillyer, Madison McGuire, and Tarik Aginar. It has been a pleasure working with them and I have been very impressed and proud of their accomplishments. Some of the work discussed here would not have been possible without their contribution.

I would like to thank all the members of my committee, Dr. Erik Lundquist, Dr. Berl Oakley, Dr Yoshiaki Azuma, and Dr. Michael Hageman, who have provided advice and guidance throughout the different stages of my doctoral studies. In particular, I would like to expressly thank Dr. Oakley, who was a collaborator on my first project and has provided extensive advice and support throughout my time at KU. I would also like to especially thank Dr. Lundquist for taking over as my official KU mentor after Dr. Gamblin moved and for providing guidance over the past year as I complete my studies. I would also like to make a special mention of Dr. Mark Richter who provided advice and guidance as one of my committee members and teachers while being at KU. Sadly, Dr. Richter passed away at the end of last year and he will be greatly missed within the department by all who knew him.

Lastly, I would like to thank my primary mentor Dr. T. Chris Gamblin for his support throughout my time at KU. He is always happy to sit down and chat through research problems and has spent countless hours helping me to develop as a scientific thinker and writer. He has provided me with lots of guidance and direction, while also allowing me space to be able to navigate my own journey. This work would not have been possible without Dr. Gamblin’s mentorship.

Table of Contents

List of Figures

*Specific contributions from collaborators and other lab members have been highlighted in the caption of the respective figures they contributed to.

List of Tables

Chapter 1: Introduction

1.1 An overview of the microtubule associated protein tau

The microtubule associated protein tau (MAPT, or tau) has been studied in the context of neurodegeneration for almost 35 years. The initial discovery of tau was due to its function as a microtubule stabilizing protein in 1975, a decade later multiple researchers identified tau as a major component of neurofibrillary tangles (NFTs), a histopathological hallmark found in Alzheimer's disease (AD)[1]. The specific role of tau in disease and normal human physiology has yet to be fully elucidated, however significant evidence supports the hypothesis that tau plays a major role in neurodegeneration, cellular death, and cellular dysfunction[2]. Tau pathology has been shown to be well correlated with disease progression in AD by using tau positron emission topography tracers, Braak staging based clinical diagnosis, and post-mortem brain dissection[3-5]. Expression of aggregation prone tau mutations in mice has been shown to cause severe neurotoxicity within relatively short time frames (< 3 weeks). Interestingly, by turning off expression of the aggregate prone tau, neurotoxicity is reversed[6]. After longer periods of aggregation prone tau expression, mice suffer non-reversible neurodegeneration. Furthermore, cortical injections of tau pathology into mice results in neurodegeneration and cell to cell transmission of tau seeds[7]. Based on these findings is it thought that stopping or reversing tau aggregation may prevent neurodegeneration and neurotoxicity in tauopathies.

Tau is expressed in the human adult brain as a combination of 6 different isoforms. These isoforms differ by the inclusion of either three, or four microtubule binding repeat (MTBR) domains (3R, 4R), or the inclusion of either zero, one, or two N-terminal domains (0N, 1N, 2N). The typical nomenclature for these six isoforms is 2N4R, 1N4R, 0N4R, 2N3R, 1N3R, and

0N3R. Often, these isoforms are grouped together as either 3R/3-repeats (2N3R, 1N3R, and 0N3R) or 4R/4-repeats (2N4R, 1N4R, and 0N4R). Although this form of grouping suggests that the N-terminal inserts do not play as significant a role in tau physiology, or pathophysiology, the incorporation of these N-terminal repeats may have much more of an impact in tau biology than previously thought[8]. Figure 1 illustrates a schematic of the *MAPT* gene and each of the 6 isoforms expressed in the adult human central nervous system (CNS).

In addition to the two N-terminal and MTBR domains of tau, there are three other regions of interest; the phosphatase activating domain (PAD) located on the most distal point of the N-terminus (aa. 2-18)[9], two proline rich domains (PRD1 and PRD2) located between residues 151-243, and the C-terminal domain (CTD), aa. 371-441. PRD1, or P1, consists of aa. 151-198 and PRD2, or P2, consists of aa. 199-243[10]. The PAD is thought to play a role in cell signaling and regulating transportation of cellular cargo along microtubules[11]. Although tau is primarily thought of as an intrinsically disordered protein (IDP), there have been several studies that have shown that long range electrostatic interactions and regions of secondary structure may allow tau to maintain a partially folded state in normal physiology either in a "hairpin" conformation or an "S" conformation[12, 13]. Exposure of the PAD is also an early marker of tau aggregation as it is thought to be inaccessible while tau is in a native conformation[13, 14]. The roles of PRDs P1 and P2 are still not fully understood, however there is evidence that they may play a role in tau's ability to interact with RNA, actin filaments, other proteins, and potentially initiate liquid-liquid phase separation[15, 16]. In AD, paired helical filaments (PHFs) of tau are often cleaved at residue E391 and there have been several studies that have associated this truncation with AD-like

pathology both *in vivo* and *in vitro* [17-19]. It is also thought that the C-terminus of tau may help in reducing tau toxicity, the spread of tau pathology, and total tau aggregation[20-23].

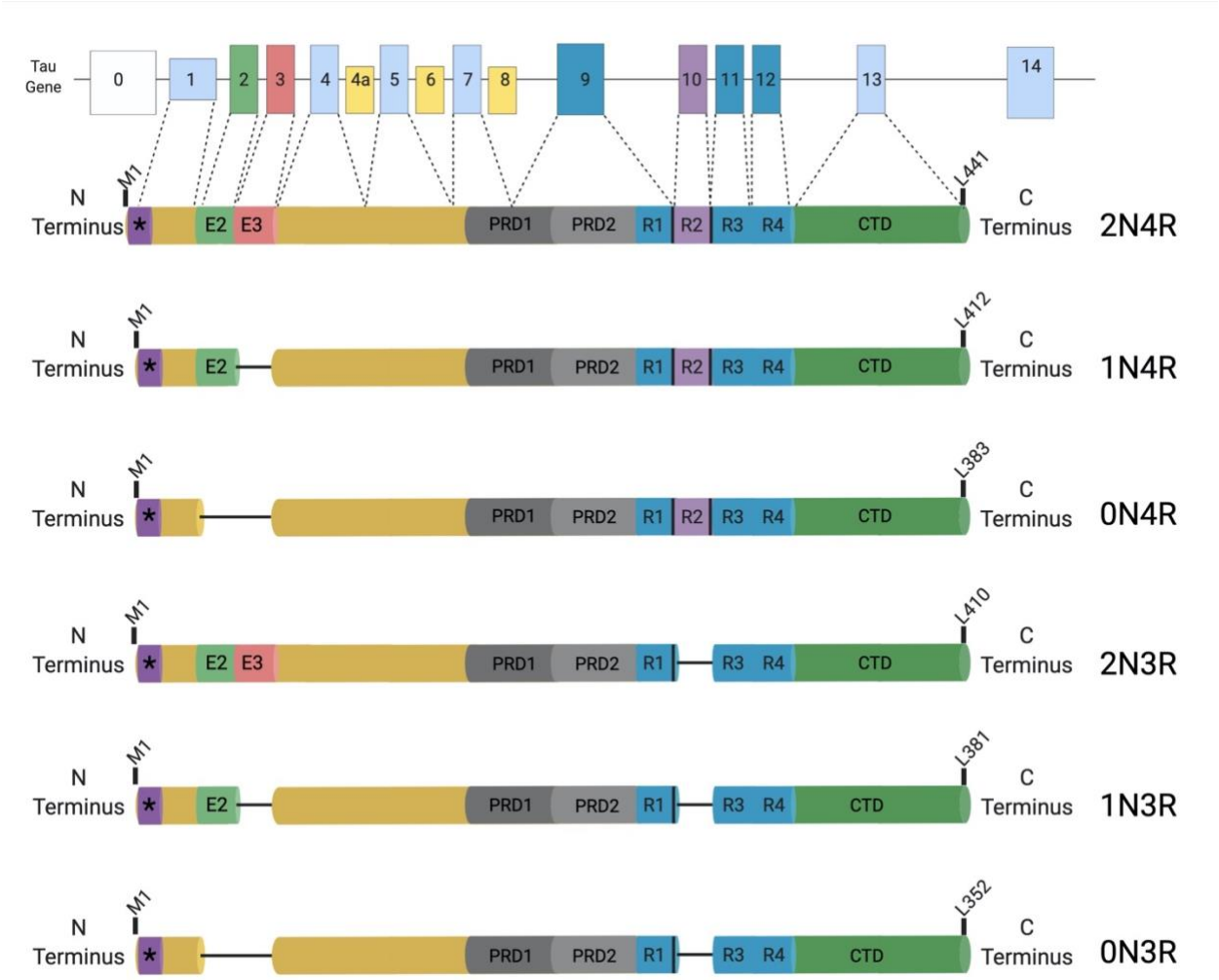

Figure 1: Schematic of the *MAPT* gene that encodes for the different tau isoforms with a schematic of the 6 isoforms of tau expressed in the adult central nervous system (CNS).
Exons 0 and 14 are transcribed, but not expressed. Exons 4a, 6, and 8 are not expressed in the (CNS). Exons 2, 3, and 10 are alternatively spliced depending on the isoform being expressed. Exons are not drawn to scale. Phosphatase activating domain (* in purple), N-terminal insert 1 (E2 in light green), N-terminal insert 2 (E3 in pink) proline rich domain 1 (PRD1 in dark gray), proline rich domain 2 (PRD2 in light gray), and microtubule binding repeat domain 1, 2, 3, and 4 (R1, R2, R3, and R4 in blue, respectively), and C-terminal domain (CTD in dark green) are indicated on each of the isoforms. This figure was created using Biorender.com and adapted from I. D'Souza and G.D. Schellenberg, 2005[24].

1.2 Tau in normal physiology

In normal human physiology 3-repeat and 4-repeat tau isoforms are expressed at approximately equal ratios. In general, the expression of N-terminal inserts appear at different levels, 9% (2N4R, 2N3R), 54% (1N4R, 1N3R), and 37% (0N4R, 0N3R) in the adult human brain, however this can vary depending on the brain region[25]. It is thought that the concentration of tau in the human brain is within the low micromolar concentration range (2-4 μM) and higher levels of expression have been associated with disease[26]. The full extent for the differences in isoform expression has yet to be clarified, however it is widely accepted that the normal regulation of isoform expression plays a role in maintaining microtubule stability, managing cellular cargo traveling throughout the cytoskeletal network, and helps maintain normal cell function through various cellular communication pathways[27-29]. The primary function of tau is to bind to and stabilize microtubules to maintain the axonal cytoskeletal network.

There are many post-translational modifications (PTMs) that can modulate the functions of tau, including phosphorylation, nitration, acetylation, ubiquitination, glycation, SUMOylation, methylation, oxidation, and glycosylation[30]. Of these PTMs, phosphorylation is by far the most well studied in the context of tau physiology and pathology. Phosphorylation of tau can occur through the action of several different kinase enzymes including glycogen synthase kinase 3 (GSK3β), cyclin dependent kinase 5 (cdk5), casein dependent kinase 1 (CK1), cyclic AMP-dependent protein kinase (PKA) and others[30]. Tau phosphorylation has typically been associated with disease due to the isolation of hyperphosphorylated tau fibrils from diseased brain compared to typical phosphorylation of tau found in healthy brain tissue. In addition, the phosphorylation of tau increases the number of negatively charged residues of the protein, thus

leading to a lower affinity towards negatively charged microtubules[2]. However, recent studies have suggested that the increase in phosphorylated tau isolated from disease, may be due to an increase of steric hinderance and electrostatic differences between aggregated tau and monomeric tau, causing phosphatases to have a higher affinity towards tau monomers[2, 30]. In addition, the interaction between tau and microtubules could be much more dynamic than previously thought, with evidence to support a "kiss and hop" mechanism where tau spends relatively short dwell times associated with microtubules[31]. This could mean hyperphosphorylation and dephosphorylation occurs in normal physiology, but this highly dynamic process is "fixed" in samples of aggregated protein. The role of other PTMs on tau in pathology is less studied, however PTMs such as acetylation, ubiquitination, SUMOylation, glycation, and methylation are all known to act on lysine residues and therefore may be important factors to study when taking into account the role of specific lysines on tau filament structure and how modified lysines may be targeted by future therapeutic molecules[32].

1.3 Tau aggregation

The initial cause of tau aggregation in disease is still unknown, and is likely to consist of a complex series of cellular events that are disease dependent. However, based on *in vitro* and *in vivo* studies, it is generally accepted that the formation of abnormal tau accumulation occurs through the following sequence of events illustrated in figure 2. 1) Tau dissociates from microtubules, either through post-translational modifications or other cellular events. 2) Soluble monomeric tau undergoes a conformational change that leads to the formation of β-sheet enriched structures allowing monomers to begin to self-associate and form dimers and oligomers. 3) Oligomers can then elongate through the recruitment of soluble monomeric protein

eventually forming larger protofilaments. 4) Protofilaments can then form filaments such as PHFs and SF that can further accumulate into larger aggregates such as NFTs[33, 34]. The details of these events are still unknown and heavily debated. In addition, several studies in recent years have also showed that the phenomenon of liquid-liquid phase separation may cause tau to accumulate at highly concentrated levels in the cellular environment and therefore promote spontaneous aggregation[35-37].

Due to recent advancements within the field of cryo-electron microscopy there are now high-resolution structures of authentic filaments isolated from several different tauopathies. These structures includes filaments from AD[38], Pick's disease (PiD)[39], corticobasal degeneration (CBD)[40], and chronic traumatic encephalopathy (CTE)[32]. In addition, a recent pre-print has been deposited in BioRxiv that claims to have solved tau filament structures from several other neurodegenerative disorders[41]. The specific amino acid residues included within the ordered fibril core isolated from AD, PiD, CBD, and CTE varies depending on the disease, but in general encompasses the MTBR region of the protein.

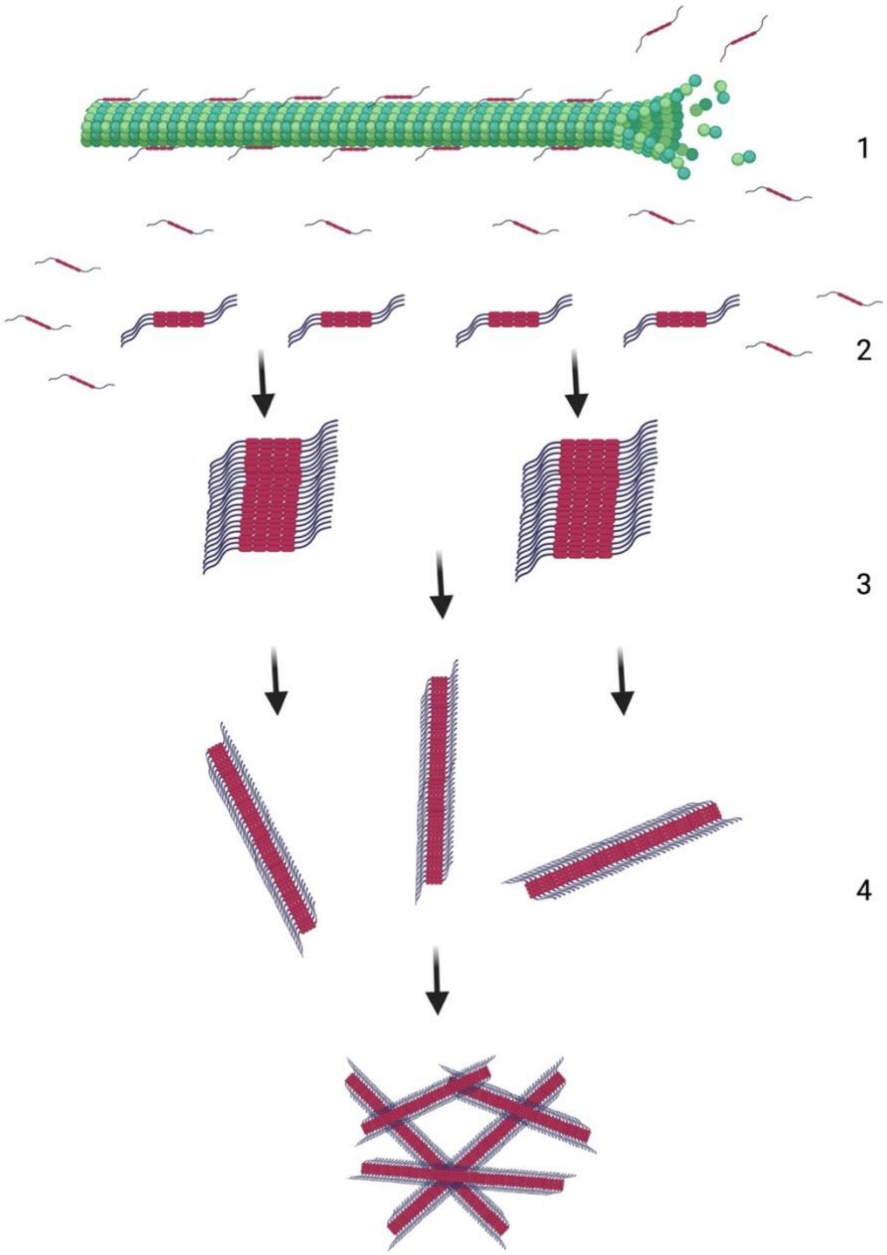

Figure 2: Schematic of sequence of events leading to tau aggregation.
1) Tau initially dissociates from microtubules either through post translation modifications, or other cellular events. 2) Tau then undergoes a conformational change that allows it to go from an inert monomer to a β-sheet enriched conformation, this allows for tau-tau binding to occur and form dimers, trimers, and larger oligomers. 3) Oligomers continue to recruit monomeric tau and elongate to form longer fibrils that can form as paired helical filaments, straight filaments, or other filamentous structures. 4) These filaments continue to aggregates forming larger complexes such as neurofibrillary tangles or neuropil threads. This figure was created using biorender.com.

1.4.1 Tauopathies and tauopathy related mutations: FTDP-17

The *MAPT* gene that encodes for the different isoforms of tau is located on the q arm of chromosome 17 at band 21 (17q.21). Frontotemporal dementia with parkinsonism linked to chromosome 17 (FTDP-17, also known as familial FTD) is a group of frontotemporal dementias that are associated with specific mutations on *MAPT*[42]. This subset of tauopathies can include Pick's disease (PiD), corticobasal degeneration (CBD), progressive supranuclear palsy (PSP), and others. However, it should be noted that not all cases of the aforementioned tauopathies are caused by tau mutations. This has resulted in a push to retire the term FTDP-17 for familial FTD as these cases appear to be clinically and pathologically similar to the sporadic forms of disease, but are associated with an autosomal dominant mutation[43]. *MAPT* mutations can include several intronic mutations flanking exon 10 that lead to changes in alternative mRNA splicing patterns that increase the frequency of 4R isoform expression. In addition, deletions, missense and silent mutations of exons 1, 9, 10, 11, 12, and 13 can lead to increased dissociation from microtubules, increased aggregation, and changes in filament morphology and aggregation dynamics[44]. Based on recent studies showing the structural heterogeneity of tauopathies and the fact that the majority of FTDP-17 associated mutations occur within the MTBR domains and therefore the ordered fibril core (figure 3), it is probable that structures of familial cases of tauopathies will differ when compared to the structures isolated from sporadic cases[41]. This will result in a divergence between clinical classification and structural classification of this group of diseases. Although a direct link between *MAPT* mutations and tau aggregation is important for highlighting the role tau plays in neurodegeneration and neurotoxicity, most tauopathies appear to be sporadic. Below is a summary of several different tauopathies that illustrates the diverse etiology and structural pathology associated with tau in disease.

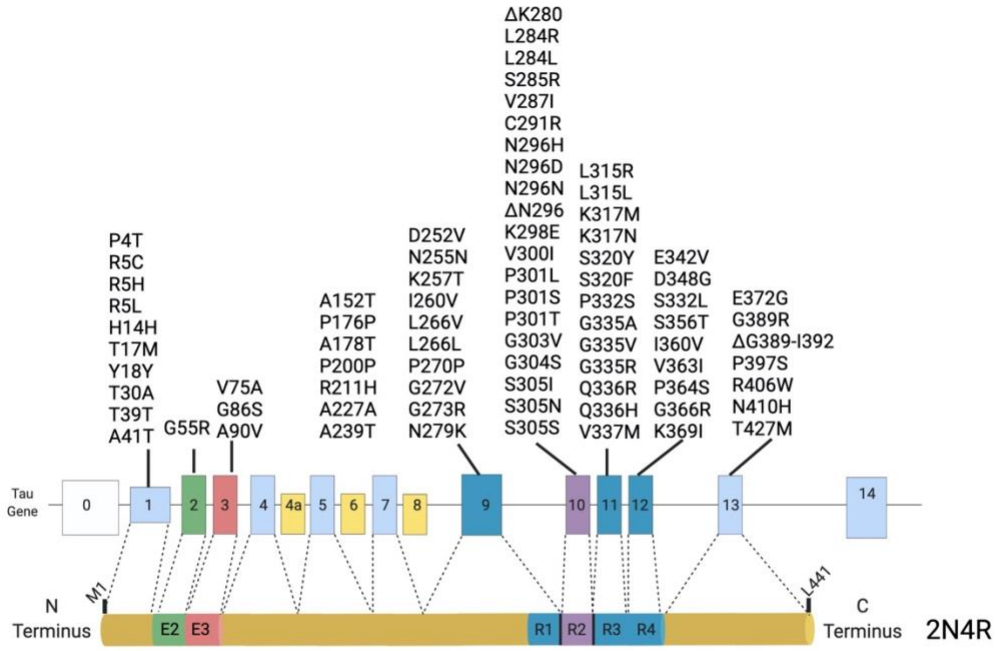

Figure 3: Schematic of exonic FTDP-17 mutations.
A schematic of the *MAPT* gene and how it relates to the MAPT protein. Known associated exonic mutations have been shown using traditional form and numbering based on full length 2N4R tau isoform. For example P301S, refers to the proline at position 301 being mutated to a serine residue, Δ refers to a deletion mutation of that specific residue or group of residues. It should be noted that there are several intronic mutations (not shown) that have been shown to alter expression of different isoforms through altering alternative mRNA splicing patterns. This figure has been made using biorender.com and was based on information found on alzforum.org/mutations/mapt and Olszewska, et. al. 2016[42].

1.4.2 Tau in Alzheimer's disease

The most prevalent and extensively studied tauopathy is Alzheimer's disease (AD). Although AD was first reported by Dr. Alois Alzheimer in 1906, the exact cause of the disease remains elusive[45]. The two histopathological hallmarks of AD include extracellular senile plaques (Aβ plaques) formed by the amyloid β peptide, and neurofibrillary tangles (NFTs) formed by the intracellular accumulation of tau[46]. In AD, tau aggregates into both paired helical filaments (PHFs) and straight filaments (SFs) beginning in the entorhinal cortex followed by

spreading to the limbic area, and eventually the neocortex[47]. Aggregation occurs primarily within neurons leading to cell death, synapse loss, and brain atrophy[48]. Although both PHFs and SFs are made up of two protofilaments, PHFs have regular twist with a half periodicity of approximately 80 nm and a width that ranges between 8 nm and 20 nm, unlike SFs that have no apparent twisting and a typical width of 15 nm[49]. These filaments are made up of both 3R and 4R co-polymerized tau isoforms. Recent advances in the field of cryo-electron microscopy have led to the first published high-resolution structures of both PHFs and SFs isolated from Alzheimer's disease[50]. The filament structures solved in Fitzpatrick et. al. 2017[50] showed fibrils from AD patients adopt a common C-shaped fold made up of 8 β-strands. Despite differences between the protofilament interface of PHFs and SFs, both types of filaments appeared to be similar in structure. These findings are based on a relatively small sample size and therefore tau filament heterogeneity amongst all AD patients cannot be ruled out. However, the findings that the AD PHF and SF filaments were made up of residues found between V306 and F378 (R3 and R4, numbering based on 2N4R isoform) and that both PHFs and SFs consisted of all six isoforms, were consistent with previous structural studies[51, 52].

1.4.3 Tau in chronic traumatic encephalopathy

Similar to AD, filaments made up of all six tau isoforms are also a histopathological hallmark of chronic traumatic encephalopathy (CTE). However, the presence of Amyloid-β plaques is not required for diagnosis of CTE, and this disorder is primarily caused by known environmental factors, such as single or repetitive head injuries. The distribution of tau filaments within CTE brain tissue differs to AD and is primarily found surrounding blood vessels and astrocytes[53]. In addition, recent cryo-EM structures have shown that although CTE tau filaments

adopt a C-shape fibril core made up of 8 β-strands of R3 and R4, these fibrils are distinct from AD-PHFs and AD-SFs[40]. Interestingly, structures solved by cryo-EM have also shown an unidentified additional density within the hydrophobic core of the tau fibrils suggesting the presence of a hydrophobic cofactor.

1.4.4 Tau in corticobasal degeneration and progressive supranuclear palsy

Corticobasal degeneration (CBD) and progressive supranuclear palsy (PSP) have long been associated with each other as they are both characterized by the formation of 4R tau fibrils with overlapping regional pathology of the basal ganglia and brainstem as well as overlapping clinical symptoms[54-56]. However, despite these similarities there are also distinct clinical symptoms and pathology that distinguish CBD and PSP. Recently, the first structure of 4R tau filaments isolated from CBD patients was solved using cryo-EM[40]. This study showed that tau filaments isolated from CBD brain tissue have a distinct fibril core from other tauopathies. Similar to fibrils isolated from CTE, the CBD filaments also contained a non-proteinaceous unidentified density buried within the ordered fibril-core. In contrast to the cofactor incorporated in the CTE fibril core, the density identified in CBD filaments interacts with three lysine residues at position K290, K294, K370, and is thought to be anionic. A recent pre-print has also been deposited on *BioRxiv* that shows a cryo-EM structure of filaments isolated from PSP differs to the previously solved CBD filament structure[57]. Interestingly, both filaments contain an 11 β-strand ordered fibril-core made up of residues K274 and E380, however, the PSP fibril core appears to have a non-proteinaceous density that interacts with a lysine at position K317 and appears to be similar to the lysine coordinated density found in CBD fibrils. The authors posit

that this may be a common negatively charged cofactor that is required to neutralize the positively charged lysine molecules during early stages of aggregation.

1.4.5 Tau in Pick's disease

In the case of Pick's disease (PiD), tau fibrils primarily form spherical Pick bodies and are made up of narrow-Pick filaments (NPFs) and wide-Pick filaments (WPFs). In contrast to the other tauopathies discussed above, fibrils isolated from Pick's disease are primarily formed by the 3R tau isoforms and result in frontotemporal atrophy[58]. As the only three repeat tau fibril structure that has been solved by cryo-EM, it is not surprising that the ordered core of filaments isolated from Pick's disease is distinct from the previously solved structures[39]. The NPFs and WPFs appear to have the same basic protofilament structure, that is formed by 9 β-strands between residues K254 and F378 (numbering based on full length 2N4R tau) with no apparent incorporated cofactors. The NPFs associated with PiD are made up a protofilament that has a single compact fold. WPFs are made up of two protofilaments that share a narrow hydrophobic interface that allows them to be approximately twice as wide as NPFs.

1.4.6 Heparin induced tau fibrils

Under typical *in vitro* conditions recombinant tau monomer does not spontaneously aggregate into disease-like filaments. In order to conduct studies that aim to screen potential tau targeted therapeutics, characterize disease related mutations, and study aggregation dynamics, it is impractical to use authentic filaments isolated from diseased brain tissue. Therefore, most researchers within the field utilize the polyanionic glycosaminoglycan heparin to induce *in vitro* tau aggregation. It should be noted that there are many other classes of anionic molecules that

can also be used to induce tau aggregation, including; fatty acids, polyphosphate, nucleic acids, anionic detergents, and planar aromatic dyes. Specific details about aggregation conditions, filament morphology, and biological relevance of the polyunsaturated fatty acid – arachidonic acid (ARA), polyanions – heparin (HEP), polyphosphate (PP), and ribonucleic acid (RNA), and two planar aromatic dyes – thiazine red (TR) and Congo red (CR) in the context of *in vitro* tau aggregation are discussed in chapter 4. To date, heparin induced filaments remain the only synthetic full length fibrils that have had their structure solved by high resolution cryo-electron microscopy[59]. The fibril cores formed by heparin appear to be polymorphic in nature and all polymorphs are structurally distinct to tau filament structures isolated from disease. It is possible that the structures induced by heparin differ to those from disease due to the lack of some other required cofactor that is present in the cellular environment. However, based on current structural data, it is likely that fibrils formed by heparin are not disease relevant and therefore may provide erroneous results when used in modeling tau aggregation.

1.5 Tau based therapeutics

Despite the identification of tau as a major component of NFTs in AD and aggregates of other tauopathies, tau-based therapeutics have remained a relatively low priority for pharmaceutical development in the treatment of AD. Following Hardy and Higgins' proposal of the "Amyloid Cascade Hypothesis" in 1992, the identification of autosomal dominant mutations associated with the amyloid precursor protein, presenilin I, and presenilin II provided a direct link between early-onset familial AD (fAD) and the amyloid β aggregation cascade[60]. This led to a wave of research interest into therapeutics targeting the pathway of Aβ-plaques. Despite repeated failures of Aβ based therapeutics and the fact that fAD accounts for <5% of AD cases,

there are still twice as many Aβ based agents (19) as tau targeting agents (9) currently in clinical trials[61]. A summary of each of the tau based therapeutic agents currently in clinical trials can be found in Table 1.

This continued effort to treat Alzheimer's disease by targeting Aβ plaques has now resulted in the first FDA approved drug to treat AD in nearly two decades. Aducanumab (or Aduhelm), is a monoclonal antibody that targets Aβ fibrils and soluble oligomers that has been shown to significantly reduce Aβ-plaques as well as some improvement in cognitive function as determined by one of two large phase III clinical trials, Emerge (NCT 0248547). However, during spring 2019, the trial's sponsor, Biogen, announced that it would be halting the development of the drug due to poor results from another phase III clinical trial that did not show any improvement over the placebo group, Engage (NCT 02477800)[62]. Despite these conflicting results, the company applied for FDA approval based on the Emerge trial and positive results from a subset of participants from the Engage trial. The approval of aducanumab has been met with much controversy by some, resulting in 3 members of the FDAs scientific advisory committee to resign. However, Aducanumab's approval was praised by others, especially AD patient and caregiver advocacy groups. Regardless of whether the positive results of the Emerge trial will hold true after the drug is available to the wider public, it is still clear that there is a need for more effective therapeutics to treat Alzheimer's disease, but also Alzheimer's disease related dementias where Aβ pathology is not present.

Of the 9 tau-based therapies currently in clinical trials only one is in phase III trials and it falls under the category of a disease modifying small molecule, TRx0237. TRx0237 (also known as

LMTX or LMTM) is discussed at length in chapter 2. Of the other 8 tau based therapeutics, 7 are classified as disease modifying biologics, and one is a small molecule, nicotinamide (vitamin B_3), a known histone deacetylase inhibitor[63].

Disease modifying biologics is a relatively new field of study especially in the modification of disease within the CNS. There are currently five tau based biologic agents that are monoclonal antibodies that target extracellular, soluble, phosphorylated, or toxic forms of tau[64]. In addition, there is currently a phase II clinical trial of the active vaccine, ACI-35. This vaccine aims to elicit an immune response against phosphorylated tau[65]. In addition to both passive and active immune based therapies, a phase II trial of the antisense oligonucleotide Ionis-MAPTRx is aimed at reducing the expression of tau without impacting neuronal function[66].

Table 1 Summary of Tau based therapeutic agents used in clinical trials

Therapeutic Agent	**Trial Phase**	**Type/target**
TRx0237™	III	Small molecule, tau aggregation inhibitor[67]
Nicotinamide	II	Conjugated nanoparticle/tau phosphorylation[63]
Semorinemab	II	monoclonal antibody/extracellular tau[68]
Ionis-MATPRx	II	Antisense oligonucleotide/*MAPT* mRNA[66]
Zagotenemab	II	monoclonal antibody/aggregated tau[69]
Tilavonemab	II	monoclonal antibody/tau N-terminus[70]
ACI-35	II	Active immunization/phosphorylated tau[71]
JNJ – 63733657	II	monoclonal antibody/phosphorylated tau[72]
Lu-AF87908	I	monoclonal antibody/phosphorylated tau[73]

1.6 *In vitro* induced tau aggregation

In vitro tau aggregation studies are useful in gaining a detailed understanding of aggregation mechanisms, the role specific regions of tau play in aggregation, the effect of PTMs, and the understanding interactions with co-factors and other binding partners. High-throughput screening (HTS) is a common approach used to identify potential therapeutic agents. Initial screenings can identify potential "hit" compounds that can then be further studied and modified through structural activity relationship (SAR) studies. As monomeric WT tau does not spontaneously aggregate under normal *in vitro* lab conditions, an additional cofactor molecule is often used to induce aggregation. These inducers can include, polyanionic chains such as heparin (HEP) (discussed above), polyphosphate (PP), and nucleic acids (RNA and DNA), free fatty acids including arachidonic acid (ARA) and docosahexanoic acid (DHA), anionic detergents such as alkyl sulfate, and planar aromatic dyes such as Congo red (CR) and thiazine red (TR)[74].

In our lab we primarily use the polyunsaturated fatty acid, arachidonic acid (ARA) as an inducer molecule. This is due to the resulting fibrils having morphological similarities to SFs found in AD, reactivity towards antibodies that have a high affinity toward tau pathology in diseased brain tissue, and ARA's role in oxidative stress within the cellular environment. However, as we do not have good structural data to compare ARA induce filaments to those identified in disease, we must still investigate other *in vitro* aggregation inducers. As part of this effort we have utilized 6 different *in vitro* tau aggregation inducer molecules to be used as potential models for *in vivo* tau aggregation (ARA, HEP, PP, RNA, TR, CR). A summary of our findings using these 6 different inducers can be found in chapter 4.

1.7 Cell culture models of tauopathies

In addition to using cell free high-throughput screening assays, many groups also utilize cell culture models to screen potential tau targeting therapeutics. This can be done by adding compounds directly to cells at an initial screening concentration and then either isolating resulting tau pathology, or lack thereof, or using biosensor cell lines that display a signal of some sort that can be used as a reporter of tau aggregation[75]. Alternatively, compounds can be incubated with pre-formed fibrils prior to using the fibrils as seeds for inducing cell based seeding[76]. For example; one of the most common cell-based systems used for modeling tau aggregation is the tau RD P301S FRET biosensor cell line developed by the Diamond Lab group. This cell line expresses the repeat domain of tau with a P301S mutation that has been tagged with either a CFP or YFP fluorescent tag. Once the monomeric RD P301S tau begins to self-associate the two fluorophores will be close enough to form a FRET (Förster Resonance Energy Transfer) signal that can then be quantified[77]. Many tau expressing cell lines also use the P301S, P301L, and ΔK280 mutations, to drive tau into filaments and PHF-like aggregates[78, 79]. Other lines utilize other FTDP-17 related mutations that are known to decrease tau's affinity towards microtubules, such as R406W.

1.8 Mouse models of tauopathies

There are almost 30 different tau pathology displaying mouse models that are currently available according to AlzForum.org. Although some of these models express WT tau and still display AD PHF-like tau pathology, the majority of models used in therapeutic studies express a disease related mutation such as P301S or P301L[80-83]. Based on the location of these mutations and how they relate to recently solved tau filament structures, it is highly likely that such a

mutation results in structurally different tau fibrils. Therefore, an aggregation inhibitor that is effective in a P301S tau mouse model should not be assumed to be effective at inhibiting authentic fibrils isolated from human tauopathy.

1.9 Summary and significance

This body of work identifies how our understanding of small molecule tau aggregation inhibitors and tau aggregation dynamics can be influenced by different *in vitro* inducers of tau filaments. Previous work using aggregation inducer molecules has relied on the principle that *in vitro* induced filaments adequately represent structures found in disease. Based on recent structural studies, we now know that tau filaments isolated from diseased brain tissue form unique structures within the ordered fibril core. These structures appear to be conserved within specific neurodegenerative disorders and differ from structures formed by the most commonly used *in vitro* inducer molecule, heparin. The contrast between *in vitro* formed filaments and those found in disease, may be the reason for unsuccessful clinical trials aimed at targeting tau pathology. Developing our understanding of how different inducer molecules interact with tau aggregation inhibitors and effect tau aggregation dynamics is important to be able to identify disease relevant inducer systems. The studies discussed here identify how using non-disease relevant inducer systems may lead to significant setbacks in our attempts to identify tau based therapeutics and better understand how tau aggregates in disease.

Chapter 2: Fungally-derived isoquinoline demonstrates inducer-specific tau aggregation inhibition

2.1 Introduction

Aggregation of the microtubule associated protein tau (MAPT, UniProtKB - P10636) is a histopathological hallmark of multiple neurodegenerative diseases such as Alzheimer's disease (AD) and Alzheimer's disease related dementias (ADRDs) including progressive supranuclear palsy (PSP), Pick's disease (PD), corticobasal degeneration (CBD), chronic traumatic encephalopathy (CTE) and frontotemporal dementias with Parkinsonism linked to chromosome 17 (FTDP-17). AD and ADRDs have huge impacts on the economy and healthcare in the United States with an estimated annual cost of more than $355 billion for 2021, that is projected to rise to over $1 trillion by 2050[84]. Tau pathology has been linked to neuronal cell death, and its progression correlates extremely well with the advancement and severity of dementia[85]. Despite the recent FDA approval of the Aβ targeting drug, aducanumab, there is still a need for effective therapeutics that can slow or prevent the development of tau pathology.

Blocking or reversing tau aggregation is considered to be a viable therapeutic approach for the treatment of AD and ADRDs for the following reasons: tau aggregation correlates with cellular dysfunction and neuronal death; there is no known normal biological function of tau aggregates; and extensive approaches targeting other pathological structures such as beta amyloid senile plaques have had limited success[2, 86]. There have therefore been multiple studies aimed at identifying small-molecule tau aggregation inhibitors (TAIs)[87]. TAIs have traditionally been identified by screening large libraries of hundreds of thousands of small molecules against tau aggregates[88]. Due to the large amount of tau aggregate that is required to conduct these screens it

is impractical to use authentic tau filaments isolated from diseased tissue. Rather, it has been necessary to use recombinant tau that has been induced to form filaments *in vitro*.

The most common inducers employed for studying tau aggregation have been polyanionic molecules such as the glycosaminoglycan heparin, polyphosphate, and RNA; planar aromatic dyes such as Congo red and thiazine red; free fatty acids such as arachidonic acid and docosahexaenoic acid; and anionic detergents such as alkyl sulfate[74]. These compounds have been used primarily because the tau filaments induced in their presence have gross morphological similarities to filaments isolated from diseased tissue. They have increased beta strand formation like disease filaments, many of them bind to dyes such as thioflavin S in a manner similar to disease filaments, and antibodies that recognize aggregated tau in disease also interact with many of the *in vitro* assembled filaments. Compounds based on a phenothiazine core structure, such as LMTX (leucomethylthionine, LMTM, or TRx0237), a compound that has had limited success in phase III clinical trials[89], were identified primarily based on their inhibition of heparin-induced tau aggregates[90].

Emerging evidence has revealed that tau aggregates from disease do not all have identical structures[91], rather, they form unique and distinct "strains" with different seeding capacities and three-dimensional structures[32, 39, 40]. This evidence strongly suggests that tau pathology between AD and other ADRDs is much more heterogeneous than previously thought[32, 38, 39]. The structural variability in aggregated tau conformations has important implications in the identification of effective TAIs.

Recently, multiple studies have shown the structure of heparin induced filaments differs from those identified in diseased tissue[59, 92]. As yet, there have not been any published high-resolution structures of arachidonic acid induced tau filaments. As is the case with filament structures identified from diseased tissue, it is likely that different aggregation inducer molecules may result in heterogeneous filament structures. Based on comparisons of filament length distributions, polymerization kinetics, and polymerization conditions, it is highly likely that the core fibril folds formed by these inducers are different[93].

We have previously identified secondary metabolites isolated from the fungus *Aspergillus nidulans* that are effective at inhibiting and disassembling arachidonic acid and heparin induced tau aggregates *in vitro*[94, 95]. The most effective of these previously studied compounds was an azaphilone compound, Aza-9 (5-bromo-3-((S,1E,3E)-3,5-dimethylhepta-1,3-dien-1-yl)-7-methyl-6,8-dioxo-7,8-dihydro-6H-isochromen-7-yl acetate). Aza-9 was able to inhibit and disassemble tau aggregates induced by both heparin and arachidonic acid. However, Aza-9 also appeared to have high levels of non-specific interactions with tubulin, as evidenced by tubulin polymerization studies[95], suggesting the possibility that it has somewhat promiscuous activity toward proteins in general.

In the present study, we show how a different fungal secondary metabolite with an isoquinoline structure, ANTC-15, (7-methyl-3-nonylisoquinoline-6,8-diol[96]) can act as a narrow spectrum TAI *in vitro.* We chose to study ANTC-15 because it is a naturally occurring compound with structural similarity to other known tau aggregation inhibitors (for example, 4-piperazine isoquinoline derivatives [97]), and shares some structural similarities with the aforementioned Aza-

9. We found that ANTC-15 both inhibits arachidonic acid (ARA) induced aggregation and disassembles ARA PFFs with a potency greater than Aza-9 and could be a good candidate for further development because even though it has a cLogP above the range of most CNS penetrant drugs, the compound has not yet been modified in any way to increase its efficacy through structure-activity relationship studies. This is an initial examination of the properties of ANTC-15 before any efforts to increase its potency and drug-like characteristics. We compared the activities of ANTC-15 and LMTX against arachidonic acid and heparin induced tau filaments as well as studying their effects on tubulin polymerization. We have found that ANTC-15 inhibits the assembly of, and promotes the disassembly of, arachidonic acid induced filaments but not heparin induced filaments. LMTX, on the other hand, inhibits the assembly of heparin induced filaments but is not effective against arachidonic acid induced filaments. These results strongly suggest that heparin and ARA induce different polymorphs and ANTC-15 and LMTX have different activities against these polymorphs.

Together these findings support the hypothesis that tau aggregation inhibitors of different classes may have inducer-specific mechanisms of action. Understanding how these different molecules interact with tau will be an important step in developing tau aggregation inhibitors that can target disease-relevant strains.

2.2 Materials and Methods

Chemicals and reagents: Full length 2N4R tau (HT40, 441 amino acids) was expressed in *E. coli* and purified, as previously described, by Ni-His Tag affinity purification and size exclusion chromatography[98]. As shown by King et. al. the polyhistidine tag does not influence

tau aggregation and therefore was not removed[99]. Tau protein concentration was quantified using a Pierce BCA protein assay kit (23225) purchased from Thermo Fisher Scientific. Tau purity and concentration was confirmed to be ~95% pure by SDS PAGE (data not shown). Individual aliquots of 50 µL were prepared and stored at -80°C to avoid protein degradation. Arachidonic acid (90010) was purchased from Cayman Chemical, (Ann Arbor, MI). Heparin sodium salt (H4784) with an average molecular weight of 17,000 Da – 19,000 Da, was purchased from Millipore Sigma, (St Louis, MO). TRx0237 mesylate salt (LMTX) (CAS: 1236208-20-0) was purchased from BOC Sciences (Shirley, NY). ANTC-15 (7-methyl-3-nonylisoquinoline-6,8-diol) was discovered as a compound produced by over-expression of a non-reducing polyketide synthase (ANID_03386.1=AN3386) in *Aspergillus nidulans*[96]. Additional quantities of ANTC-15 were synthesized by the University of Kansas synthetic chemical biology core facility. The structure of the synthesized compound was confirmed using ^{1}H NMR (500 MHz, DMSO-d_6), ^{13}C NMR (126 MHz, DMSO), and high-resolution mass spectrometry (HRMS). A schematic diagram and description of the synthesis can be found in figure 10. TOC1 and TNT1 capture antibodies were a kind gift from Dr. Nicholas Kanaan, Michigan State University. The primary detection antibody was an anti-tau polyclonal rabbit antibody (A002401-2) purchased from Agilent (Santa Clara, CA). A goat anti-rabbit IgG (H+L) antibody with an HRP conjugate (1706515, Bio-Rad, Hercules, CA) was used as a secondary detection antibody.

Inhibition of tau aggregation: Inhibition assays of arachidonic acid induced filaments were performed as previously described[95]. Two µL of various concentrations of test compounds dissolved in DMSO were added to 190.5 µL of polymerization buffer (PB) in 1.7 mL microcentrifuge tubes to give a final compound concentration range of 0.8 µM to 200 µM. Final

DMSO concentration was 1%. PB final concentrations were 100 mM NaCl, 5 mM DTT, 10 mM HEPES (pH 7.64), 0.1 mM EDTA, and 2 µM 2N4R tau. These mixtures of compound and monomeric tau were incubated for 20 minutes at room temperature before the addition of 7.5 µL of 2 mM arachidonic acid (ARA) dissolved in 100% ethanol (final volume 200 µL, final ARA concentration 75 µM). Reactions were carried out overnight (20 hours) at 25°C. A no-compound polymer control containing 1% DMSO and 75 µM arachidonic acid and a no-compound monomer control of 1% DMSO and 0 µM arachidonic acid were used as positive and negative controls respectively. Inhibition assays of heparin induced filaments were carried out similarly but with the following modifications: final NaCl concentration was 25 mM with a final concentration of 0.5 µM heparin dissolved in ddH_2O, no ethanol was added to any of the heparin reactions. Incubation was completed at 37°C for 48 hours.

Disassembly of pre-formed tau filaments: Disassembly reactions were completed by setting up reactions in PB as described above prior to adding inhibitor compounds dissolved in DMSO. The reactions were given time for tau to completely polymerize (6 hours for arachidonic acid induced reactions and 48 hours for heparin induced reactions) before adding inhibitor compound dissolved in DMSO to give a final compound concentration range of 0.8 µM to 400 µM (final DMSO concentration of 1%) in a 1.7 mL microcentrifuge tube. The reactions were then left to incubate for 24 hours at 25°C for arachidonic acid induced filaments and 37°C for heparin induced filaments.

Sandwich ELISA: Following inhibition and disassembly reaction incubations samples were analyzed using a modified sandwich ELISA assay based on conditions previously described by

Combs et. al. [100]. Briefly, a Corning 3590 EIA/RIA 96 well microplate was coated with 100 µL/well of capture antibody [either TOC1 (2 ng/µL) or TNT1 (1 ng/µL)], sealed and incubated with gentle agitation overnight at 4ºC. Capture antibodies were diluted in BSB capture buffer (100 mM boric acid, 25 mM sodium tetraborate, 75 mM NaCl, 250 µM thimerosal, pH 8.56). The plate was then washed 2x with 300 µL/well of BSB wash buffer (100 mM boric acid, 25 mM sodium tetraborate, 75 mM NaCl, 250 µM thimerosal, 60 mM BSA, 0.1% Tween 20, pH 8.56). Each well was then blocked with 300 µL of 5% non-fat dry milk (NFDM) dissolved in BSB wash buffer, sealed and incubated at room temperature for 1.5 hours with gentle agitation. Inhibition or disassembly reaction samples were diluted in 5% NFDM BSB wash buffer to a concentration of 100 nM for TOC1 capture antibody and 25 nM for TNT1. To provide an internal standard curve, dilution series of no compound polymer and monomer controls were added to the plate at a range of (3.125 nM - 400 nM for TOC1 and 3.125 nM - 75 nM for TNT). In our hands, the EC_{50} of the polymerized tau affinity curve was found to be ~105 nM and ~28 nM for TOC1 and TNT1 respectively (see figure 11, for antibody binding affinity curves). Samples were added to a volume of 100 µL/well. Plates were sealed and incubated at room temperature for 1.5 hours with gentle agitation. Plates were then washed 2x using BSB wash buffer. Next, 100 µL/well of polyclonal rabbit detection antibody diluted to a concentration of 50 ng/mL in 5% NFDM BSB wash buffer was added. Plates were sealed and incubated at room temperature for 1.5 hours with gentle agitation. Plates were washed 2x using BSB wash buffer before the addition of 100 µL/well of the goat anti-rabbit IgG secondary detection antibody diluted 1:5,000 in 5% NFDM BSB wash buffer. The plate was sealed and incubated at room temperature with gentle agitation for 1.5 hours. Plates were then washed 3 x using BSB wash buffer before the addition of 50 µL per well of tetramethylbenzidine (TMB) substrate. The plates

were then covered and incubated with gentle agitation at room temperature for 20 minutes before the addition of 50 µL of a 3.6% H_2SO_4 stop solution. Readings were taken at an absorbance of 450 nm using a Varian Cary 50 UV Vis spectrophotometer with a Varian Cary microplate reader. Raw data readings were zeroed against the no compound monomeric control and then converted to % light absorbance and normalized using the internal no compound polymer control. Half maximal inhibitory concentration (IC_{50}) and half maximal disassembly concentration (DC_{50}) values were calculated by fitting the data to a log(inhibitor) vs response – variable slope, non-linear regression curve using Graphpad Prism 8.0. Curves were fit using the following variation of the 4PL equation where *Top* and *Bottom* refer to the upper and lower plateau of the response curve, respectively.

$$Y = Bottom + (Top - Bottom)(1 + 10^{LogIC50-X} * Hillslope))$$

Equation 1: Log inhibitor vs response – variable slope

Statistical analyses were completed using a one-way ANOVA multiple comparison Tukey's test to compare values at 200 µM screening concentration and no compound control. Statistical significance was defined as $* \, p \leq 0.05; \; ** \; p \leq 0.01; \; *** \, p \leq 0.001$. A full summary of p-values for all ARA induced filament screening experiments can be found in table 2, and all HEP induced filament screening experiments in table 3.

Transmission electron microscopy: Inhibition and disassembly samples were diluted 1:10 in polymerization buffer and fixed with 2% glutaraldehyde for 5 minutes at room temperature. The samples were then affixed to a 300-mesh carbon formvar coated copper grid, purchased from

Electron Microscopy Sciences, (Hatfield, PA) by floating the grid on a 10 µL droplet of sample for 1 minute. The grid was then blotted on filter paper and washed on a droplet of ddH_2O before being blotted and stained by floating the grid on a droplet of 2% uranyl acetate as previously described[101]. The grids were imaged using a JEOL JEM 1400 transmission electron microscope fitted with a LaB_6 electron source (Electron Microscopy Research Lab, University of Kansas Medical Center). Five random images per grid were taken at a 5,000x magnification. Images were analyzed using Image Pro Plus 6.0 software by measuring the number, length, area, and perimeter of filaments >25 nm in length. Under our experimental conditions, it is very difficult to reliably identify filaments less than 25 nm, therefore the assay is limited to tau filaments and oligomers greater than 25 nm. IC_{50} and DC_{50} values were determined by fitting the data to a log(inhibitor) vs response – variable slope non-linear regression curve in Graphpad Prism 8.0 (see equation 1).

Tubulin polymerization: Assays were completed in triplicate using tubulin polymerization assay kits (BK006P) purchased from Cytoskeleton Inc. (Denver, CO). Following the manufacturer's protocol for screening proteins for effects on tubulin polymerization activity, 0.5 µM tau was added using a multichannel pipette to a final concentration of 2 mg/mL of tubulin protein with or without 40 µM of ANTC-15 or LMTX diluted in DMSO. Tubulin polymerization was monitored at 340 nm using a Varian Cary UV Vis Spectrophotometer with Varian Cary microplate reader at 37°C. Readings were taken every 60 seconds for 61 minutes. Data were fitted to the Finke-Watzky polymerization equation shown below and analyzed using a paired t-test in Graphpad Prism 8.0.

$$[B]_t = [A]_0 - \frac{\frac{k_1}{k_2} + [A]_0}{1 + \frac{k_1}{k_2[A]_0}\exp\,(k_1 + k_2[A]_0)t}$$

Equation 2: Finke-Watzky Polymerization Equation.

Where $[B]_t$ is the amount of tubulin polymerization at time t, k_1 is the nucleation rate and k_2 is the elongation rate (reported k_1 and k_2 values can be found in figure 12).

Acoustic shearing of heparin filaments: No compound 1% DMSO heparin induced fibrils were formed as described above. Samples at volumes of 130 µL were transferred to Covaris microtube-130 AFA fiber pre-slit snapcap tubes (PN 500514). Samples were then sheared for 0 seconds, 30 seconds, 180 seconds, and 450 seconds using a Covaris ME220 focused-ultrasonicator (Covaris Inc. Woburn MA) at 20 °C on settings of 50 W peak power, 20% duty factor, and 200 cycles per burst. Using right-angled laser light scattering samples were analyzed for their ability to scatter light as previously described [102]. Briefly, samples were transferred to a 5 mm × 5 mm optical glass cuvette (Starna Cells, Atascadero, CA) in the light path of a 532 nm wavelength 12 mW solid-state laser operating at 7.6 mW (B&W Tek Inc. Newark, DE) and images were captured using a Sony XC-ST270 digital camera with an aperture of f.s. 5.6. Images were analyzed using Adobe Photo Shop 2021 by taking histogram readings of the pixel intensity across the scattered light path. Following the sandwich ELISA protocol described above, samples were analyzed for their affinity towards TOC1 and TNT1 capture antibodies as well as being imaged by TEM as described above.

2.3 Results

In previous studies of secondary metabolites isolated from the fungus *Aspergillus nidulans,* we have identified multiple compounds that can both inhibit and disassemble tau filaments induced by arachidonic acid[94, 95]. We have since identified a new class of fungal secondary metabolite that may act as a tau aggregation inhibitor. The isoquinoline, ANTC-15 (figure 4A), was studied for its ability to inhibit and disassemble tau filaments *in vitro*. As an external benchmark we wanted to compare the inhibitory activity of ANTC-15 to that of a known and extensively studied tau aggregation inhibitor, LMTX (figure 4B). LMTX has been shown to inhibit and disassemble tau aggregates in both *in vitro* and *in vivo* models. In phase 3 clinical trials it has shown limited success in the treatment of mild to moderate Alzheimer's disease patients [67, 89].

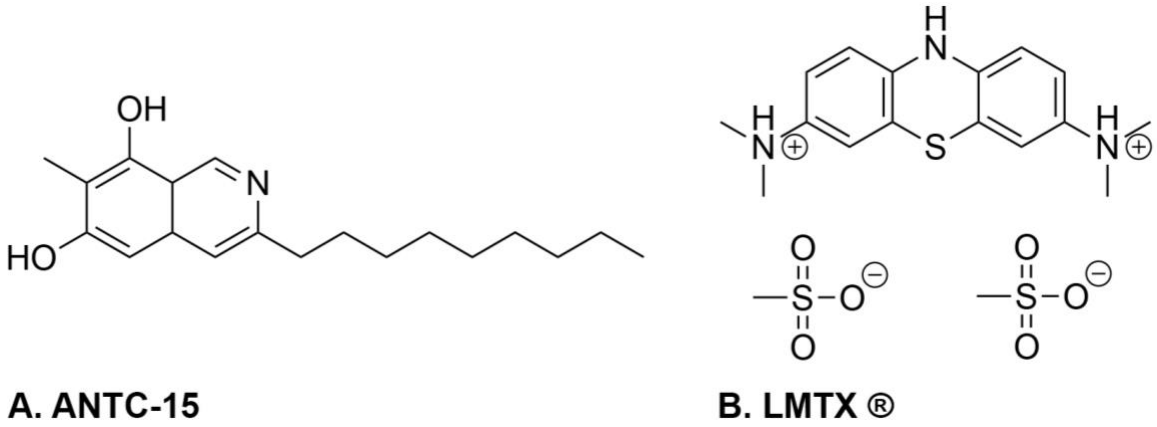

Figure 4: a. Chemical structure of the isoquinoline, ANTC-15 (7-methyl-3-nonylisoquinoline-6,8-diol). b. Chemical structure of the phenothiazine, LMTX® (TRx0237, leuco-methylthionine mesylate salt).
Initial discovery and isolation of ANTC-15 as a fungal secondary metabolite was complete by Dr. Berl Oakley's lab group and initial identification of ANTC-15 as a tau aggregation inhibitor was completed by Bryce Blankenfeld.

Assembly inhibition assays:

Typical tau aggregation inhibitor screening studies utilize high throughput methods, such as thioflavin T and thioflavin S fluorescence. During studies of both of these compounds we found

that they interfered with thioflavin fluorescence at our initial screening concentration of 200 µM (Figure 13). We also found that both compounds scattered light in aqueous solution, and we were therefore unable to use the standard right-angled laser light scattering aggregation assay (Figure 13). We therefore used a quantitative sandwich ELISA technique to determine the ability of ANTC-15 and LMTX to inhibit *in vitro* arachidonic acid (ARA) induced tau filament formation at an initial concentration of 200 µM (figure 5 A, B). The sandwich ELISA utilizes a polyclonal rabbit total tau detection antibody (A0024) and two monoclonal toxic-conformation-sensitive capture antibodies (TOC1 and TNT1) that have a high affinity for toxic tau species that are enriched during aggregation[100] with a linear dependence on the total amount of aggregates (figure 11). The tau oligomeric complex (TOC1) antibody recognizes toxic tau oligomers that are induced by arachidonic acid and heparin, as well as pathological tau from Alzheimer's disease (AD) and chronic traumatic encephalopathy (CTE) brain tissue[103-105]. The tau N-terminal (TNT1) antibody recognizes the phosphatase-activating domain (PAD) of the N terminus of tau, an epitope that is present in early-stage tau aggregation generated *in vitro* and found in both AD and CTE brain tissue[14, 104].

In these assays, ANTC-15 almost completely inhibited the formation of both TOC1 and TNT1 reactive tau species that were induced by ARA (figure 5 A, B). In contrast, LMTX had no significant effect on the formation of TNT1-reactive species and caused a significant increase in the amount of TOC1-reactive species (Figure 5 A, B). Transmission electron microscopy (TEM) was used to visualize the effect of these compounds at a range of concentrations (3 µM to 200 µM). Representative TEM micrographs show the effects of ANTC-15 (figure 5 E-H) and LMTX (figure 5 I-L) on ARA-filament formation. Quantification of both the average number of filaments per image and total filament length present on the TEM micrographs treated with 200

µM ANTC-15 confirmed that ANTC-15 significantly decreased the number and total length of tau filaments induced by ARA. LMTX at 200 µM, however, caused an increase in the length and numbers of filaments (figure 14).

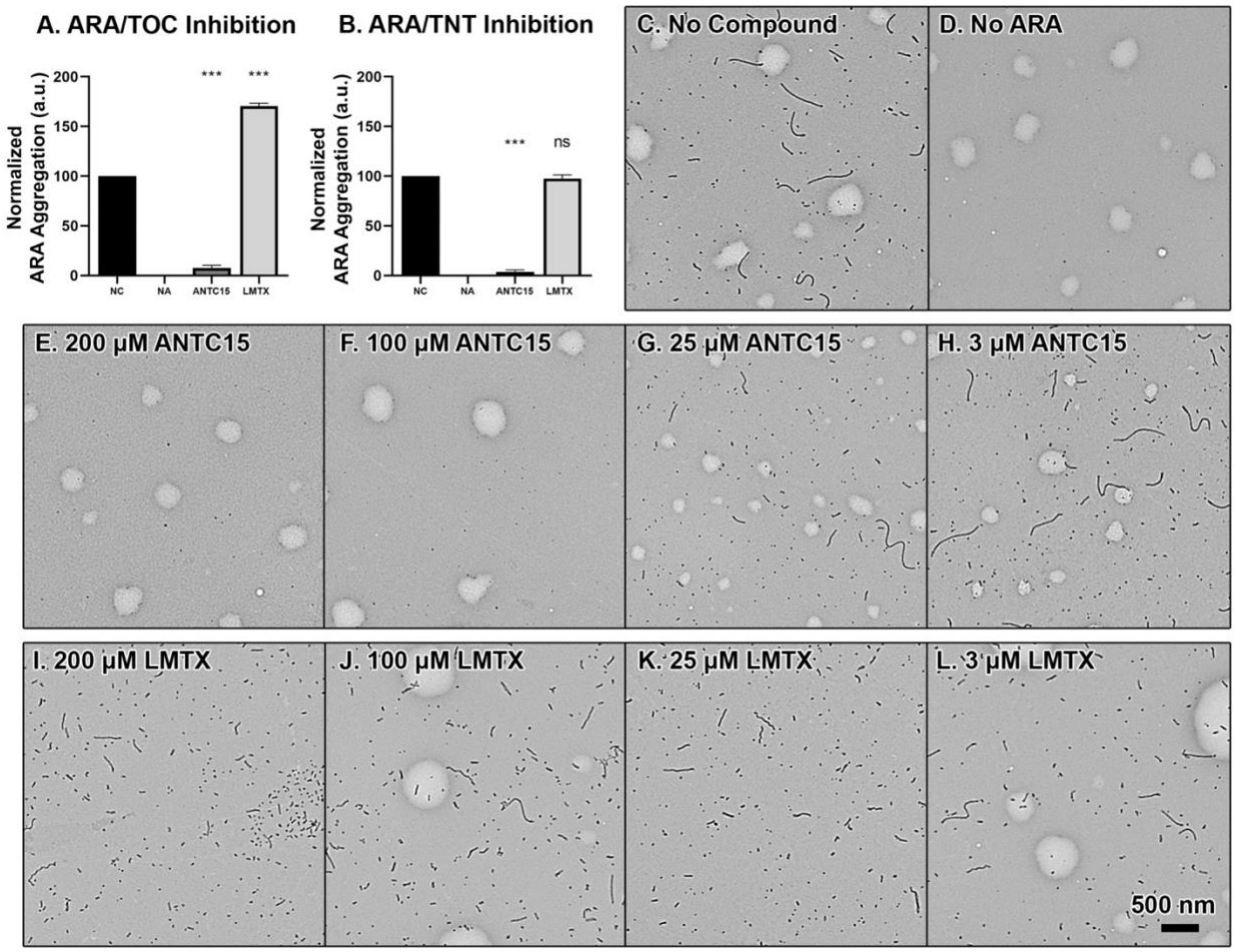

Figure 5: Inhibition of ARA induced filaments.
Initial inhibition assay of 200 µM ANTC-15 and LMTX against arachidonic acid (ARA) induced tau filaments. Sandwich ELISA using TOC1 capture antibody and TNT1 capture antibody (A and B, respectively) normalized against 1% DMSO no compound control (No compound =100). Samples were compared to no compound control using a Tukey's multiple comparison test, (p-values of all comparisons can be found in **Table 2**), $* \; p \leq 0.05$; $**$ $p \leq 0.01$; $*** \; p \leq 0.001, ns \; denotes \; no \; significant \; difference$. Representative transmission electron micrographs at 5000x magnification of no compound control (C), no arachidonic acid monomer control (D), ANTC-15 (E-H) and LMTX (I-L) at concentrations of 200 µM, 100 µM, 25 µM, 3 µM (left to right). Scale bar in 2L represents 500 nm for all images.

LMTX was first identified as a potent inhibitor of heparin induced filaments[90]. We therefore compared the ability of LMTX and ANTC-15 to inhibit heparin induction of tau aggregation (figure 6). There was a significant decrease in TOC1 and TNT1 reactive species in the presence

of 200 µM LMTX, however, no significant difference was observed in the presence of 200 µM ANTC-15. Quantification of the average number of filaments per image and total filament length based on TEM micrographs confirmed the finding from the ELISA experiments that LMTX significantly inhibited the number and total length of heparin induced filaments (figure 14). Representative TEM micrographs (figure 6 E-H) show the effects of ANTC-15 and LMTX (figure 6 I-L) on heparin induced filament formation.

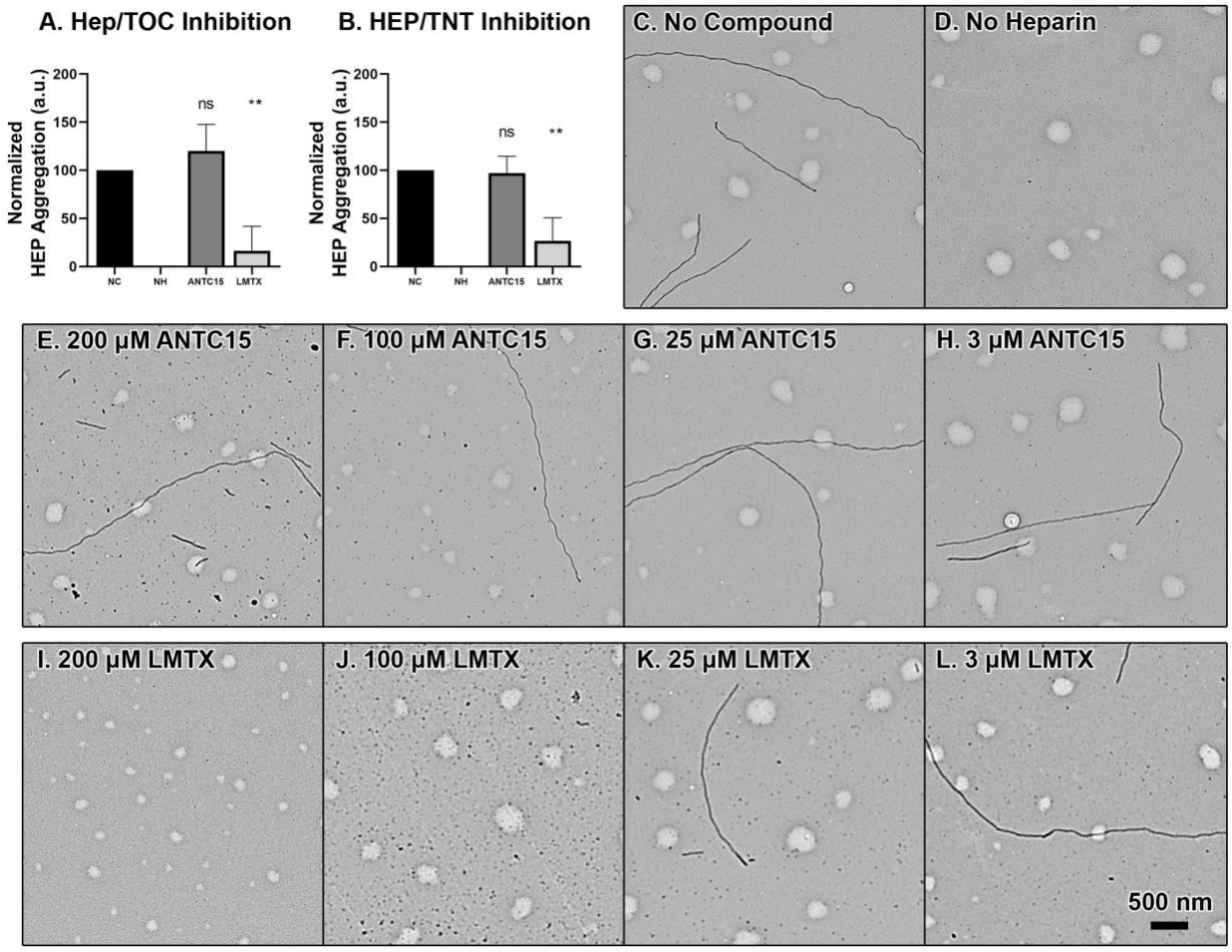

Figure 6: Inhibition of heparin induced filaments.
A, B: Initial inhibition assay of 200 µM compound concentration of ANTC-15 and LMTX against heparin (Hep) induced tau filaments. Sandwich ELISA using TOC1 capture antibody and TNT1 capture antibody (A and B, respectively) normalized against 1% DMSO no compound control (No compound =100). Samples were compared to no-compound controls using a Tukey's multiple comparison test, (p-values of all comparisons can be found in **Table 3**) $* \; p \leq 0.05$; $** \; p \leq 0.01$; $*** \; p \leq 0.001$, ns denotes no significant difference. Representative transmission electron micrographs at 5000x magnification of no compound control (C), no heparin monomer control

(D), ANTC-15 (E-H) and LMTX (I-L) at concentrations of 200 µM, 100 µM, 25 µM, 3 µM (left to right). Scale bar in 2L represents 500nm for all images.

Disassembly assays:

In disease, tau pathology is thought to develop long before symptom onset[29]. Therefore, when identifying compounds that act as TAIs, it is also useful to determine if these molecules can disassemble pre-formed fibrils (PFFs). In addition, due to the structural stability of amyloid folds, compounds that are able to disassemble PFFs are unlikely to inhibit tau aggregation through interfering with the inducer mechanism. To evaluate the abilities of ANTC-15 and LMTX to disassemble PFFs, we added each compound after the filaments had fully polymerized, incubated the PFFs with compound for 24 hours and then determined the amount of remaining aggregates by sELISA.

When ARA induced PFFs were treated with 200 µM ANTC-15, there was a significant decrease in TOC1 and TNT1 reactive species (figure 7 A, B). There was approximately a 50% reduction in TOC1 reactive species and 40% reduction in TNT1 reactive species. The addition of LMTX to ARA-PFFs caused an increase in TOC1 reactive species and had no effect on TNT1 reactive species (figure 7 A, B), which is consistent with results from ARA-aggregation induction trials (compare to figure 5).

We also compared the activity of ANTC-15 and LMTX to disassemble heparin PFFs. There was no significant change in heparin induced TOC1 and TNT1 reactive species with 200 µM ANTC-15 (figure 7 C, D). There were significant increases in TOC1 species in samples treated with 200 µM LMTX (figure 7 C), however, changes in TNT1 reactive species were not significantly different from the no-compound control when analyzed using a Tukey's multiple comparison test

(figure 7 D). We were interested to see if the increase in TOC1 and TNT1 species observed in the presence of LMTX could be caused by the change in filament length distributions. Therefore, we used quantitative TEM to measure the changes in filament length distribution in samples treated with 200 µM LMTX. Compared to the no compound control, an increase in the number of small filaments (25 nm - 50 nm) was observed with 200 µM LMTX (figure 15).

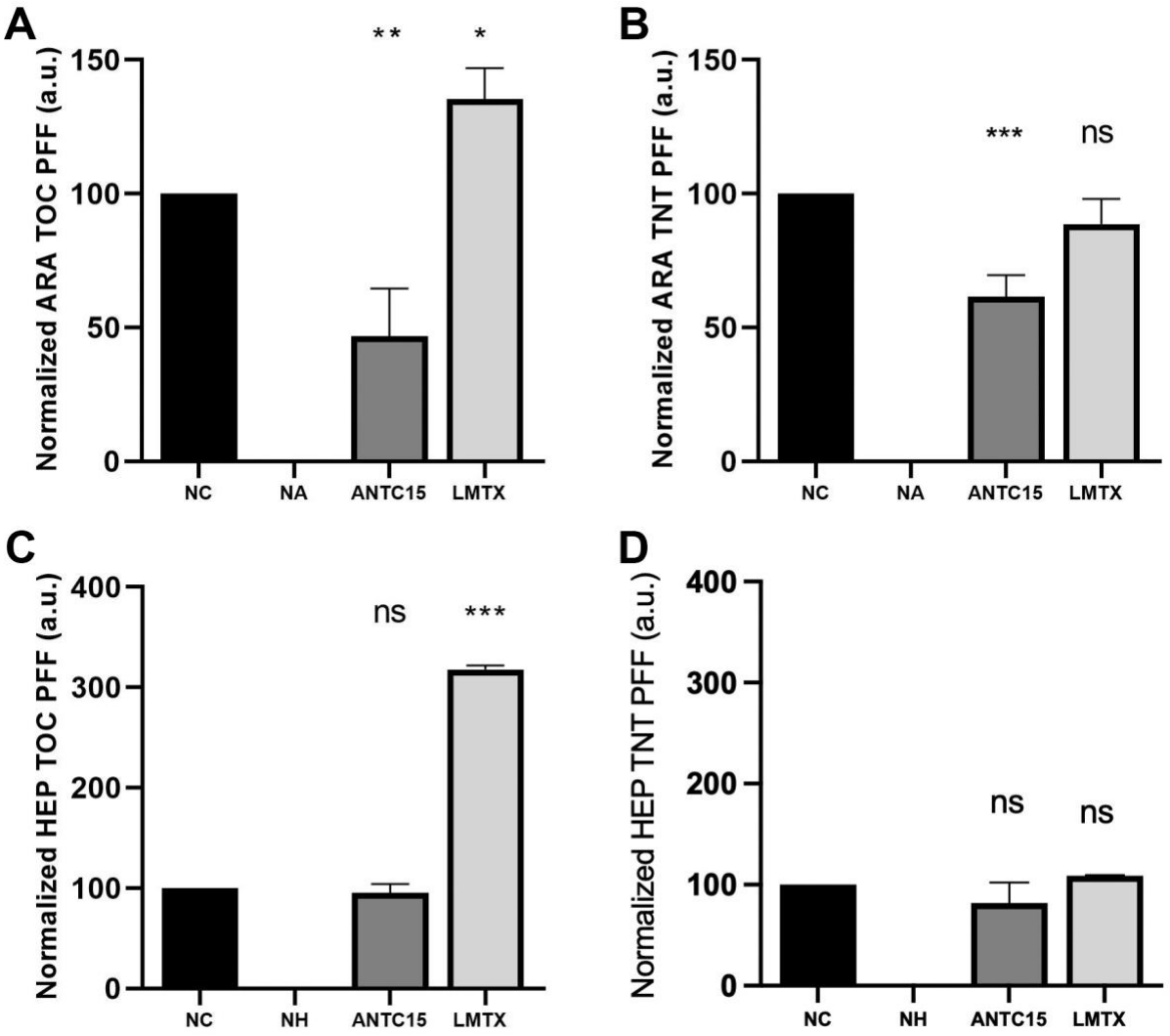

Figure 7: Disassembly of ARA and heparin PFF.
Disassembly assay of 200 µM of ANTC-15 and LMTX against arachidonic acid (ARA) induced tau filaments (A-B) and heparin (Hep) induced tau filaments (C-D). Sandwich ELISA using TOC1 capture antibody (left) and TNT1 capture antibody (right) normalized against 1% DMSO no compound control (No compound =100). Samples were compared to no compound control using a Tukey's multiple comparison test, (p-values of all comparisons can be found in **Table 2**). $* \, p \leq 0.05$; $** \, p \leq 0.01$; $*** \, p \leq 0.001$, ns denotes no significant difference.

Dose dependence studies:

Due to ANTC-15's ability to inhibit and disassemble ARA induced filaments at high concentrations, we sought to measure the relative efficacy of ANTC-15 by determining the values for IC_{50} and DC_{50} (figure 8). ANTC-15 concentrations ranged from 3 µM to 400 µM and experiments were completed in triplicate to establish an IC_{50} and DC_{50} for each of two antibodies that recognize toxic species of tau (TOC1 and TNT1) and by average number of filaments per image and total length of filaments as measured by transmission electron microscopy. Similar IC_{50} values were obtained by sandwich ELISA for TOC1 and TNT1 tau species for ANTC-15, (35 µM and 47 µM respectively). These values were in general agreement with IC_{50} values obtained by quantitative EM for the average number of filaments per image (33 µM) and the total filament length (25 µM) (figure 8 A, C, and E). By both sandwich ELISA and EM, complete inhibition of ARA-induced aggregation occurred at approximately 100 µM.

Disassembly was determined by quantitation of TOC1 and TNT1 species remaining after incubation of ARA-PFFs. At the highest concentration tested ANTC-15 reduces the amount of PFF approximately 50% and 40% respectively (Figure 8 B). We cannot accurately determine the value of the DC_{50} by sELISA because, by definition, there cannot be a half maximal concentration for disassembly if the amount of disassembly does not reach 100%. However, the sELISA results with TOC1 indicates that there is an estimated 50% reduction in PFF at an approximate concentration of 200 µM compound. Our analysis of the average number of filaments remaining after treatment of ARA-PFFs with ANTC-15 using TEM revealed a decrease of approximately 90% in the average number of filaments at the highest ANTC-15 concentrations used (figure 8 D) and a decrease of in total filament length of approximately 80%

(figure 8 F). Again, we are not able to accurately determine an absolute value for the DC_{50} as determined by TEM, but a rough estimation of the data suggests that there is a 50% reduction in the average number of PFF at 200 µM and a 50% reduction in the total mass of ARA PFF at 250 µM.

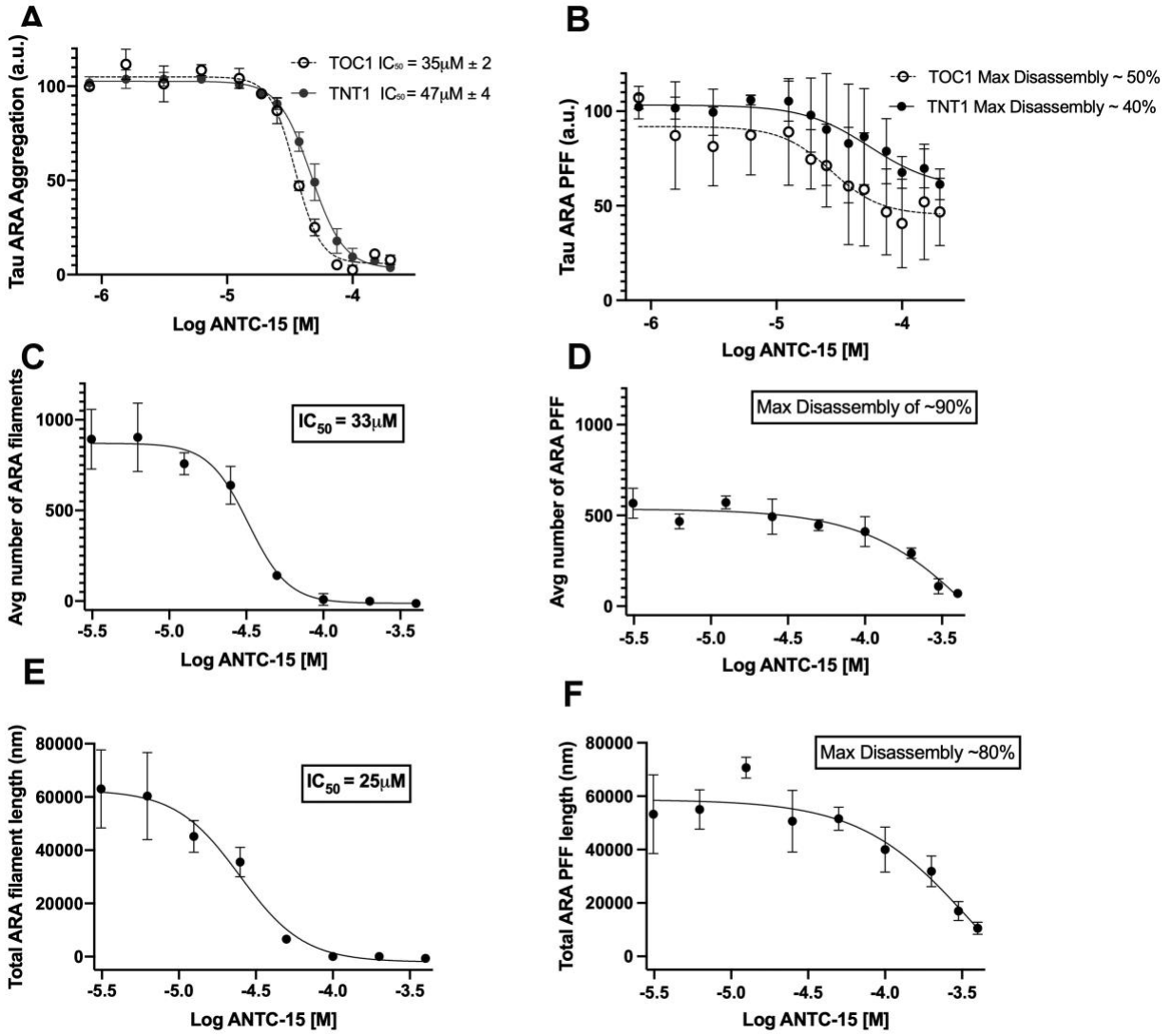

Figure 8: Dose dependence of ARA induced filaments using ANTC-15.
ANTC-15 dose dependence: inhibition of ARA-filaments (A, C, & E) and disassembly of ARA pre-formed filaments (PFF) (B, D, & F). Inhibition and disassembly of both TOC1 (open circles) and TNT (closed circles) reactive species as shown by sandwich ELISA at different concentrations of ANTC-15 (A & B). Inhibition and disassembly of the average number of filaments as determined by TEM at different concentrations of ANTC-15 (C & D). Inhibition and disassembly of total filament length as determined by TEM at different concentrations of ANTC-15 (E & F).

The analogous experiments using heparin induced filaments to identify a dose dependent response to LMTX were also completed (figure 16). However, the data from these experiments could not be used to calculate an IC_{50} and DC_{50} for the following reasons. 1) LMTX appears to form many small tau oligomers that are reactive to both TOC1 and TNT1 antibodies, as well as being detectable by TEM. Other groups have shown that this is the case with the closely related compound, methylene blue with a reported IC_{50} value of 1.9 µM [106]. 2) the previously reported IC_{50} values of LMTX inhibition of tau filament formation in a cell free environment have been shown to be much lower than the IC_{50} based on cell free tau-tau binding assays (analogous to the sandwich ELISA assay used in this study) [107]. Therefore, LMTX appears to interact with tau through two different mechanisms; one that breaks down larger filaments into small oligomers within a low micromolar concentration range, and one that blocks tau-tau binding at a high micromolar concentration range. 3) Due to heparin induced filaments being much longer than those induced by ARA, it is difficult to reliably measure subtle changes in total filament length and number of filaments to be able to calculate IC_{50} and DC_{50} values. 4) The differences of how LMTX, and other closely related molecules interact with heparin induced tau filaments and cell-based tau aggregation assays have been extensively studied by other groups and therefore were considered to be outside the scope of this study[106, 107].

Tubulin polymerization:

An important feature of any potential TAI should be that it does not inhibit the normal functions of tau, due to the large potential for side effects through a toxic loss of tau function. We therefore compared the microtubule stabilization properties of tau with and without ANTC-15 and LMTX

(figure 9). The probability that the differences occurred by chance is 78% for ANTC-15 (p=0.78) and 9% for LMTX (p=0.09), which are both higher than the widely accepted 5% threshold for significance (p=0.05). Similarly, neither ANTC-15 nor LMTX caused a significant alteration of the nucleation rate (k_1) in comparison with the tubulin-with-tau control, although the p-values once again suggest ANTC-15 has less effect than LMTX (0.7 and 0.13 respectively). However, the analysis did show a significant difference between the tubulin-with-tau elongation rate (k_2) and the samples with LMTX, but not with ANTC-15 (p-values of 0.021 and 0.24, respectively). Figure 12 contains a summary table of tubulin polymerization assay p-values along with graphs of the maximum polymerization, elongation rate (k_1), elongation rate (k_2), as well as graphed data for tubulin only with and without ANTC-15 and LMTX.

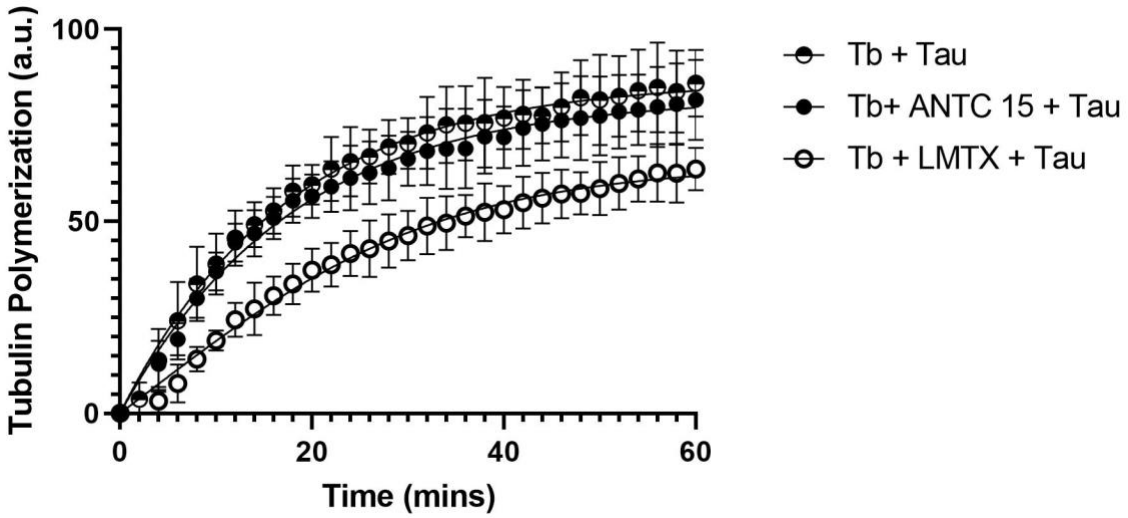

Figure 9: Tubulin polymerization in the presence of ANTC-15 and LMTX.
Tubulin (Tb) at a final concentration of 2 mg/mL was incubated at 37°C with or without inhibitor compound at a concentration of 40 µM in the presence of tau at a concentration of 0.5 µM. Data was then normalized against a taxol (10 µM) positive control and fit to a Finke-Watzky polymerization curve.

2.4 Discussion

There has been a recent realization of the need for treatments for Alzheimer's disease and Alzheimer's disease related dementias that directly reduce the pathological accumulation of aggregated tau. There are efforts to reduce the expression of tau, to reduce post-translational modifications of tau, to increase the clearance of abnormal tau, to repair the functional loss of tau by stabilizing microtubules, to reduce the prion-like spread of tau, and to inhibit or reverse the aggregation of tau[108].

Techniques such as PET imaging, cognitive diagnostic tests, and analysis of post mortem tissue have shown that the underlying pathology of tau aggregation can occur in neurons many years, or even decades prior to symptom onset and disease diagnosis[109]. Therefore, it is important to be able to develop compounds that can not only inhibit filament formation, but also disassemble previously formed filaments. Due to the thermodynamic stability of the amyloid fold formed during tau aggregation, filaments are extremely stable. This stability means using inhibitory molecules to prevent the conversion of inert monomeric tau to aggregate competent monomer, or aggregated tau, is not sufficient to disassemble previously formed filaments. Unfortunately, current compound screening approaches have not yet provided a viable therapeutic that has been successful in phase III clinical trials. The phenothiazine tau aggregation inhibitor compound LMTX showed some promise in early clinical studies, but did not meet pre-trial objectives in comparison with the placebo control of low LMTX dosage[89]. Further trials with low dosages of LMTX are currently underway[67].

Our efforts to identify TAIs from the fungal secondary metabolome of *A. nidulans* has yielded several compounds with TAI activity[94, 95], including the isoquinoline compound ANTC-15

identified in this study. ANTC-15 almost completely inhibited the formation of ARA induced filaments at a concentration of 100 µM compound as shown by oligomer specific antibody ELISA and by electron microscopy. ANTC-15 also disassembled ARA-preformed filaments at high compound concentrations by almost 50% as determined by ELISA and 80-90% as determined by electron microscopy. We interpret this difference as potentially being due to differences in the sensitivity of the assays. For example, the capture antibodies used in the sandwich ELISA are conformationally sensitive antibodies with a high affinity towards aggregated tau protein. The protocol was carefully optimized by titering the antibodies against a standard curve of diluted aggregate and monomeric samples to ensure that the differentiation between monomeric and aggregate tau in our reactions was in a linear range (figure 11). However, it is likely that TOC1 and TNT1 antibodies bind to structures smaller than the approximately 25 nm limit of resolution by TEM.

Using dose dependence studies of ANTC-15 to inhibit ARA induced fibrils, we were able to calculate the IC_{50} of ANTC-15 being between 25 µM and 47 µM, depending on the assay used, ELISA or TEM (figure 8 A, C, and E). The inhibition dose-response curves show high *Hill* coefficients (>1.5) as summarized in table 4. *Hill* coefficient values >1 are typically considered to be an indication of a complex inhibitory mechanism. Many previously identified tau aggregation inhibitors have also been reported to have *Hill* coefficients >1 as shown by the NIH databank entry AID 1460. As discussed by Heino Prinz[110], there could be several reasons for a *Hill* coefficient other than 1, including; ligand cooperativity or ligand micellization, protein and ligand stoichiometry other than 1:1, protein denaturation that leads to an increase in the number of ligand binding sites, or a complex mixture of several of these factors.

Due to the hydrophobic nature of ANTC-15 it is unlikely to be a biologically useful compound in its current form. In addition, potential hydrophobic interactions between ANTC-15 and the ARA inducer molecule cannot be ignored. However, the ability of ANTC-15 to disassemble the extremely stable ARA PFF suggests that its activity is not solely due to interactions with the ARA inducer.

Although ANTC-15 has activity to inhibit tau aggregation and disassemble pre-formed filaments, the micromolar concentration required for this activity are too high for it to be consider a potential therapeutic candidate as most drugs tend to be effective at nanomolar concentrations. However, we were interested to see if ANTC-15 could be used as a molecular probe for further investigation of *in vitro* tau aggregation models. We therefore used the TAI LMTX as an external benchmark that had already been shown to inhibit tau filament formation at relatively low concentrations in both *in vitro* and *in vivo* assays. To our surprise, LMTX had very little effect on the formation of ARA-filaments or in disassembling ARA-preformed filaments both in ELISA assays and as determined by electron microscopy.

Because LMTX was first identified as a TAI using heparin as an inducer of tau aggregation rather than ARA[90], we sought to test both ANTC-15 and LMTX against heparin induced filaments. The results were opposite to those obtained with ARA-induced filaments: LMTX was effective as a TAI against heparin induced filament formation while ANTC-15 had little to no TAI activity against heparin induced aggregation. The most striking example of this is that at 200 μM LMTX, the very long filaments characteristic of heparin-induced aggregation were virtually

non-existent. In the presence of ANTC-15, there was little to no reduction in the number of long heparin-induced filaments (although there was an increase in smaller filaments). ANTC-15 also had no effect on heparin pre-formed filaments, while the addition of LMTX to heparin pre-formed filaments actually increased the number of TOC1 reactive species and had no significant effect on TNT1 reactive species while an increase in the number of smaller filaments was observed by electron microscopy. This increase in smaller filaments could account for the increase in TOC1 reactive species as breaking down filaments can result in increased antibody binding site availability. For example, acoustic shearing can be used to break apart long filaments into small oligomers and therefore increase the number of available binding sites of both TOC1 and TNT1 antibodies (figure 17). Although tau aggregation in disease is still not fully understood, it is widely accepted that small oligomers may play an important role in pathology[111-113]. Therefore, potential therapeutic candidates that inhibit tau filament formation, but promote the formation of smaller oligomers may potentially increase the neurotoxic or neurodegenerative effects of tau aggregation. There is also a growing consensus that the spread of tau aggregation occurs in a prion-like fashion, where inert monomeric tau is converted to a seed-competent tau aggregate that can further oligomerize[12]. For these reasons, it is important to study the effects of TAIs on the formation of large filaments and oligomers using visualization methods such as TEM as well as conformation changes to the protein using immunohistochemical techniques.

Recent developments in cryo-electron microscopy have allowed researchers to solve high resolution structures of tau fibrils isolated from multiple tauopathies[32, 39, 40]. These discoveries have shed new light on, and garnered support for, the hypothesis that tau fibrils from different

diseases are distinct structures with unique properties. In light of this finding, it is important that we identify inducers that form disease relevant filaments *in vitro* to screen potential therapeutic TAI compounds. *In vitro* models will likely have to be disease specific. For example, a potent compound that targets the interface between PHFs in AD is unlikely to be as effective against the different set of residues at the interface of filaments from Pick's disease. In addition, cryo-EM and pulsed electron paramagnetic resonance structural studies have revealed that at least one common *in vitro* aggregation inducer (heparin) does not appear to form structures relevant to disease[59, 114]. These findings may explain why potential therapeutic molecules that inhibit filaments *in vitro* and in specific *in vivo* models, have poor results when used in humans in clinical trials[115]. In this study we have shown how two different small molecules can have quite different effects on assembly and disassembly of filaments induced by ARA versus those induced by heparin.

Molecular dynamics and drug discovery efforts using heparin induced tau filaments may not represent the true nature of authentic tau aggregation *in vivo*. While a compelling argument can be made for arachidonic acid as a biologically relevant aggregation inducer of tau due to: 1) its relative abundance in the cell, especially during times of oxidative stress, 2) *in vitro* filaments appearing to have similar gross morphological traits as the straight filaments isolated from AD in regards to average length, width, and periodicity[99] and 3) antibodies that have been raised against ARA induced filaments having a high affinity to epitopes in diseased AD brain tissue, as well as tissue isolated from CTE brains[14, 103], to date there are no high-resolution structures of arachidonic acid induced filaments and therefore, the atomic similarities to filaments from diseases are unknown.

Our data are consistent with the possibility that ARA and heparin induce the formation of tau aggregates that are structurally distinct and that ANTC-15 and LMTX have differing activities against the two structures. Because of the differences in properties of the inducers and because of differences in the chemical structures of the compounds, we cannot rule out the possibility that our results could be explained by a more complex mechanism beyond any potential structural differences in ARA and heparin filaments. For example, ANTC-15 is highly hydrophobic and could have a preferential interaction with ARA or ARA/tau complexes. Similarly, LMTX could have a preferential interaction with the polyanionic heparin inducer. These and potentially other complexities could help to explain the very steep dose-response curves of inhibition observed. Further experimentation will be required to fully elucidate the mechanisms of inhibition and disassembly. However, unless future structural studies can demonstrate that these *in vitro* filaments have structures related to those found in disease, the mechanisms of inhibition may not have direct biological relevance to AD and ADRDs.

Our data suggests that it is important to begin developing new screening techniques that utilize a range of different types of tau aggregation inducer molecules, seeding assays, and spontaneous aggregation models, rather than relying on one particular inducer molecule. Long term goals must aim to identify whether artificially induced aggregates *in vitro* generate structures relevant to disease and also identify to which disease they are specific, to enhance the potential for success in future clinical trials. Until we can verify that artificially induced *in vitro* tau aggregates have sufficient structural similarities to those found in disease, the evaluation of potential TAIs such as ANTC-15 must be interpreted with an abundance of caution.

2.5 Supplementary Information:

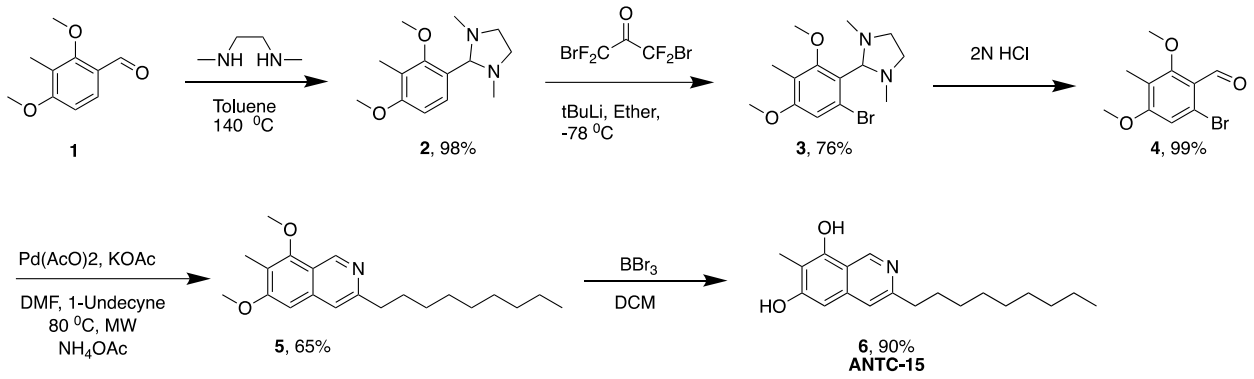

Figure 10: Synthesis scheme for ANTC-15 completed by Shibin Chacko and Chamani Perera.

Synthesis of ANTC-15

7-methyl-3-nonylisoquinoline-6,8-diol (ANTC-15, 6): Synthesis of ANTC-15 (**6**) was carried out according to the scheme illustrated in **Figure 10**. First 2,4-dimethoxy-3-methylbenzaldehyde (**1**) was protected using N, N dimethyl ethylenediamine to give compound **2** in 98% yield. Compound **2** was then brominated in the presence of tBuLi to give the bromo compound **3**. Deprotection of **3** in the presence of 2N HCl resulted in aldehyde **4**. Subsequent Palladium mediated alkylation of **4** with 1-Undecyne followed by cyclization in the presence of ammonium acetate gave compound **5**. Final removal of the methoxy groups in the presence of BBr_3 resulted in the desired compound ANTC-15 (**6**) in 90% yield as a yellow solid. **^{1}H NMR (500 MHz, DMSO-d_6):** δ 9.34 (s, 1H), 7.83 (s, 1H), 6.93 (s, 1H), 2.90 (t, *J* = 7.7 Hz, 2H), 2.21 (s, 3H), 1.75-1.69 (m, 2H), 1.38 – 1.14 (m, 12H), 0.85 (t, *J* = 6.9 Hz, 3H).**^{13}C NMR (126 MHz, DMSO):** δ 166.3, 155.4, 145.2, 140.9, 139.5, 119.7, 114.4, 114.2, 100.4, 32.5, 31.7, 29.3, 29.1 (2C), 29.0, 28.8, 22.5, 14.4, 9.7. **HRMS for** $C_{19}H_{28}NO_2$ $(M + H)^+$ Calculated 302.2120; Found 302.1327.

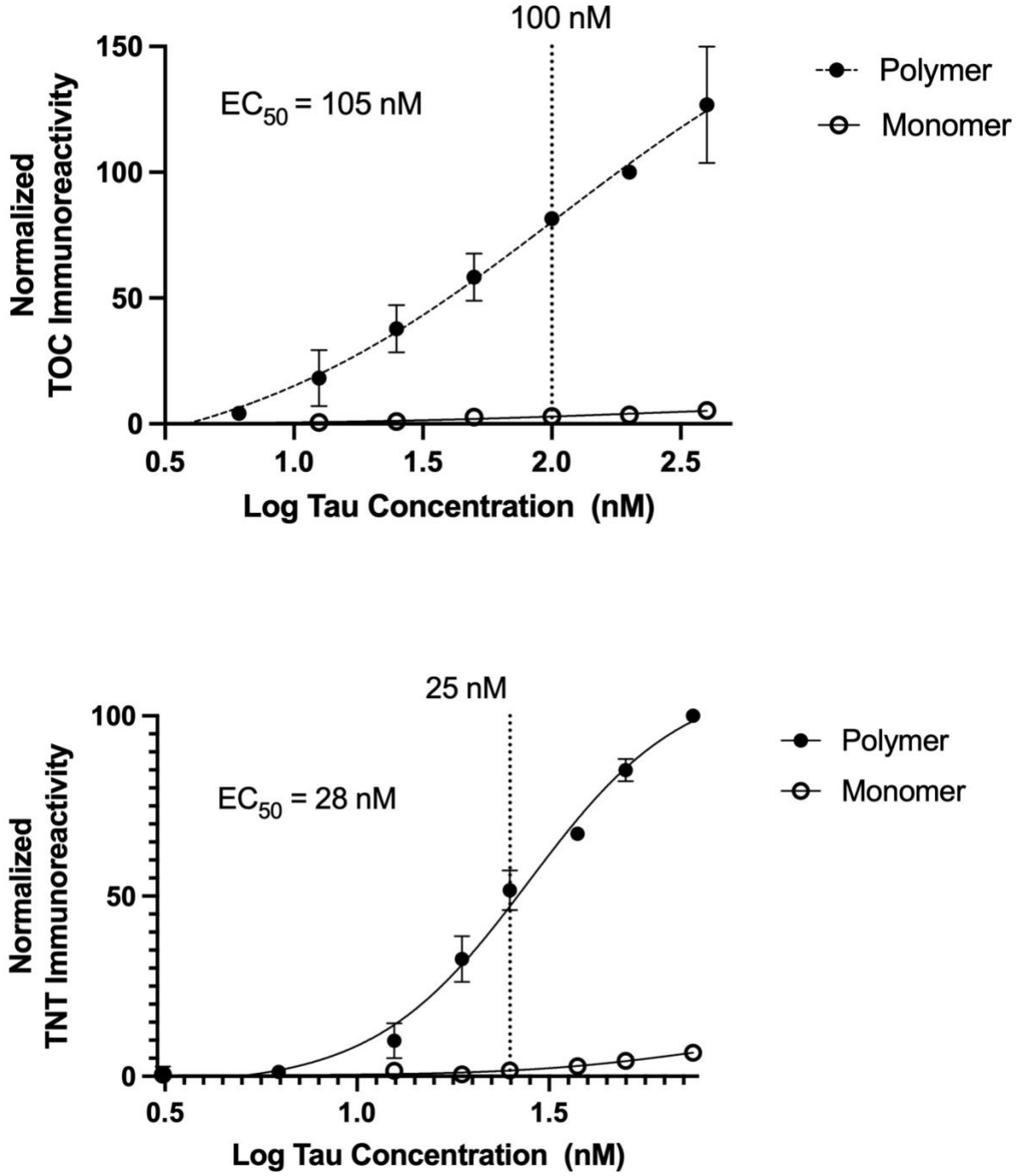

Figure 11: Affinity curves for TOC1 and TNT1.
Affinity curve of TOC1 (top) and TNT1 (bottom) monoclonal antibodies against a series dilution of aggregated and monomeric tau using ELISA. Y-axis signal has been converted to % light absorbed and normalized against an internal positive control. EC_{50} represents the concentration of aggregated tau at which a 50% signal is present based on the best fit of the following agonist vs response equation.

A

p-value when compared to no compound tubulin + tau control			
Compound	Maximum Polymerization	Nucleation Rate (k1)	Elongation Rate (k2)
ANTC-15	0.78	0.7	0.24
LMTX	0.086	0.13	0.021**

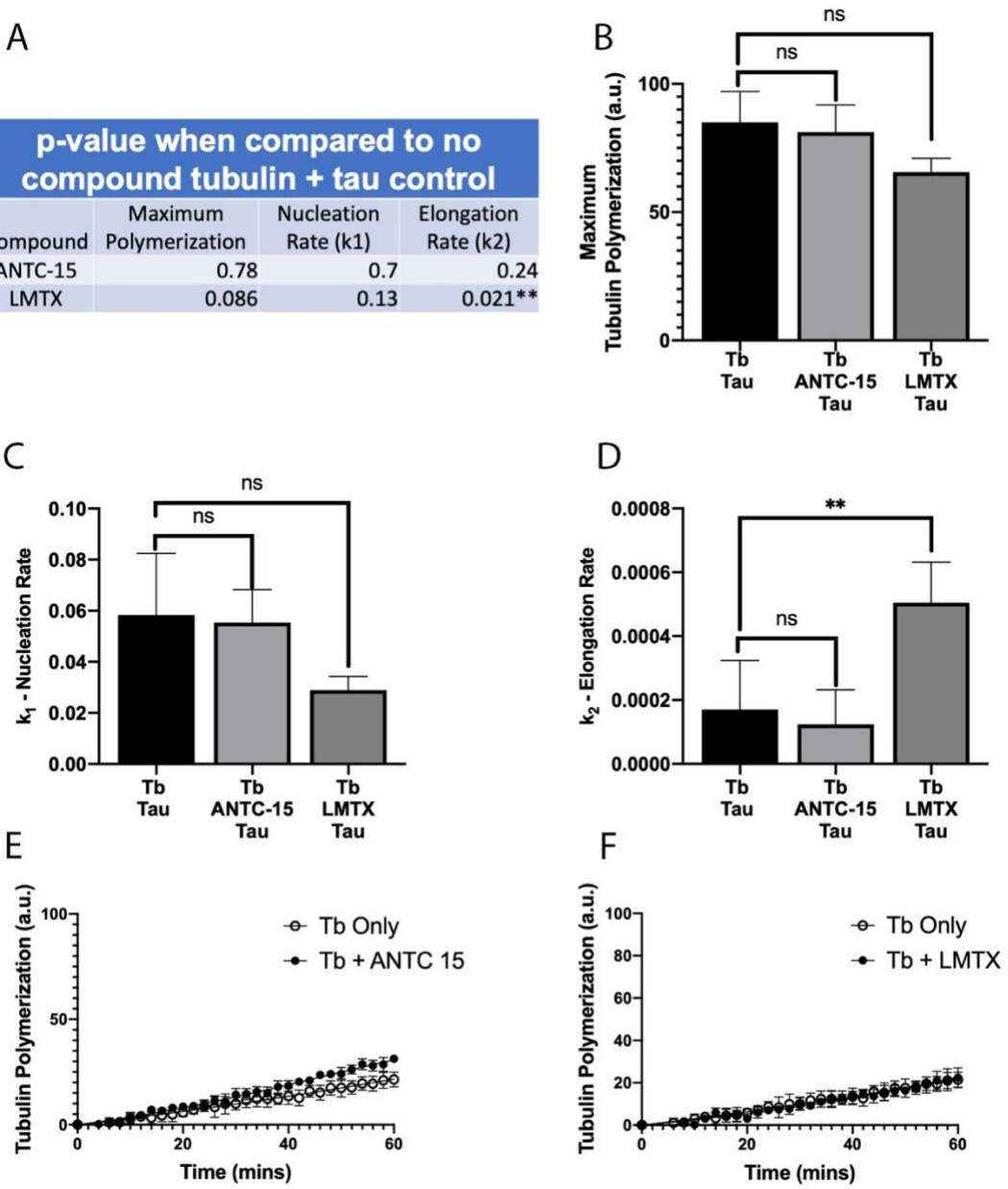

Figure 12: Tubulin polymerization assay supplementary information.
Tubulin Polymerization Assay: Summary table of p-value results following t-test analysis comparing tubulin with tau and with either ANTC-15, or LMTX, to tubulin with tau no compound (1% DMSO) control (A). Graphed data summarized in table 1; maximum tubulin polymerization (B), nucleation rate (k_1) (C), and elongation rate (k_2) (D). Tubulin only (open circles) and tubulin with 40µM ANTC-15 (E, closed circles) or 40µM LMTX (F, closed circles) polymerization data fitted to F-W polymerization curve. Samples were compared to no compound control using a t-test.
$* \ p \leq 0.05; \ ** \ p \leq 0.01; \ *** \ p \leq 0.001$, ns denotes no significant difference.

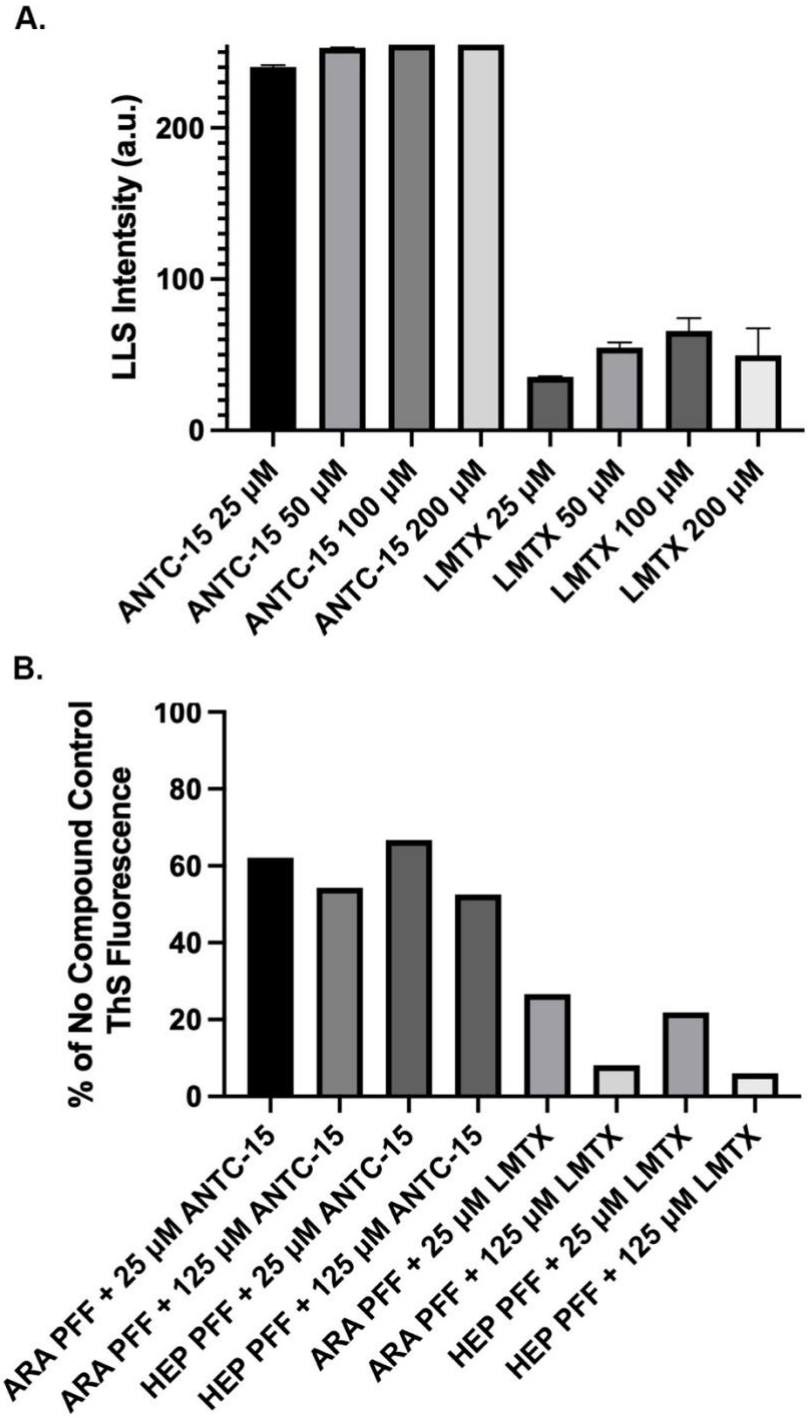

Figure 13: Compound interference with LLS and ThS assays.

Compound interference with LLS and ThS assays: Right-angled laser light scattering intensity (a.u.) with a maximum y-axis saturation of 255, showing light scattering of compounds in aqueous polymerization buffer conditions. Samples were zeroed against a 1% DMSO control, A. Thioflavin S fluorescence showing the effect of compound on a standard ThS fluorescence assay. Values were normalized as a percentage of no compound (1% DMSO) control. All compounds, or DMSO, were added to polymerized filaments immediately prior to completing the ThS assay, B.

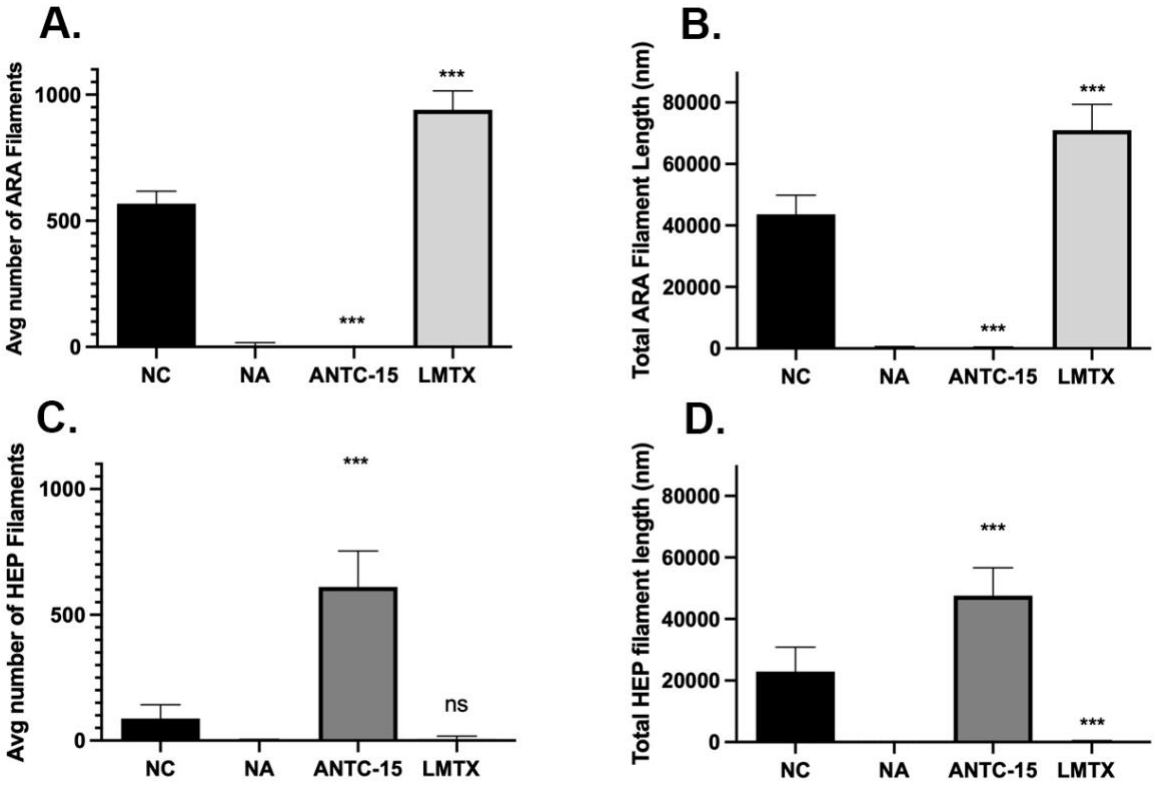

Figure 14: Quantification of TEM micrographs of initial inhibition assay using ANTC-15 and LMTX. Quantification of TEM micrographs of initial inhibition assay of 200 µM ANTC-15 and LMTX against arachidonic acid (ARA) and heparin (Hep) induced tau filaments with no compound (NC) and no arachidonic acid or no heparin (NA and NH respectively). Number of filaments induced by ARA (A), total filament length induced by ARA (B), number of filaments induced by heparin (C), total filament length induced by heparin (D). Samples were compared to no compound control using an unpaired t-test, $* \; p \leq 0.05$; $** \; p \leq 0.01$; $*** \; p \leq 0.001$.

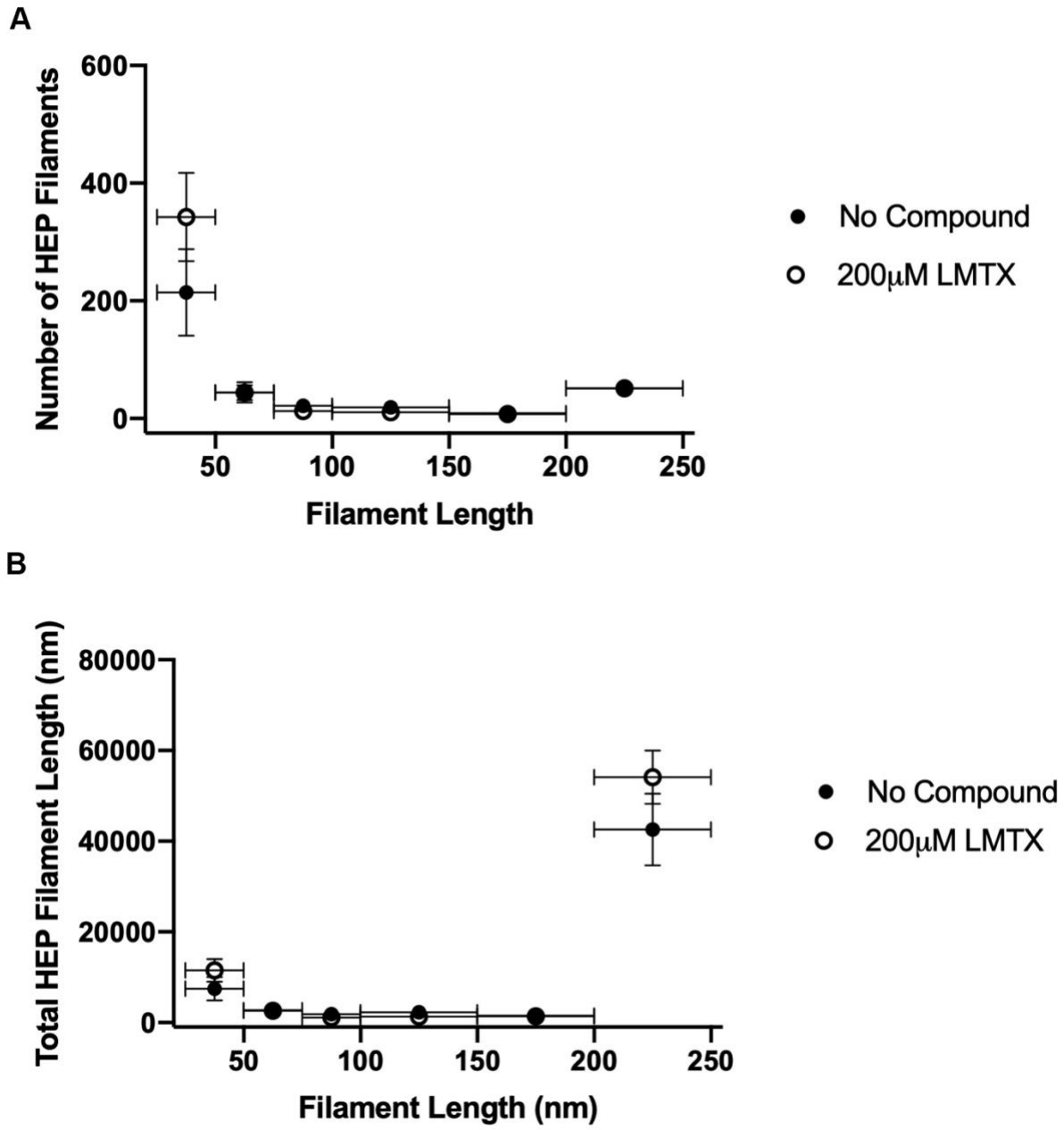

Figure 15: Length distribution of pre-formed heparin filaments treated with LMTX.
Length distribution (determined by TEM) of pre-formed filaments induced by heparin treated with 200μM LMTX as compared to a no-compound control. Horizontal bars represent bin sizes, vertical error bars represent standard deviation. A. Average number of filaments per image. B. total filament length.

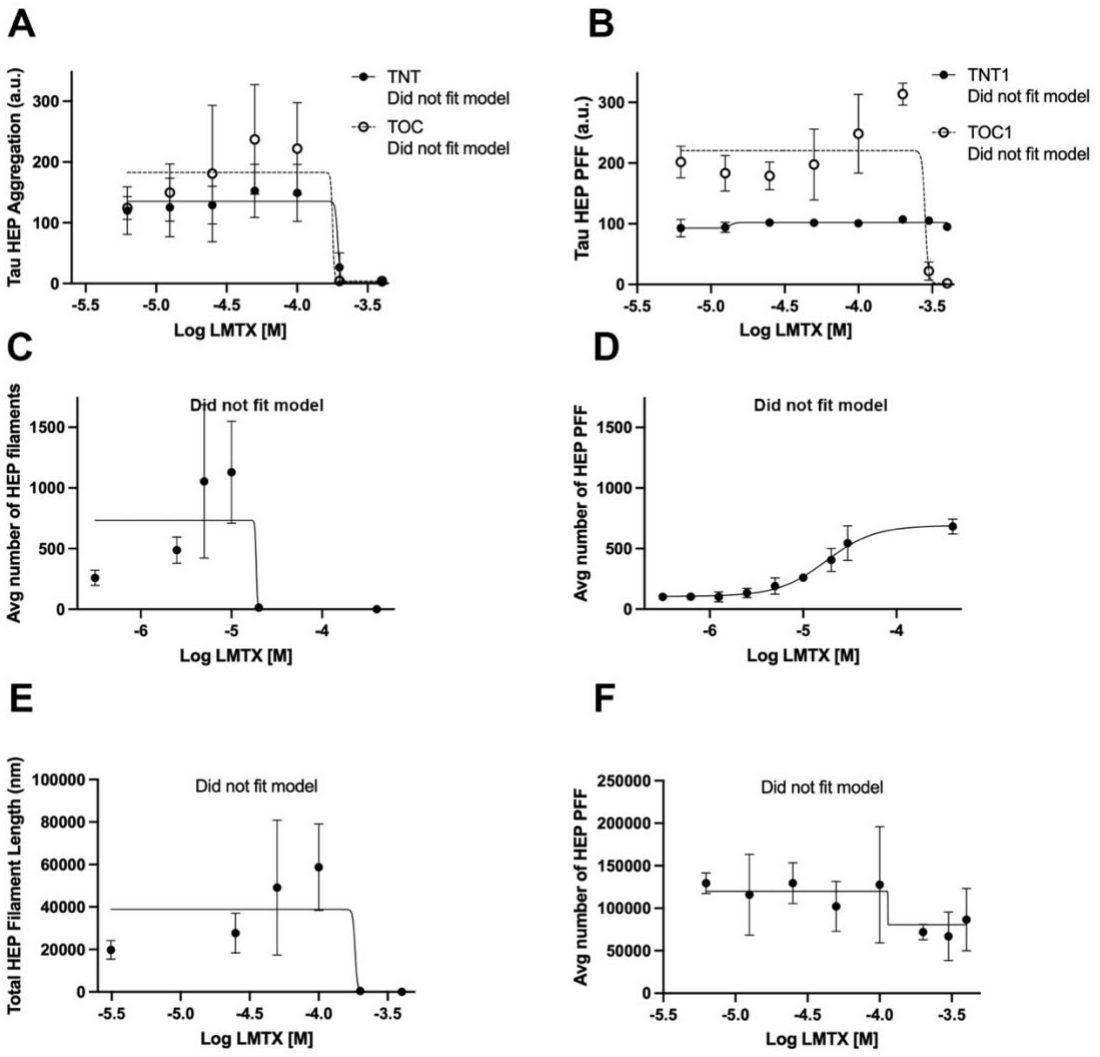

Figure 16: LMTX dose dependence studies.
LMTX dose dependence: inhibition of HEP-filaments (A, C, & E) and disassembly of HEP pre-formed filaments (PFF) (B, D, & F). Inhibition and disassembly of both TOC1 (open circles) and TNT (closed circles) reactive species as shown by sandwich ELISA at different concentrations of LMTX (A & B). Inhibition and disassembly of the average number of filaments as determined by TEM at different concentrations of LMTX (C & D). Inhibition and disassembly of total filament length as determined by TEM at different concentrations of LMTX (E & F). "Did not fit model" refers to use of a log inhibitor vs response – four parameter equation (equation 1 in methods), the data collected in these experiments did not fit this equation.

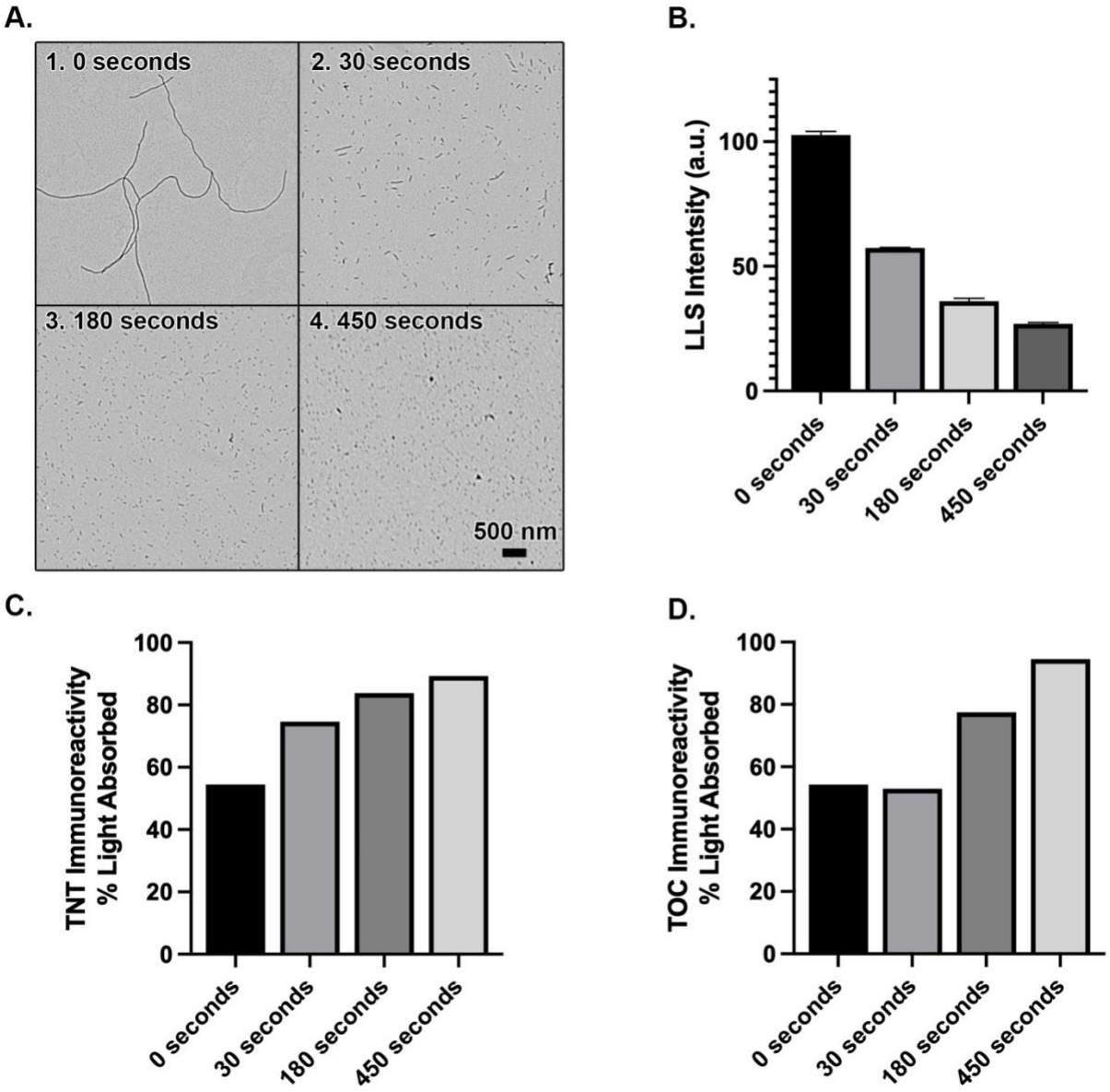

Figure 17: Acoustic shearing of heparin induced filaments.
Shearing of HEP induced tau filaments. Representative TEM micrograph showing filaments after acoustic shearing for 0 seconds A1., 30 seconds A2., 180 seconds A3., and 450 seconds A4. Scale bar in figure A4 represents 500 nm for all images. Changes in right-angled laser light scattering of each sample using a IIIb laser light source with a wavelength of 532 nm, B. Immuno-reactivity by ELISA of each sample using capture antibody TNT1 9C and TOC1 9D.

Table 2			
ARA Inhibition - TOC		ARA Inhibition - TNT	
Comparison	Summary/p-value	Comparison	Summary/p-value
NC vs NA	***/<0.001	NC vs NA	***/<0.001
NC vs ANTC-15	***/<0.001	NC vs ANTC-15	***/<0.001
NC vs LMTX	***/<0.001	NC vs LMTX	ns/0.5
NA vs ANTC-15	**/0.005	NA vs ANTC-15	ns/0.18
NA vs LMTX	***/<0.001	NA vs LMTX	***/<0.001
ANTC-15 vs LMTX	***/<0.001	ANTC-15 vs LMTX	***/<0.001
ARA Inhibition - Total Filament Length		ARA Inhibition - Average Number of Filaments	
Comparison	Summary/p-value	Comparison	Summary/p-value
NC vs NA	***/<0.001	NC vs NA	***/<0.001
NC vs ANTC-15	***/<0.001	NC vs ANTC-15	***/<0.001
NC vs LMTX	***/<0.001	NC vs LMTX	***/<0.001
NA vs ANTC-15	ns/>0.999	NA vs ANTC-15	ns/>0.999
NA vs LMTX	***/<0.001	NA vs LMTX	***/<0.001
ANTC-15 vs LMTX	***/<0.001	ANTC-15 vs LMTX	***/<0.001
ARA Disassembly - TOC		ARA Disassembly - TNT	
Comparison	Summary/p-value	Comparison	Summary/p-value
NC vs NA	***/<0.001	NC vs NA	***/<0.001
NC vs ANTC-15	**/0.001	NC vs ANTC-15	***/<0.001
NC vs LMTX	*/0.01	NC vs LMTX	ns/0.19
NA vs ANTC-15	**/0.003	NA vs ANTC-15	***<0.001
NA vs LMTX	***/<0.001	NA vs LMTX	***/<0.001
ANTC-15 vs LMTX	***/0.001	ANTC-15 vs LMTX	**/0.003
ARA Disassembly - Total Filament Length		ARA Disassembly - Average Number of Filaments	
Comparison	Summary/p-value	Comparison	Summary/p-value
NC vs NA	***/<0.001	NC vs NA	***/<0.001
NC vs ANTC-15	***/<0.001	NC vs ANTC-15	***/<0.001
NC vs LMTX	***/<0.001	NC vs LMTX	ns/0.9737
NA vs ANTC-15	***/<0.001	NA vs ANTC-15	***/<0.001
NA vs LMTX	***/<0.001	NA vs LMTX	***/<0.001
ANTC-15 vs LMTX	***/<0.001	ANTC-15 vs LMTX	***<0.001

Table 2: ARA Tukey's multiple comparison p-value summary.

Summary of Tukey's multiple comparison test p-values from ARA induced inhibition and disassembly screening experiments. Using 200 μM LMTX or ANTC-15 compound concentration compared to NC (no compound, 1% DMSO) positive control and NA (no ARA, 1% DMSO) negative control. TOC and TNT results are based on sELISA experiments, and total filament length and average number of filaments was determined by quantitative transmission electron microscopy. $* \; p \leq 0.05$; $** \; p \leq 0.01$; $*** \; p \leq 0.001$.

Table 3

HEP Inhibition - TOC		HEP Inhibition - TNT	
Comparison	Summary/p-value	Comparison	Summary/p-value
NC vs NH	***/<0.001	NC vs NH	***/<.001
NC vs ANTC-15	ns/0.57	NC vs ANTC-15	ns/>.99
NC vs LMTX	**/0.003	NC vs LMTX	**/0.001
NH vs ANTC-15	***/<0.001	NH vs ANTC-15	***/<0.001
NH vs LMTX	ns/0.71	NH vs LMTX	ns/0.2
ANTC-15 vs LMTX	***/<0.001	ANTC-15 vs LMTX	**/0.002
HEP Inhibition - Total Filament Length		HEP Inhibition - Average Number of Filaments	
Comparison	Summary/p-value	Comparison	Summary/p-value
NC vs NH	***/<0.001	NC vs NH	ns/0.3067
NC vs ANTC-15	***/<0.001	NC vs ANTC-15	***/<0.001
NC vs LMTX	***/<0.001	NC vs LMTX	ns/0.3647
NH vs ANTC-15	***/<0.001	NH vs ANTC-15	***/<0.001
NH vs LMTX	ns/0.999	NH vs LMTX	ns/0.9993
ANTC-15 vs LMTX	***/<0.001	ANTC-15 vs LMTX	***/<0.001
HEP Disassembly - TOC		HEP Disassembly - TNT	
Comparison	Summary/p-value	Comparison	Summary/p-value
NC vs NH	***/<0.001	NC vs NH	***/<0.001
NC vs ANTC-15	ns/0.66	NC vs ANTC-15	ns/0.2
NC vs LMTX	***/<0.001	NC vs LMTX	ns/0.71
NH vs ANTC-15	***/<0.001	NH vs ANTC-15	***/<0.001
NH vs LMTX	***/<0.001	NH vs LMTX	***/<0.001
ANTC-15 vs LMTX	***/<0.001	ANTC-15 vs LMTX	*/0.04
HEP Disassembly - Total Filament Length		HEP Disassembly - Average Number of Filaments	
Comparison	Summary/p-value	Comparison	Summary/p-value
NC vs NH	***/<0.001	NC vs NH	***/<0.001
NC vs ANTC-15	ns/0.9954	NC vs ANTC-15	*/0.0198
NC vs LMTX	ns/0.3640	NC vs LMTX	ns/0.1124
NH vs ANTC-15	***/<0.001	NH vs ANTC-15	**/0.0047
NH vs LMTX	***/<0.001	NH vs LMTX	***/<0.001
ANTC-15 vs LMTX	ns/0.4883	ANTC-15 vs LMTX	***/<0.001

Table 3: Heparin Tukey's multiple comparison p-value summary.
Summary of Tukey's multiple comparison test p-values from HEP induced inhibition and disassembly screening experiments. Using 200 µM LMTX or ANTC-15 compound concentration compared to NC (no compound, 1% DMSO) positive control and NH (no heparin, 1% DMSO) negative control. TOC and TNT results are based on sELISA experiments, and total filament length and average number of filaments was determined by quantitative transmission electron microscopy. $* \; p \leq 0.05$; $** \; p \leq 0.01$; $*** \; p \leq 0.001$.

Dose dependence inhibition experiment	Hill Slope ± Standard deviation
ANTC-15 Inhibition of ARA TOC1 reactive species (ELISA)	-4.52 ± 0.99
ANTC-15 Inhibition of ARA TNT1 reactive species (ELISA)	-3.38 ± 0.61
ANTC-15 Inhibition average number of ARA filaments (TEM)	-3.44 ± 1.2
ANTC-15 Inhibition of total ARA filament length (TEM)	-1.92 ± 1.14

Table 4: Summary of ANTC-15 ARA inhibition Hill slopes.
Summary of hill slope values calculated by fitting dose dependence data to a four parameter logistic inhibitor vs response non-linear regression equation. Hill slope values are reported as negative due to the plot being of an antagonistic response.

$$Y = Bottom + (X^{Hillslope}) * \frac{Top - Bottom}{X^{Hillslope} + EC50^{Hillslope}}$$

Chapter 3: *In vitro* tau aggregation inducer molecules dictate our understanding of the effects of *MAPT* mutations on aggregation dynamics.

3.1 Introduction

Neurodegenerative disorders are often characterized by the aggregation of one or more proteins[116]. In Alzheimer's disease (AD) and Alzheimer's disease related dementias (ADRDs), the microtubule associated protein tau accumulates within neurons and glia of the central nervous system. These terminal maladies are not only devastating to the 6.2 million Americans who suffer from them, but also cause patients to require round the clock care during advanced stages of disease. This effect is felt more broadly by society as AD and ADRDs are estimated to have associated health care costs of $355 billion in the United States for 2021 and an estimated 11 million unpaid caregivers[84]. To make matters worse, the number of cases and associated costs of AD and ADRDs are expected to rise dramatically over the next few decades.

The aberrant accumulation of tau into beta sheet enriched amyloid folds correlates strongly with the progression and severity of cognitive decline in AD patients[85]. In AD, tau primarily accumulates into twisted filamentous structures called paired helical filaments (PHFs) and straight filamentous structures called straight filaments (SFs). Other tauopathies can include PHFs or SFs, but many are characterized by tau filaments dissimilar to those found in AD. ADRDs include Pick's disease, progressive supranuclear palsy, corticobasal degeneration, chronic traumatic encephalopy, as well as other frontotemporal dementias with Parkinsonism linked to chromosome 17 (FTDP-17, or familial frontotemporal dementias - fFTD). FTDP-17 tauopathies are of particular interest to the research field because as well as having tau

accumulation as a histopathological hallmark, they have been associated with over 50 different intronic and exonic mutations of the *MAPT* gene that encodes the expression of all six isoforms of tau in the human adult central nervous system[42].

The nomenclature of the 6 tau isoforms expressed in adults is based on the inclusion of 0, 1, or 2 N terminal domains, as well as the inclusion of 3 or 4 microtubule binding repeat domains (MTBR). This results is the 6 tau isoforms of the central nervous system being named 2N4R, 1N4R, 0N4R, 2N3R, 1N3R, or 0N3R[2]. Each of the microtubule binding repeats ends with a PGGG motif. Interestingly, a P to S substitution mutation on three of the four PGGG motifs has been associated with cases of FTDP-17 at positions 301[117], 332[118], 364[119] (numbering based on full length 2N4R human tau isoform). In addition, P301S is one of the most common mutations used in both *in vitro* and *in vivo* tau aggregation model systems, primarily due to the formation of PHF-like filaments, pro-aggregation properties, and relatively poor affinity towards microtubules[120]. The PGGG motif found at the end of microtubule binding repeat 1, position 270, has not been associated with disease linked mutations. Although recent structural studies of tau filaments isolated from disease have shown that this region of tau, MTBR 1, does form part of the ordered filament core isolated from the three repeat tauopathy [Pick's disease (PiD)[121]], it is not found as part of the ordered fibril core of mixed 3R-4R tauopathies [AD[50] and chronic traumatic encephalopathy (CTE)[32]], as well as the 4R tauopathy, [corticobasal degeneration (CBD)[40]].

In this study, we sought to compare the aggregation characteristics of three of these FTDP-17 P to S mutations, as well as the non-disease related P270S mutation, to WT 2N4R tau. We used

site directed mutagenesis to recombinantly express and purify each of the P to S mutations at positions 270, 301, 332, and 364 in the full-length isoform of human tau, 2N4R (HT40) (see figure 18).

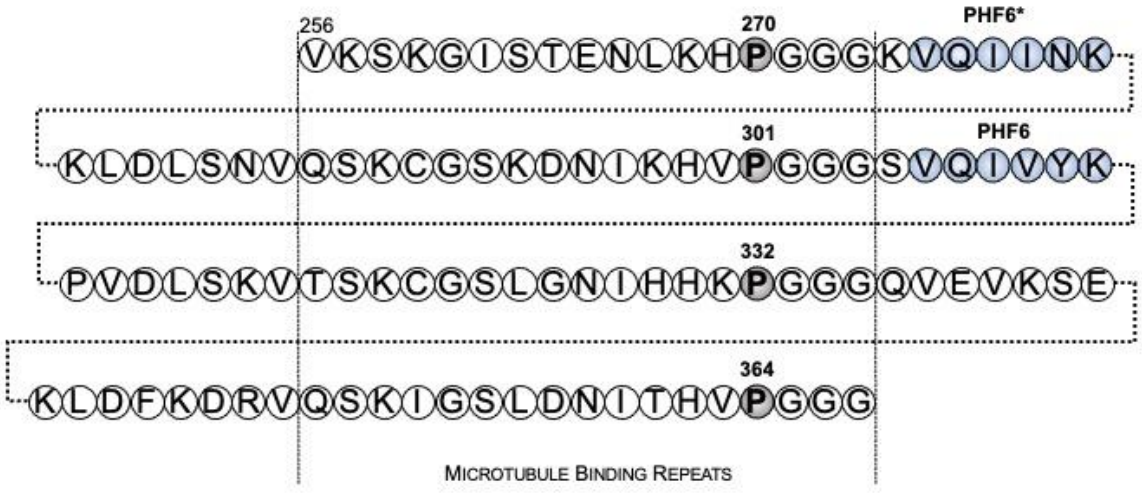

Figure 18: Schematic location of the PGGG motifs at the end of each microtubule binding repeat.
Motifs are found at position at the end of each microtubule binding repeat region P270 (MTBR 1), P301 (MTBR 2), P332 (MTBR 3), and P364 (MTBR 4). P270 is proceeded by the hexapeptide PHF6* motif, and P301S is proceeded by the hexapeptide PHF6, both are thought to be important in the formation of tau filaments. Site directed mutagenesis, expression, and purification of each of the mutants was completed by Kelsey Hillyer and myself. Figure was created by Dr. T. Chris Gamblin.

However, because tau is natively unfolded, contains high numbers of both positively and negatively charged residues, and is highly soluble in solution, it is resistant to spontaneous aggregation[2]. Therefore, biochemical "inducers" of tau aggregation are widely employed to initiate and enhance the aggregation of tau *in vitro*. One of the most commonly used tau aggregation inducers, heparin[59], induces polymorphic tau aggregate structures that are dissimilar to any structures found in filaments isolated from disease[59, 114]. Heparin is therefore not likely to be a useful model in studies characterizing and identifying tau aggregation-based therapeutics or the molecular dynamics of aggregation. Therefore, we chose three alternative inducers of tau

aggregation for this study: the polyunsaturated fatty acid arachidonic acid (ARA), polyphosphate, and RNA, although to date there have not been any high-resolution structures published of *in vitro* tau filaments generated with these inducers.

We have previously found that ARA rapidly polymerizes tau to form filaments that have similar morphological characteristics to straight filaments isolated from AD[99]. In addition, ARA is found within the intracellular environment at elevated levels during times of oxidative stress and could play numerous roles in the pathology of AD[122] . Furthermore, antibodies raised against ARA induced filaments have been shown to have a high affinity towards aggregated tau in diseased brain tissue[14, 103]. We have also shown that two different small molecule tau aggregation inhibitors (TAIs), the isoquinoline ANTC-15 and the phenothiazine LMTX, appear to inhibit heparin and ARA induced filaments in an inducer-specific manner[123]. ANTC-15 inhibits ARA induced filaments, but not heparin induced filaments. Conversely, LMTX inhibits heparin induced filaments, but not those induced by ARA. It is therefore likely that the polymorphs formed from ARA and heparin induction are structurally distinct. Polyphosphate is present in mammalian neurons and has been shown to induce the aggregation of tau *in vitro*[124-126]. RNA has been shown to induce the aggregation of tau *in vitro* [127, 128] and tau aggregates in disease can sequester RNA[129]. Although the structures formed by ARA, polyP, and RNA are not known and it is unclear whether they play a direct role in tau aggregation in disease progression, they have the potential to form biologically relevant, and potentially disease relevant, aggregates of tau.

Using right-angle laser light scattering, transmission electron microscopy, and a conformationally sensitive ELISA we were able to compare the maximum protein aggregation, filament length, morphology, and immuno-reactivity of toxic tau species.

To our knowledge, not only is this the first study to complete a direct biochemical comparison of this group of disease related mutations, it is also the first to directly compare multiple *in vitro* aggregation inducers to study biochemical characteristics of multiple disease related mutations. Using this combination of approaches we have found that different classes of tau aggregation inducer molecules can not only influence typical aggregation characteristics such as length of filaments and total amount and rate of aggregation, but also, the type of inducer used can have effects on the fundamental differences between wild type tau and mutant constructs as well as immunoreactivity towards conformationally sensitive antibodies. The data strongly supports the hypothesis that filaments formed in the presence of different inducer molecules have different characteristics in terms of aggregation morphology, aggregation dynamics, assay compatibility, and immuno-reactivity. These findings illustrate the importance of identifying disease relevant inducer molecules to be used in studies of characterizing disease related mutations.

3.2 Materials and Methods

Chemicals and reagents: Full length 2N4R tau (HT40, 441 amino acids) and all mutant constructs were expressed and purified as previously described[98]. Using the HT40 Pt7c WT construct, amino acid substitutions were introduced using a QuickChange II XL site directed mutagenesis kit (200521) purchased from Agilent (Santa Clara, CA). Mutagenesis and protein expression and purification were completed by Kelsey M. Hillyer with the assistance of myself. After transformation into *BL21-Gold (DE3)* competent cells, protein was expressed and purified

using Ni-His Tag affinity purification and size exclusion chromatography. King et. al. has shown that the poly-histidine tag does not appear to influence tau aggregation and therefore was not removed prior to concentration quantification and subsequent *in vitro* studies. The concentration of protein was quantified using a Pierce BCA protein assay kit (23225) purchased from Thermo Fisher Scientific (Rockford, IL), each protein prep was at a concentration between 1 and 2 mg/mL. Tau purity and concentration was confirmed by SDS PAGE. Individual aliquots of 50-100 µL were prepared and stored at -80°C and a fresh aliquot was used for each experiment to avoid repeated freeze/thaw cycles. Arachidonic acid (90010) was purchased from Cayman Chemical, (Ann Arbor, MI). Polyphosphate medium chain – [P100 (EUI005) - a heterogenous mixture with most chains being between 45-160 phosphate units and a purity of <1% monophosphate] and long chain - [P700 (EUI002) – a heterogenous mixture with most chains between 200 and 1300 phosphate units and a purity of <1% monophosphate] was purchased from Kerafast (Boston, MA). TOC1, TNT1, and Tau 5, Tau 7, and Tau 12 antibodies were a kind gift from Dr. Nicholas Kanaan, Michigan State University. Each of these antibodies was at a concentration of approximately 1 mg/mL. T22 antibody (ABN454) was purchased from Millipore Sigma, (Burlington, MA). The primary detection antibody (Tau 5, 7, and 12 were used as primary detection against T22 capture antibody) was an anti-tau polyclonal rabbit antibody (A002401-2) purchased from Agilent (Santa Clara, CA). A goat anti-rabbit IgG (H+L) and goat anti-mouse IgG (H+L) antibody with HRP conjugate (1706515 and 1706516, respectively, Bio-Rad, Hercules, CA) was used as a secondary detection antibody. Qiagen miRNeasy mini kit (217004) and Qiagen RNeasy minielute clean up kit (74204) was purchased from Qiagen (Germantown, MD). HEK293T cells (ATCC CRL-3216) were kindly provided by Dr. David Davido, University of Kansas. Mini Trans-Blot pre-cut filter paper (1703932) and 0.22 µm

nitrocellulose membrane (16020112) was purchased from Bio-Rad (Hercules, CA). Chemiluminescent kit was a Supersignal West pico plus chemiluminescent substrate (34577) purchased from Thermo Scientific (Rockford, IL).

RNA Isolation: Mammalian RNA was isolated from HEK293t cells using 2 different procedures. HEK 293T (ATCC CRL-3216) cells were maintained in Dulbecco's Modified Eagle's Medium (Cytiva) and supplemented with 5% fetal bovine serum (FBS), 2mM L-glutamine, 10 U/mL penicillin, 10 U/mL Streptomycin. Cells were grown in BioLite 175 cm^2 vented flask (Thermo Scientific) and maintained in a humidified incubator containing 5% CO_2 at 37 °C.

To isolate the small RNA (RNA <200 nts) and long RNA (RNA >200 nts) separately, a modified version of the Qiagen miRNeasy mini kit and minielute cleanup kit isolation procedure was used to isolate samples into small RNA or long RNA fractions. The cells were lysed using QIAzol Lysis Reagent by adding 8.75 mL to the cell-culture dish. The lysate was collected and vortexed to mix, then stored in 700 µL aliquots at -80 °C. After thawing, the homogenate was incubated at room temperature (~20 °C) for 5 minutes. Under a fume hood, 140 µL of chloroform was added to the tube containing the homogenate and vortexed vigorously for 15 s. The tube was incubated at room temperature for 2-3 minutes and then centrifuged for 15 minutes at 12,000 × g at 4 °C. The upper aqueous phase was transferred to a new collection tube and 1 volume of 70% ethanol was added and mixed thoroughly by vortexing. The sample was pipetted into a RNeasy Mini spin column placed in a 2 mL collection tube and centrifuged at 10,000 × g for 15 s at room temperature (15–25 °C). The flow-through was pipetted into a 2 mL reaction tube. The used spin

column was set aside to isolate long RNA. 450 µL of 100% ethanol was added to the flow-through and mixed thoroughly by vortexing. 700 µL of the sample was pipetted into a RNeasy MinElute spin column placed in a 2 ml collection tube, then centrifuged for 15 s at 10,000 × g at room temperature. The flow-through was then discarded and this was repeated until the whole sample had been pipetted into the spin column. 500 µL Buffer RPE was then pipetted into the RNeasy MinElute spin column and centrifuged for 15 s at 10,000 × g, the flow-through being discarded. Next, 500 µL of 80% ethanol was added to the RNeasy MinElute spin column and centrifuged for 2 min at 10,000 × g to dry the spin column membrane. The flow-through and collection tube were discarded. The spin column was placed into a new 2 mL collection tube and centrifuged for 5 min at 10,000 × g. The RNeasy MinElute spin column was then placed into a 1.5 mL collection tube and 14 µL RNase-free water was pipetted onto the spin column membrane. It was then centrifuged for 1 min at 10,000 × g to elute the small RNA-enriched fraction.

Using the previously reserved RNeasy Mini spin column, the long RNA was eluted. 700 µL of Buffer RWT was added into the RNeasy Mini spin column and centrifuged for 15 s at 10,000 × g to wash the spin column membrane. The flow-through was discarded and 500 µL of Buffer RPE was added to the RNeasy Mini spin column. It was centrifuged for 15 s at 10,000 × g and the flow-through was discarded. Another 500 µL of Buffer RPE was added into the RNeasy Mini spin column and centrifuged for 15 s at 10,000 × g. The flow-through and collection tube were discarded. The RNeasy Mini spin column was placed in a new 2 mL collection tube and centrifuged at16,000 × g for 1 min. The RNeasy Mini spin column was then placed into a new 1.5 mL collection tube and 30 µL of RNase-free water was pipetted directly onto the spin column

membrane. It was centrifuged for 1 min at 10,000 × g to elute the total RNA. This process was repeated for all samples of HEK293t cells. After this protocol was completed, a high sensitivity RNA TapeStation was used to run 2 μL samples of both fractions of RNA to confirm the size fractioning, the results of which showed significant size fractioning was achieved (figure 30). In order to determine the concentration of the differing RNA samples, readings were taken using a nanodrop and diluted to a concentration of 270 ng/μL using RNase-free water. The samples were stored at -80 °C until used in reactions.

Aggregation Reactions: Reactions were set up using each of the P to S tau mutations, P270S, P301S, P332S, P364S, as well as wild type (WT) tau. A no tau inducer only negative control and no inducer tau only negative control was also prepared and incubated with all other samples. Each mutant and WT tau were induced with small RNA, long RNA, P100, P700, or ARA in separate reaction tubes. All reactions were performed in 1.5 mL reaction tubes with a total volume of 200 μL. Ultrapurified molecular biology grade H_2O was added first, followed by 4 μl of 250 mM DTT to the reaction tube and mixed by pipetting and lightly tapping the reaction tube. 1 M NaCl was added to bring the final NaCl concentration to 100 mM for ARA reactions or 25 mM for polyphosphate and RNA reactions. Again, each sample was mixed by pipetting and gentle tapping. HEPES at a pH of 7.64 was added in 8 μL volume of 250 mM to a final concentration of 10 mM. After mixing by pipetting and gentle tapping 20 μL of 1 mM EDTA stock was added in the same manner for a final concentration of 0.1 mM.

To ensure RNase activity did not degrade the RNA inducer, a stock of EDTA, HEPES, NaCl, and DTT was also made using DEPC treated H_2O. However, there was no significant changes to

RNA induced aggregation of WT tau using DEPC treated reagents when compared to preliminary studies that did not use DPEC treated H_2O (data not shown). Either WT or mutated tau was then added to a final concentration 2 μM and mixed by pipetting and gently tapping. Inducer was then added as follows to the respective samples, 10 μL of either small RNA or long RNA was added for a final RNA concentration of 13.5 ng/μL, 10 μL of either P100 or P700 was added for a final concentration of 10 ng/μL, and 7.5 μL of 2 mM ARA diluted in 100% ethanol was added to give a final concentration of 75 μM ARA 3.75% ethanol. For the controls, a Sup200 buffer (250 mM NaCl, 10 mM HEPES, 0.1 mM EGTA, pH 7.64) was used in place of the tau and RNase-free water was used in place of the RNA inducer, molecular biology grade H_2O was used for no polyphosphate control and 7.5 μL of ethanol for the no ARA control. The reaction tubes were then incubated without agitation at 37 °C for 72 hours for RNA, 48 hours at 37 °C for polyphosphate, and 20 hours at 25 °C for ARA.

Sandwich ELISA: Following aggregation reactions, samples were analyzed using a modified sandwich ELISA assay based on previously described conditions[100, 123]. Capture antibody was used to coat Corning 3590 EIA/RIA 96 well microplate wells at a volume of 100 μL/well of either TOC1 (2 ng/μL), TNT1 (1 ng/μL), T22 (1ng/μL), or a mixture of Tau 5, Tau 7, and Tau 12 antibodies (referred to as 5,7,12) (1 ng/μL each). Capture antibodies were diluted in BSB capture buffer (100 mM boric acid, 25 mM sodium tetraborate, 75 mM NaCl, 250 μM thimerosal, pH 8.56). Plates were then sealed and incubated with gentle agitation overnight at 4 ºC. After capture antibody incubation, the plate was blotted and washed 2x with 300 μL/well of BSB wash buffer (100 mM boric acid, 25 mM sodium tetraborate, 75 mM NaCl, 250 μM thimerosal, 60 mM BSA, 0.1% Tween 20, pH 8.56). Plates were then blocked and incubated for

a further 1.5 hours with 300 µL of 5% non-fat dry milk (NFDM) dissolved in BSB wash buffer sealed at room temperature with gentle agitation. Samples were diluted in 5% NFDM BSB wash buffer to a concentration of 100 nM for TOC1 capture antibody, 25 nM for TNT1, 50 nM for T22, and 50 nM for 5,7,12. To provide an internal standard curve, dilution series of no compound polymer and monomer controls were added to the plate at a range of (3.125 nM - 400 nM for TOC1, 3.125 nM - 75 nM for TNT, and 1.5 nM-150 nM for T22). In our hands, the EC_{50} of the polymerized tau affinity curve was found to be 105 nM, 28 nM, and 35 nM for TOC1, TNT1, and T22 respectively. As 5,7,12 detects total tau, only a monomer standard curve was used at dilutions of 5-200 nM. Samples were added to a volume of 100 µL/well. Plates were sealed and incubated with gentle agitation for 1.5 hours at room temperature. Following incubation, plates were washed 2× using BSB wash buffer. A primary detection antibody was added at volumes of 100 µL/well. For TNT1, TOC1, and 5,7,12, polyclonal rabbit detection antibody diluted to a concentration of 50 ng/mL in 5% NFDM BSB wash buffer was added. For T22 capture antibody, 5,7,12 was added at a concentration of 1:1,000 dilution. Further incubation was carried out after sealing the plate at room temperature for 1.5 hours with gentle agitation. Following incubation with primary detection antibody, plates were washed 2× using BSB wash buffer before the addition of appropriate secondary detection antibody (100 µL/well of the goat anti-rabbit IgG for TOC1, TNT1, and 5,7,12 capture antibody, and 100 µL/well of goat anti-mouse IgG for T22 capture antibody). Both secondary detection antibodies were diluted 1:5,000 in 5% NFDM BSB wash buffer. The plate was sealed and incubated at room temperature with gentle agitation for 1.5 hours. After incubation, plates were washed 3× using BSB wash buffer before the addition of 50 µL per well of tetramethylbenzidine (TMB) substrate. Plates were then covered and incubated with gentle agitation at room temperature for 20 minutes

before the addition of 50 µL of a 3.6% H_2SO_4 stop solution. Readings were taken at an absorbance of 450 nm using a Varian Cary 50 UV Vis spectrophotometer with a Varian Cary microplate reader. Raw data readings were zeroed against a monomeric control of each mutant and then converted to % light absorbance. In the case of 5,7,12 capture antibody ELISA, the polymerized reactions were normalized against the monomeric protein for each mutation and WT. Statistical analyses were completed using an un-paired t-test to compare each mutation to WT 2N4R for TOC1, TNT1, and T22 ELISAs. In the case of 5,7,12, a Tukey's multiple test was completed. For both tests statistical significance was defined as $* \ p \leq 0.05; \ ** \ p \leq 0.01; \ *** \ p \leq 0.001$.

For this experiment four different capture antibodies were used, 5,7,12 (a mixture of 3 monoclonal total tau antibodies that bind to residues 9-18 tau-12[130], 218-225 tau-5, and 430-441 tau-7[131],), TNT1[14] (binds to the phosphatase activating domain epitope at residues 7-12 that are made accessible through tau fibrilization), TOC1[103] (recognizes an epitope between residues 209-224 with a high affinity for small tau oligomers and larger aggregates), T22[132] (has been shown to bind specifically to tau oligomers that have been seeded using Aβ42 oligomers as well as *in vitro* heparin induced oligomers).

Transmission electron microscopy: Samples were diluted 1:10 in polymerization buffer and fixed with 2% glutaraldehyde for 5 minutes at room temperature. The samples were then affixed to a 300-mesh carbon formvar coated copper grid, purchased from Electron Microscopy Sciences, (Hatfield, PA) by floating the grid on a 10 µL droplet of sample for 1 minute. The grid was then blotted on filter paper and washed on a droplet of ddH_2O before being blotted and stained by floating the grid on a droplet of 2% uranyl acetate as previously described[101]. Each

grid was imaged using a JEOL JEM 1400 transmission electron microscope fitted with a LaB_6 electron source (Electron Microscopy Research Lab, University of Kansas Medical Center). Five random images per grid were taken at a 5,000× magnification (to improve statistical power, 15 images were taken for both small RNA and long RNA induced filaments. Images were analyzed using Image Pro Plus 6.0 software by measuring the number, length, area, and perimeter of filaments >25 nm in length. Under our experimental conditions, it is very difficult to identify filaments less than 25 nm. To avoid erroneous results the assay has been limited to measuring tau filaments and oligomers greater than 25 nm.

Right-angle laser light scattering: Aggregation reactions were analyzed using right-angle laser light scattering as previously described[102] to determine the amount of aggregated material. The average light intensity measured of each sample was zeroed against a no inducer monomeric control for the respective tau mutant being imaged, and a no tau/inducer-only control by subtracting the background signal from the measured signal of the endpoint aggregation reactions. Briefly, samples were transferred to a 5 mm × 5 mm optical glass fluorometer cuvette (Starna Cells, Atascadero, CA) in the light path of a 532 nm wavelength 12 mW solid-state laser operating at 7.6 mW (B&W Tek Inc. Newark, DE) and images were captured using a Sony XC-ST270 digital camera with an aperture of f/ 5.6. Images were analyzed using Adobe Photo Shop 2021 by taking histogram readings of the pixel intensity across the scattered light path.

Right-angle laser light scattering kinetics of aggregation: Using the right-angle laser light scattering assay described above, samples were placed into a cuvette at time zero prior to the addition of the respective inducer molecule. An image was captured prior to induction and at

time 0 immediately after induction of each protein with either ARA, P100 or P700 as inducers. In the case of ARA, readings were taken every 5 minutes between 0- and 30- minutes post induction (p.i.), then at 45, 60, 90 and 120 minutes p.i. then every hour until 6 hours p.i. In the case of P700, images were taken at subsequent time points every 5 minutes p.i. for the first 60 minutes p.i. then at the following p.i. time points: 1.5hrs, 2hrs, 3hrs, 4hrs, 6hrs, 8.5hrs, 10hrs 40 minutes, 15hrs, and 16hrs. In the case of P100, images were taken at the same timepoint p.i. as for P700 (except 16hrs p.i.) with additional readings at 24 and 48 hours.

Thioflavin fluorescence: A standard assay in tau aggregation studies is thioflavin fluorescence using thioflavin S or thioflavin T. While thioflavin fluorescence is a useful tool in monitoring ARA and polyphosphate induced filament formation, we found that RNA gave a false positive result when using thioflavin T and quenched fluorescence of thioflavin S (data not shown).

Dot-blot assay: A 0.22 µm nitrocellulose membrane was pre-soaked for 10 minutes in Tris Buffered Saline (TBS – 500 mM NaCl, 20 mM Tris, pH 7.5). Polymerized 2N4R tau samples were diluted to a concentration of 20 ng/uL in TBS and added to the membrane using a dot-blot manifold (no vacuum). Samples were incubated on the membrane for 30 minutes at room temperature before removal of excess liquid and blocking the membrane with 5% non-fat dried milk (NFDM) in TBST (TBS + 0.05% Tween 20). The membrane was blocked for 1.5 hours with gentle agitation at room temperature. After incubation, the membrane was washed for 5 minutes 3× with TBST. The T22 primary detection antibody was diluted at 1:1,000 concentration in 5% NFDM in TBST, the membrane was submerged in T22 and incubated at

room temperature for 2 hours with gentle agitation. Secondary antibody (Goat anti-rabbit IgG) was diluted in 5% NFDM in TBST to a 1:3,000 concentration. The membrane was washed 2× in TBST, before being submerged in secondary antibody at room temperature for 2 hours with gentle agitation. The membrane was once again washed for 5 minutes 2× using TBST before being developed using Thermo Fisher Supersignal West Pico Plus chemiluminescent substrate (catalog number 34580). An image of the blot was taken using UVP Chemidoc IT_2 western blot imager and analyzed using Adobe Photoshop software using the histogram function to measure dot-blot intensity (figure 33).

3.3 Results

ARA induced tau aggregation:

Using ARA as an inducer molecule, we initially completed LLS and TEM endpoint studies by allowing aggregation experiments to run for 20 hours (figure 19). The results from the LLS experiments (figure 19A) revealed that the P301S mutation caused significantly more aggregation in comparison with the WT. In addition, P332S led to a significant decrease in aggregation in comparison with the WT. Although not statistically significant, the average total amount of aggregation of the P270S mutation appeared to decrease (approximately 15% less than WT), and P364S showed no change when compared to WT.

Quantitative TEM was used to measure average filaments length (figure 19B), total filament mass (figure 19C), and number of filaments (figure 19D). Consistent with the findings of the LLS experiments, the difference in filament mass of P270S filaments was not statistically significant when compared to WT. However, the P270S mutation caused a greater average

number of filaments that were shorter than WT filaments. Consistent with results from other studies, P301S filaments induced by ARA were significantly longer than WT filaments, however, there were also fewer P301S fibrils. This resulted in P301S having a higher average mass per image, but not enough to reach the threshold of statistical significance (p-value < 0.05). No significant difference in average filament length was seen when comparing WT to the P332S mutation, however there were fewer filaments that resulted in a significant decrease in filament mass, consistent with the LLS results. The P364S mutation cause no significant difference in filament length, mass, or number of filaments when compared to WT tau.

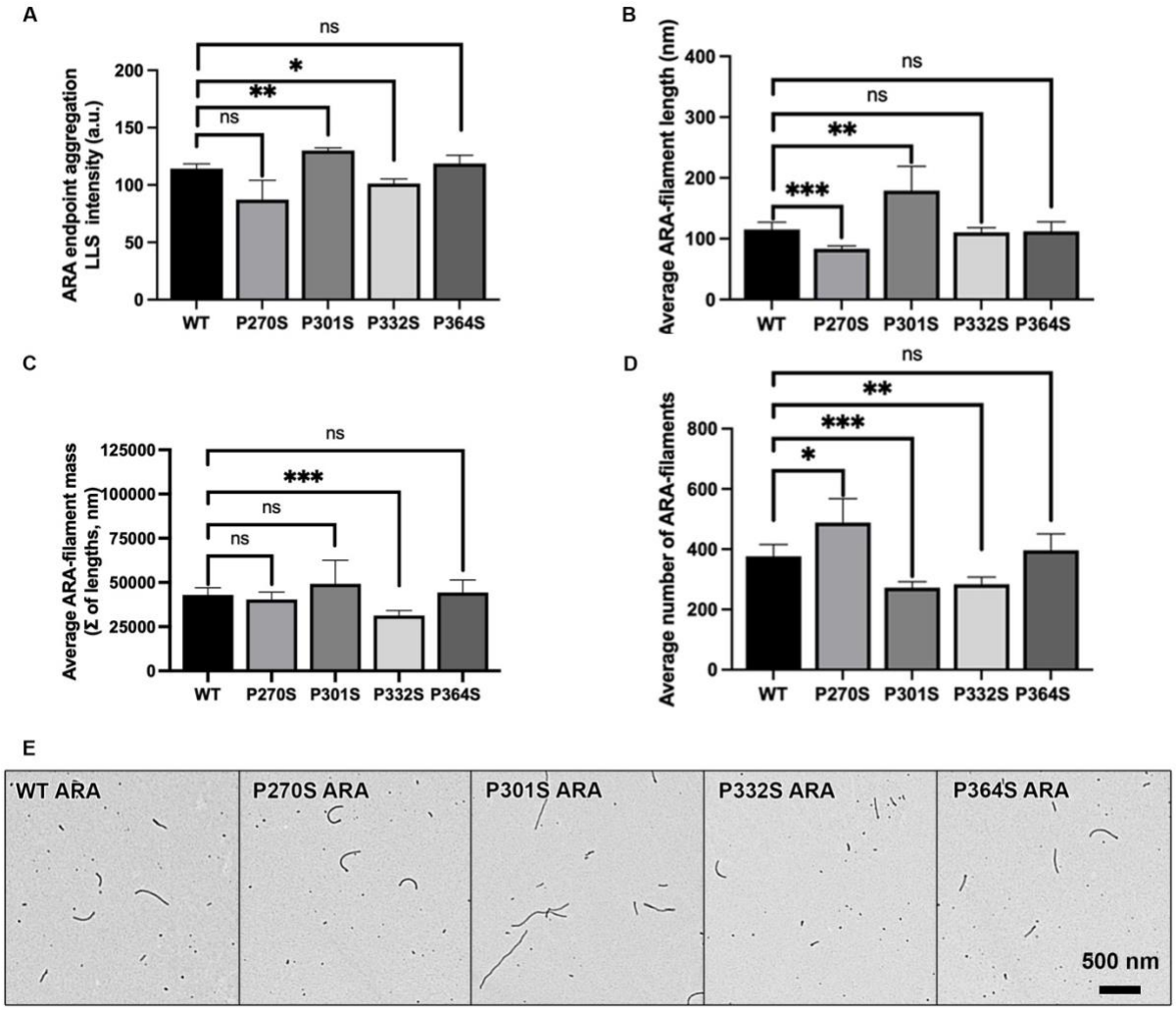

Figure 19: LLS and TEM endpoint measurements of ARA aggregation reactions.
A) Endpoint total amount of aggregation of ARA induced aggregation for WT and each of the four P to S mutations, quantified using laser light scattering (n=3 ± s.d.). 5 different TEM images selected at random were quantified to measure. B) average ARA induced filament length (>25 nm) ± s.d., C) average ARA filament total filament mass of each micrograph ± s.d., and D) average number of filaments (>25 nm) per micrograph ± s.d.. E) Representative TEM micrographs of WT and each of the four P to S mutations (see labeling in upper left corner of each micrograph). Scale bar in bottom right corner of P364S image represents 500 nm and applies to each micrograph. LLS and TEM grid preparation was completed by Kelsey M. Hillyer. Error bars on figures A-D represents SD of each data set. Each P to S mutation in A-D was compared to WT using an unpaired t-test. $ns\ p > 0.05$, $*\ p \leq 0.05$; $**\ p \leq 0.01$; $***\ p \leq 0.001$. *ns* = not significant.

ARA induced aggregation measured by sandwich ELISA:

The 5,7,12 ELISA showed no significant difference between WT and any of the P to S mutations (figure 20A). This shows that the mutations themselves do not appear to significantly inhibit the affinity of the two total tau antibodies; either polyclonal rabbit or 5,7,12 (figure 20A). In contrast with the LLS results, there was no significant difference between ARA induced WT tau and any of the mutations when detecting with either TNT1 or TOC1 antibody (figure 20 B-C). However, the TOC1 ELISA did show that the average P301S signal was higher than WT, but not enough to meet the pre-determined p-value threshold of 0.05. Based on the LLS results we would have expected the TNT1 ELISA to show an increase for P301S and a decrease for P332S. Interestingly, ARA induced P301S, P332S, and P364S had significantly less reactivity with the T22 antibody than ARA induced WT tau, however P270S was not significantly different (figure 20D).

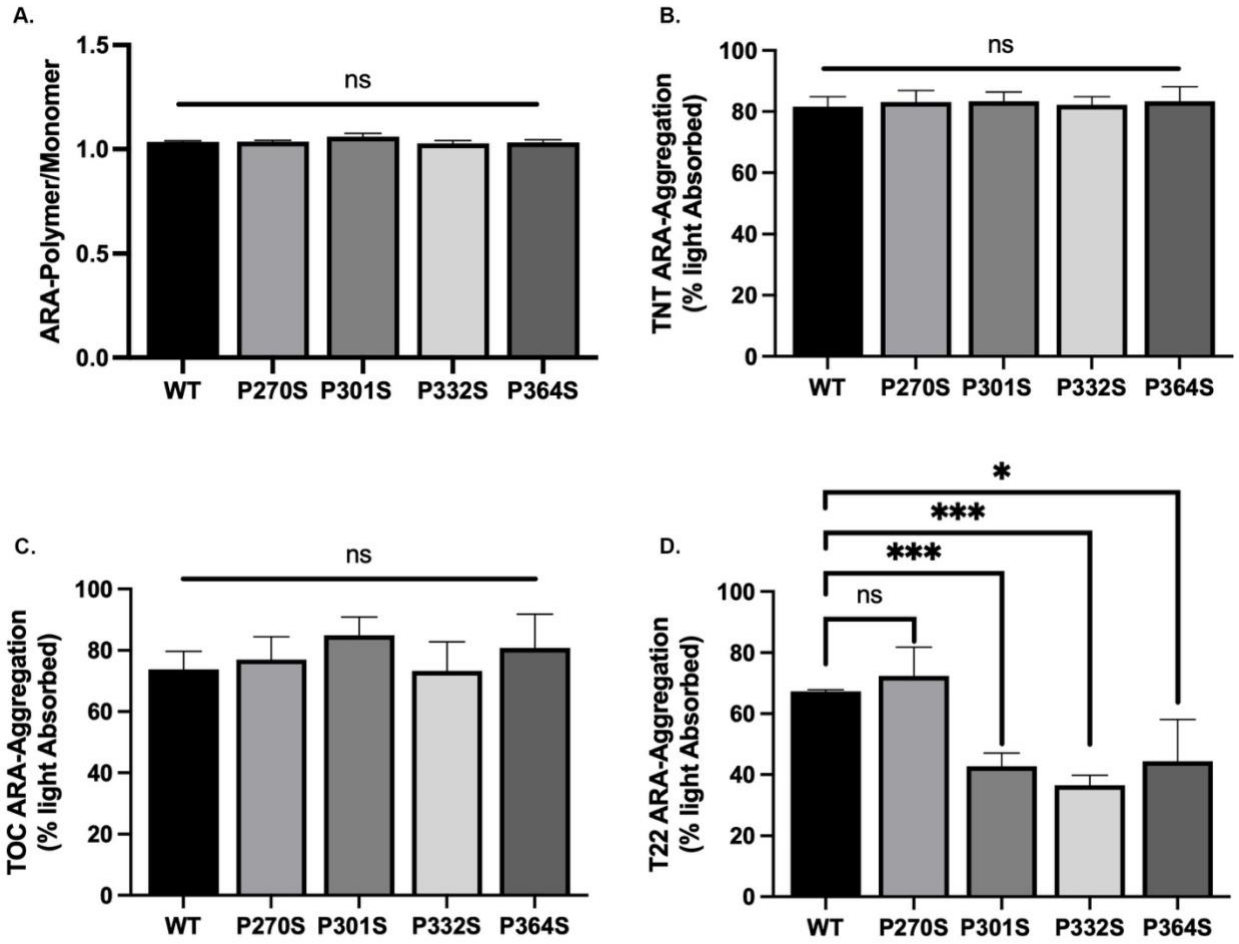

Figure 20: ARA ELISA data.
ELISA results using 5,7,12 monoclonal total-tau antibody mixture as a capture antibody. The signal for each aggregate was divided by the signal for monomeric tau (either WT or the respective P to S mutations). Y axis represents a fraction of monomeric tau signal (e.g. 1=100%). B-D, ELISA results of conformationally sensitive antibodies TNT1 (B), TOC1 (C), and T22 (D). Y-axis represents % light absorbed value (converted from A450 reading). Error bars represent SD of 3 independent experiments and data sets were compared to WT 2N4R tau using an unpaired t-test. "ns" indicates no significant difference when compared to WT 2N4R control. Statistical significance was defined as $ns\ p > 0.05,\ *\ p \leq 0.05;\ **\ p \leq 0.01;\ ***\ p \leq 0.001$.

ARA Aggregation Kinetics:

In addition to studying total aggregation, filament morphology, and immuno-reactivity, we also compared the kinetics of aggregation of each mutant to WT tau in the presence of ARA. When comparing WT tau to P270S, P332S, and P364S there was no significant difference in the maximum polymerization, rate of aggregation, and lag time (figure 21). However, the P301S mutation caused a significant increase in maximum polymerization consistant with the results of the LLS endpoint reactions (figure 21B). Although the P301S rate of polymerization was less than WT, it did not meet the statistical threshold to be considered signficantly different (figure 21C). However, P301S did cause a significant increase in the lag time when compared to WT (figure 21D). Typically, a longer lag time and slower rate of polymerization is indicative of fewer filaments with a longer average length. Therefore, the results from these aggregation kinetic experiments support, at least in part, the findings from the TEM studies (figure 19).

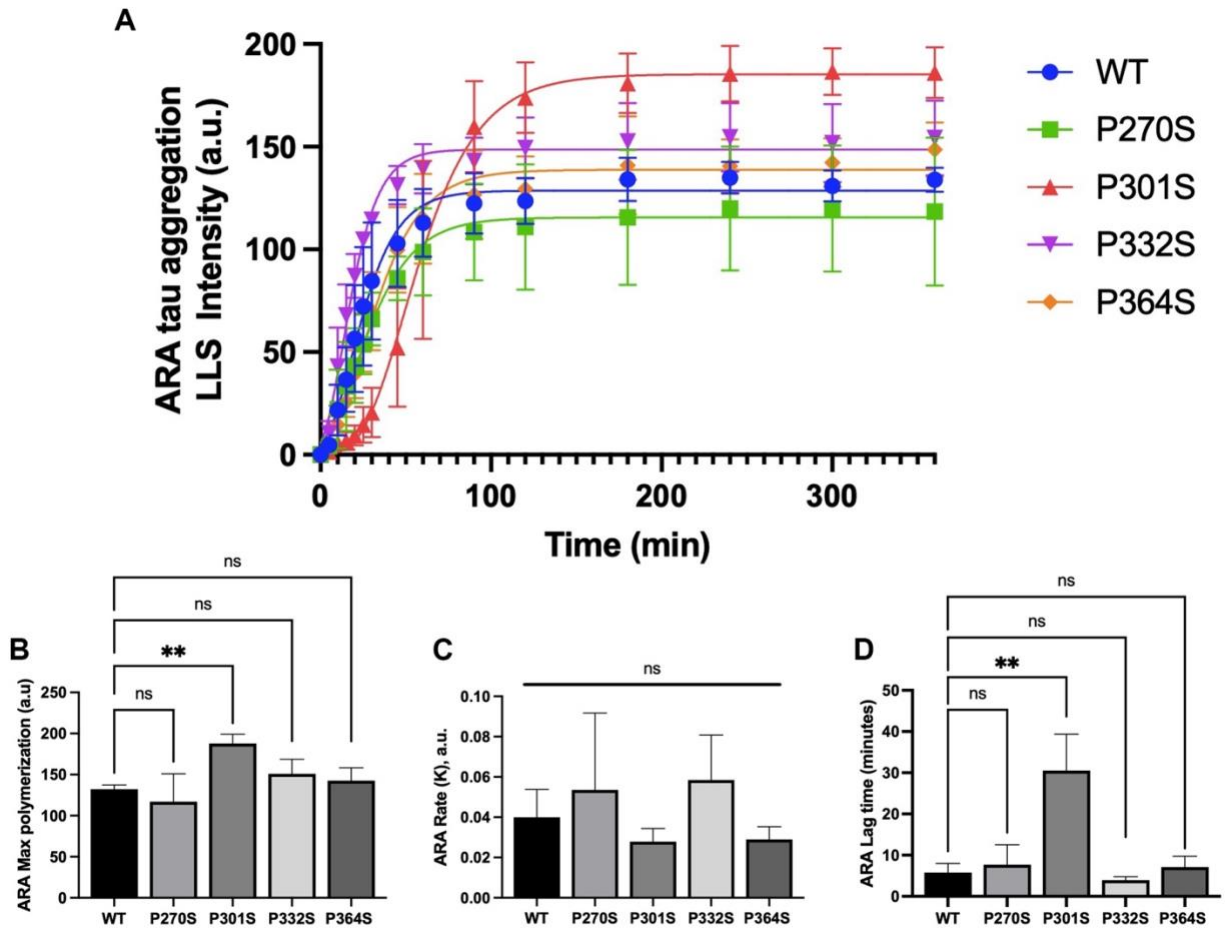

Figure 21: ARA induced aggregation kinetics.
Three independent data sets of ARA induced reactions monitored by LLS were fit to a plateau followed by one phase association non-linear curve. A) average LLS intensity over the course of 6 hours (360 minutes) were plotted for WT (blue dots), P270S (green squares), P301S (red triangles), P332S (purple inverted triangles), and P364S (orange diamonds). B) Average maximum polymerization, C) average rate of polymerization, and D) average lag time of each mutation was shown in a bar graph (n=3 ± s.d.). ARA induced kinetic experiments were completed by Kelsey M. Hillyer. Each P to S mutation was compared to WT using an unpaired t-test. Significance was identified as $ns\ p > 0.05$, $*\ p \leq 0.05$; $**\ p \leq 0.01$; $***\ p \leq 0.001$. *ns* = not significant.

ARA Results Summary:

In summary, when compared to WT tau, the P270S mutation effects average filament length and average number of filaments. In contrast, P301S causes difference in total polymerization, filament length, number of filaments, T22 immuno-reactivity, and aggregation kinetics. Compared to WT, P332S also has a significant effect on total polymerization, number of filaments, and T22 reactivity. The P364S mutation had no effect on total polymerization, filament morphology as shown by TEM, and aggregation kinetics. However, there was a significant decrease in T22 reactivity.

P100 induced endpoint aggregation experiments:

In the presence of P100 as an inducer molecule, the P270S mutation resulted in a significant decrease in LLS when compared to WT (figure 22). Also, in contrast to the ARA induced reactions, the P270S filaments were significantly longer than WT. Interestingly, P100 induction of P301S did not show a significant increase in aggregation as detected by both LLS and TEM. However, there was a decrease in the number of filaments. Both P332S and P364S mutations resulted in filaments that were significantly longer than WT. In addition, there was a significant reduction in the number of filaments and an overall decrease in filament mass as determined by TEM. However, LLS did not reveal a significant difference between either P332S or P364S when compared to WT.

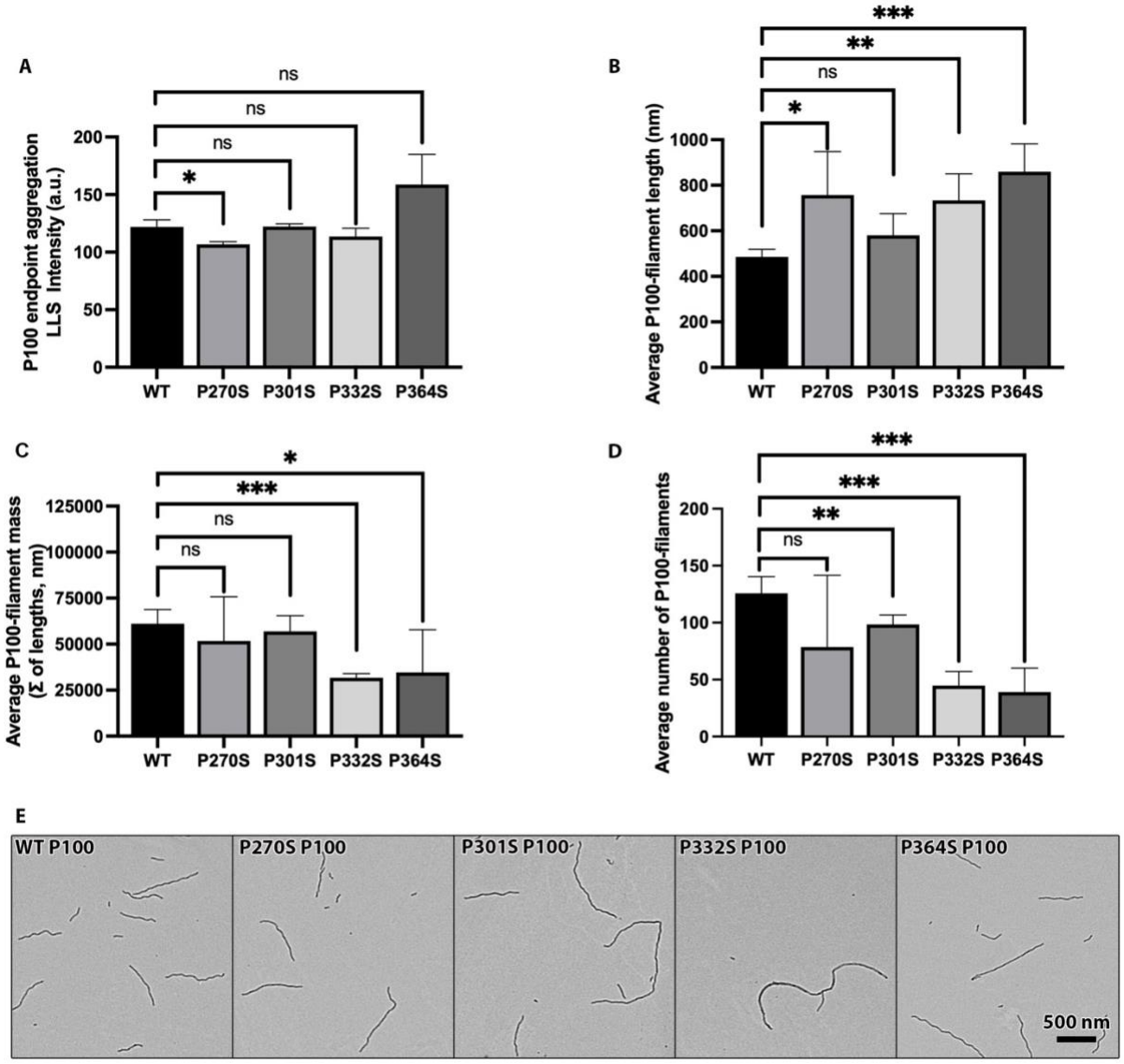

Figure 22: LLS and TEM endpoint measurements of P100 polyphosphate reactions.
A) Endpoint total amount of aggregation by LLS (n=3 ± s.d.). 5 different random micrographs taken from a single EM grid at a 5,000x magnification were quantified to obtain measure B) average filament length (± s.d), C) average filament mass (± s.d), and D) average number of filaments (± s.d). E) Representative TEM micrographs of WT and each of the four P to S mutations (see labeling in upper left corner of each micrograph). Scale bar in bottom right corner of P364S P100 image represents 500 nm for each micrograph. Each P to S mutation was compared to WT using an unpaired t-test. $ns\ p > 0.05$, $*\ p \leq 0.05$; $**\ p \leq 0.01$; $***\ p \leq 0.001$. *ns* = not significant.

P700 induced endpoint aggregation experiments:

Using P700 as an inducer molecule resulted in filaments that were shorter on average than those induced with P100, and therefore more similar in average filament length to those induced by ARA. Although, the P270S mutation did not cause any difference in the amount of LLS (figure 23), it did result in significantly fewer, but longer, filaments when compared to WT. In contrast to the LLS results, P270S caused a significant decrease in filament mass. When comparing P301S induced by P700 to WT tau, there is a significant increase in LLS, as well as significantly fewer, but longer filaments. These results were consistent with the ARA induced experiments, however, P301S filament mass was not statistically different from WT. LLS results of P332S showed no significant difference when compared to WT, however, TEM revealed fewer P332S filaments with a much longer average filament length and overall less filament mass. Both LLS and TEM-filament mass showed no significant difference between P364S and WT. Although TEM did reveal the P364S mutation to form fewer, but longer filaments when compared to WT.

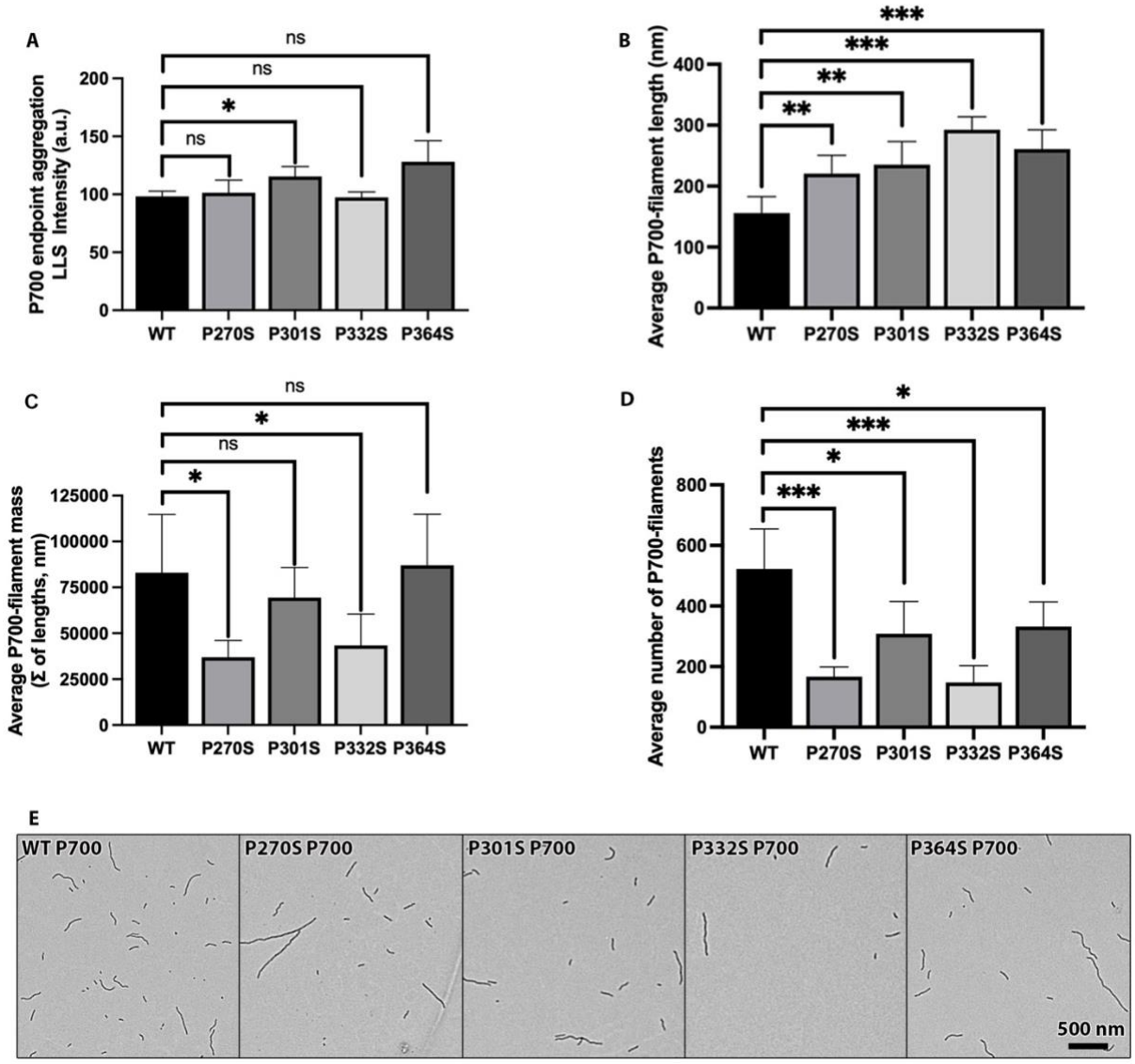

Figure 23: LLS and TEM endpoint measurements of P700 polyphosphate reactions.
A) Endpoint total amount of aggregation by LLS (n=3 ± s.d.). 5 different random micrographs taken from a single EM grid at a 5,000x magnification were quantified to obtain measure B) average filament length (± s.d), C) average filament mass (± s.d), and D) average number of filaments (± s.d). E) Representative TEM micrographs of WT and each of the four P to S mutations (see labeling in upper left corner of each micrograph). Scale bar in bottom right corner of P364S P700 image represents 500 nm for each micrograph. Each P to S mutation was compared to WT using an unpaired t-test. $ns\ p > 0.05$, $*\ p \leq 0.05$; $**\ p \leq 0.01$; $***\ p \leq 0.001$. *ns* = not significant.

Polyphosphate induced aggregation measured by sandwich ELISA:

Similar to filaments induced by ARA we saw no significant difference between WT and any of the P to S mutations using the 5,7,12 capture antibody ELISA when induced with either P100 or P700 (see figure 31). In addition, we also saw no significant effect from any of the mutants in either the TNT1 and TOC1 ELISAs using both polyphosphate inducers (figure 24). However, it does appear that the TOC1 antibody has a lower affinity towards polyphosphate induced filaments than ARA induced filaments (see figure 32 comparing WT aggregates in the presence of each inducer). However, the most striking difference in the immuno-reactivity experiments was seen using T22 as a capture antibody. Both WT (figure 32) and each of the P to S mutants (data not shown) induced by either P100 or P700 had no reactivity towards T22 in the ELISA experiment. Therefore, we were unable to compare the effect of the mutations using this particular antibody. We suspected that this may be due to the inducer molecule blocking the T22 binding site. This was tested by performing a dot-blot experiment to compare both WT and P301S induced by ARA, P100, P700, long RNA, and small RNA and detected using T22. In this experiment, T22 did detect the polyphosphate and RNA induced aggregates (figure 33).

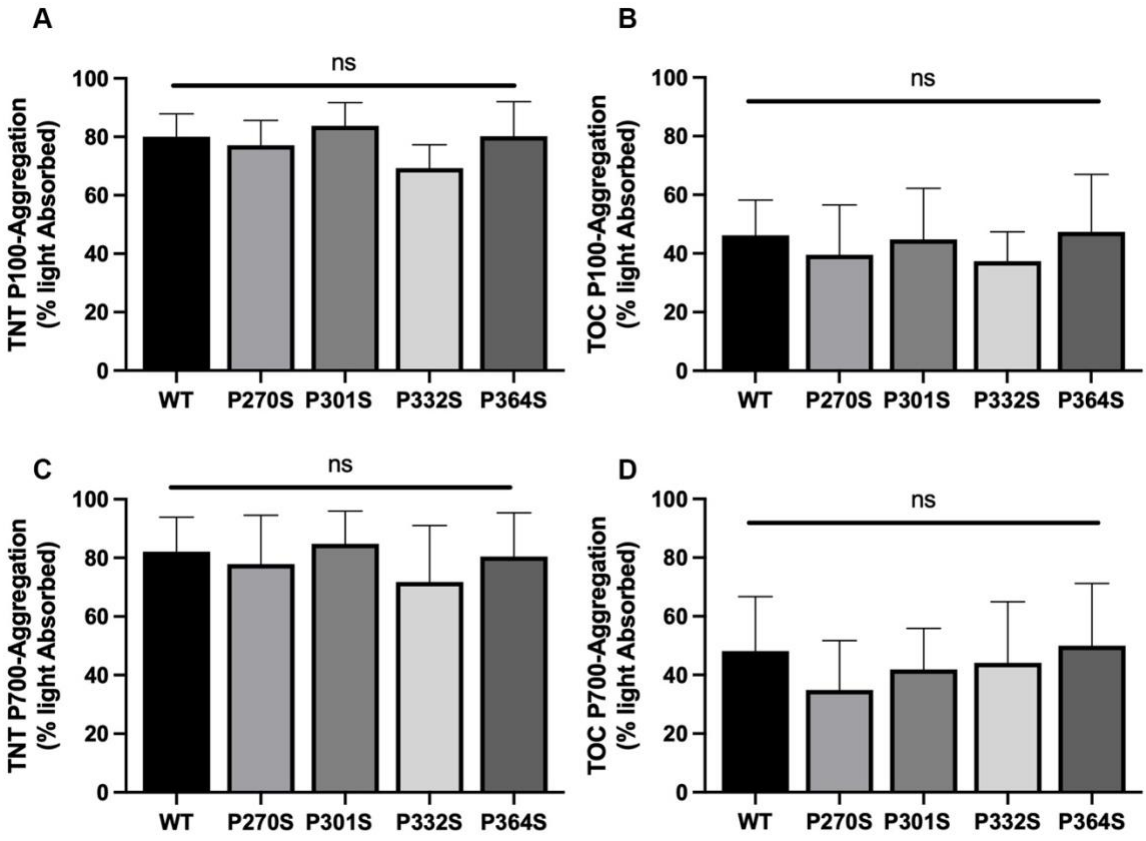

Figure 24: Polyphosphate TNT and TOC ELISA data.
ELISA results using TNT (A & C) and TOC (B & D) capture antibodies against P100 (A & B) and P700 (C & D) induced filaments. Y-axis represents % light absorbed value (converted from A450 reading). Error bars represent SD of 3 independent experiments. Each P to S mutation was compared to WT using an unpaired t-test. $ns\ p > 0.05$, $*\ p \leq 0.05$; $**\ p \leq 0.01$; $***\ p \leq 0.001$. *ns* = not significant.

P100 aggregation kinetics:

Similar to the ARA aggregation studies, we used LLS to monitor protein aggregation over time. Compared to WT tau, P332S had a significant decrease in rate of polymerization (*K*), but was similar in terms of maximum polymerization. Although the difference in lag time between WT and both P270S and P332S was not statistically significant due to the high variability in lag time, the average was much higher than WT, which had essentially no lag period. Similarly, P301S also appeared to have no lag period and total polymerization was similar to WT. However, the rate of polymerization for P301S was much faster than WT. This is in stark contrast to the results seen from the ARA induced aggregation kinetic experiments, which showed P301S to have a longer lag time, greater maximum polymerization, and no significant difference in rate (Compare figure 21 to figure 25). The P364S mutation caused a significant decrease in maximum polymerization and a significant increase in the lag time, but no change to rate of polymerization.

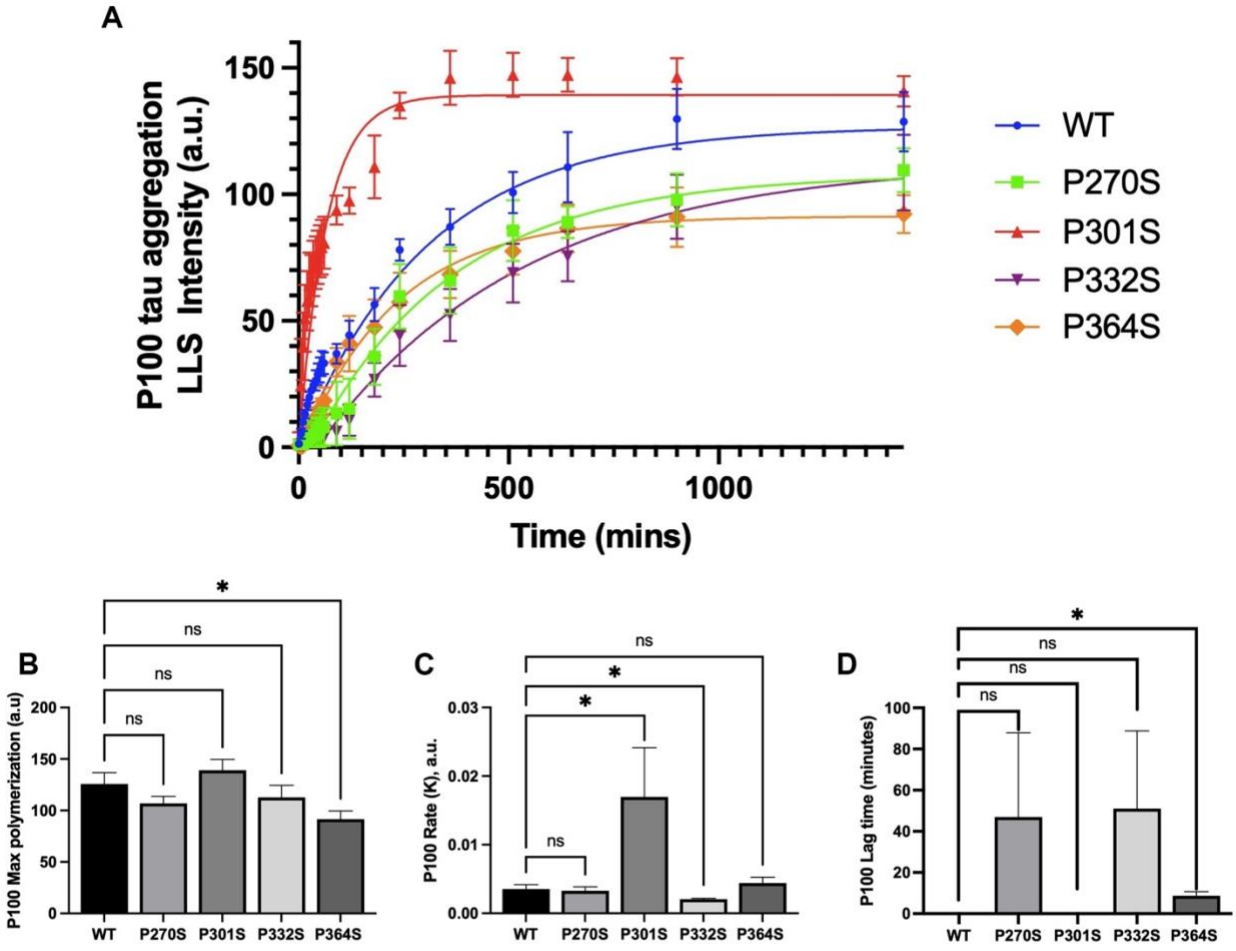

Figure 25: P100 induced aggregation kinetics.
Three independent data sets of P100 induced reactions monitored by LLS were fit to a plateau followed by one phase association non-linear curve. A) average LLS intensity over the course of 24 hours (1440 minutes) were plotted for WT (blue dots), P270S (green squares), P301S (red triangles), P332S (purple inverted triangles), and P364S (orange diamonds). B) Average maximum polymerization, C) average rate of polymerization, and D) average lag time of each mutation was shown in a bar graph with error bars representing standard deviation. Each P to S mutation was compared to WT using an unpaired t-test. $ns\ p > 0.05$, $*\ p \leq 0.05$; $**\ p \leq 0.01$; $***\ p \leq 0.001$. *ns* = not significant.

P700 aggregation kinetics:

In the presence of P700 as an inducer molecule, the P270S mutation did not significantly affect maximum polymerization (figure 26). P270S did have a significantly faster rate of polymerization when compared to WT and although not significant, the average lag time was higher than WT. In the case of P301S, the P700 inducer had the same effect as P100 as shown by the significant increase in the rate of polymerization, but no change in maximum polymerization or lag time. In contrast to the P100 induced kinetic experiments, P332S was the only mutation that caused a significant decrease in maximum polymerization. This difference was particularly striking as it was approximately 1/3 of the WT maximum polymerization. Despite this large difference, there was no change in the rate of polymerization, although the increase in lag time was statistical significance. In contrast to the results from the P100 induced experiments, but more similar to the ARA induced experiments, P364S had no significant effect on maximum polymerization, rate, or lag time.

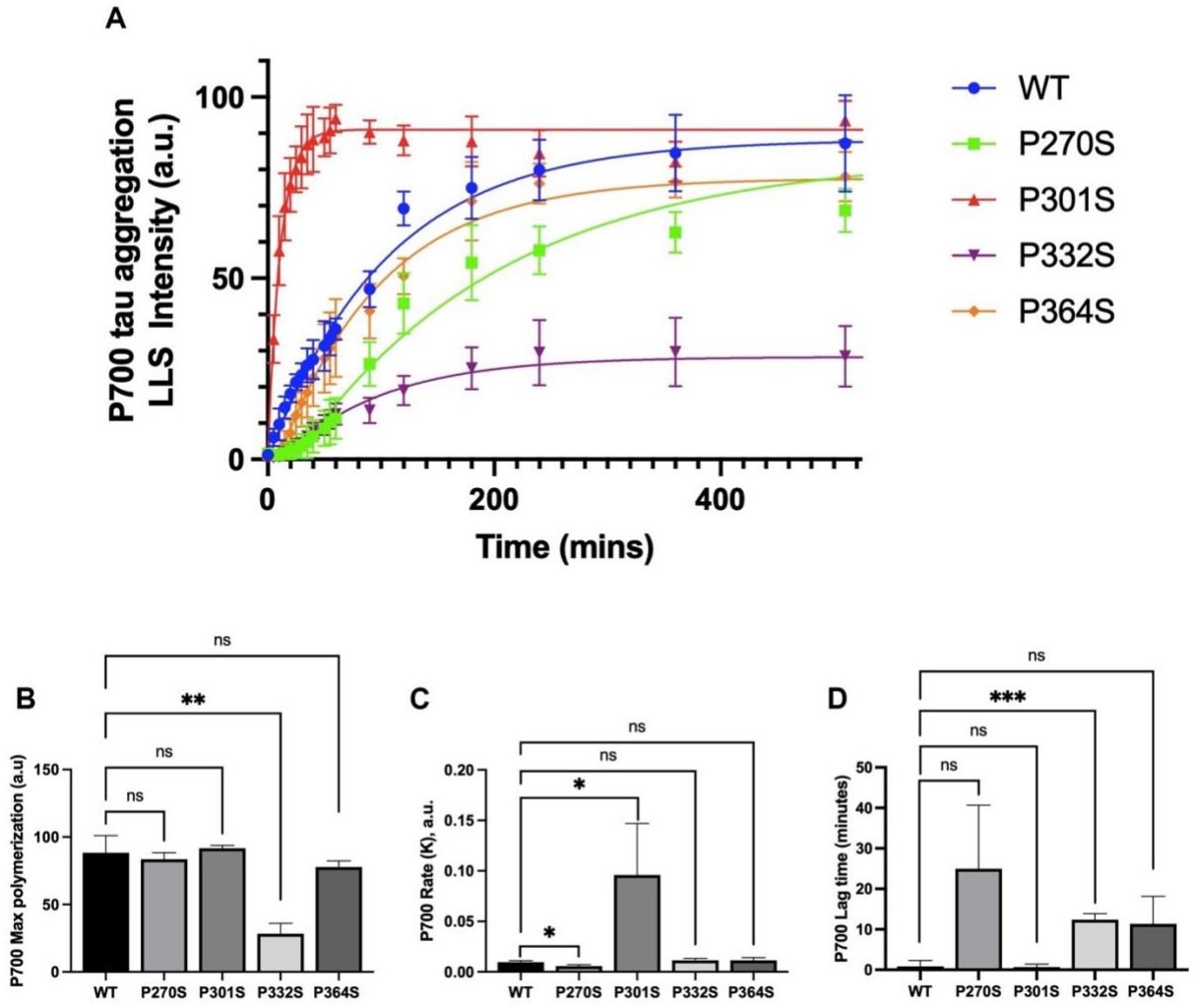

Figure 26: P700 induced aggregation kinetics.
Three independent data sets of P700 induced reactions monitored by LLS were fit to a plateau followed by one phase association non-linear curve. A) average LLS intensity over the course of 8.5 hours (510 minutes) were plotted for WT (blue dots), P270S (green squares), P301S (red triangles), P332S (purple inverted triangles), and P364S (orange diamonds). B) Average maximum polymerization, C) average rate of polymerization, and D) average lag time of each mutation was shown in a bar graph with error bars representing standard deviation. Each P to S mutation was compared to WT using an un-paired t-test. Significance was identified as $ns\ p > 0.05$, $*\ p \leq 0.05$; $**\ p \leq 0.01$; $***\ p \leq 0.001$. *ns* = not significant.

Polyphosphate Summary:

The P270S mutation, previously shown to have no effect on total aggregation, a decrease of average filament length, and an increase in the number of filaments when induced by ARA, causes a decrease in total aggregation as measured by LLS and an increase in average filament length as measured by TEM when induced with P100. When P270S is induced with P700, the average filament length is still longer, but there are fewer filaments and less overall filament mass. In addition, analysis of P700 induced kinetic data revealed a decrease in rate of polymerization for P270S. The P301S mutation causes a decrease in the number of filaments as measured by TEM and a significant increase in rate of polymerization when induced with both P100 and P700. When induced with P700, there was an increase in total aggregation as determined by LLS, and an increase in average filament length as measured by TEM. Both P100 and P700 induced P332S reactions showed similar changes in filament length, mass, and number of filaments. P100 induced P332S caused a decrease in rate of polymerization and P700 induced filaments showed a decrease in the maximum polymerization and increase in lag time. While both P100 and P700 induced P364S reactions showed an increase in average filament length and decrease in the number of filaments, only P100 induced reactions had a negative effect on total filament mass and maximum polymerization (as determined by kinetic analysis). In addition, P100 induced P364S also caused a decrease in maximum polymerization and increase in lag time as shown by kinetic analysis. None of these differences were shown when inducing P364S with ARA. Both WT and each of the P to S mutations induced with either P100 or P700, did not react with T22 in the ELISA experiment.

RNA induced aggregation:

Endpoint aggregation experiments were performed using small RNA and long RNA as inducers and the analysis of aggregation was completed using LLS and TEM (figure 27 and figure 28) similar to ARA, P100, and P700. WT tau and many of the mutants had total amounts of aggregation that were much lower than reactions induced with ARA, P100, and P700 (compare to figure 19, figure 22, and figure 23).

Long RNA endpoint aggregation experiments:

In contrast to the results using ARA, P100, and P700, total filament mass as determined by TEM (figure 27C) showed P270S mutation caused a significant increase in aggregation when induced with long RNA. As measured by LLS, the P301S mutation caused a significant increase of more than 5-fold when compared to WT tau (figure 27A). This was further supported by an approximate 5-fold increase in filament mass (figure 27C). In contrast to the results of the ARA induced reactions, P301S induced with long RNA did not result in increased filament length, but did result in an increase in the total number of filaments (compare figure 19 B&D to figure 27 B&D). Similarly, the P332S mutation also resulted in an increase in filament mass and number (figure 27 C&D). Although P364S induced reactions did result in significantly higher light scattering (figure 27A), no filaments were detected using TEM (figure 27 B-E). This suggests that either long RNA induced P364S aggregates are not stable and depolymerize during TEM grid preparation, filaments are below the TEM detection threshold (<25 nm), that RNA interacts with P364S causing it to scatter light, but not form filaments, or that long RNA induced P364S aggregates have properties that reduce their adherence to EM grids.

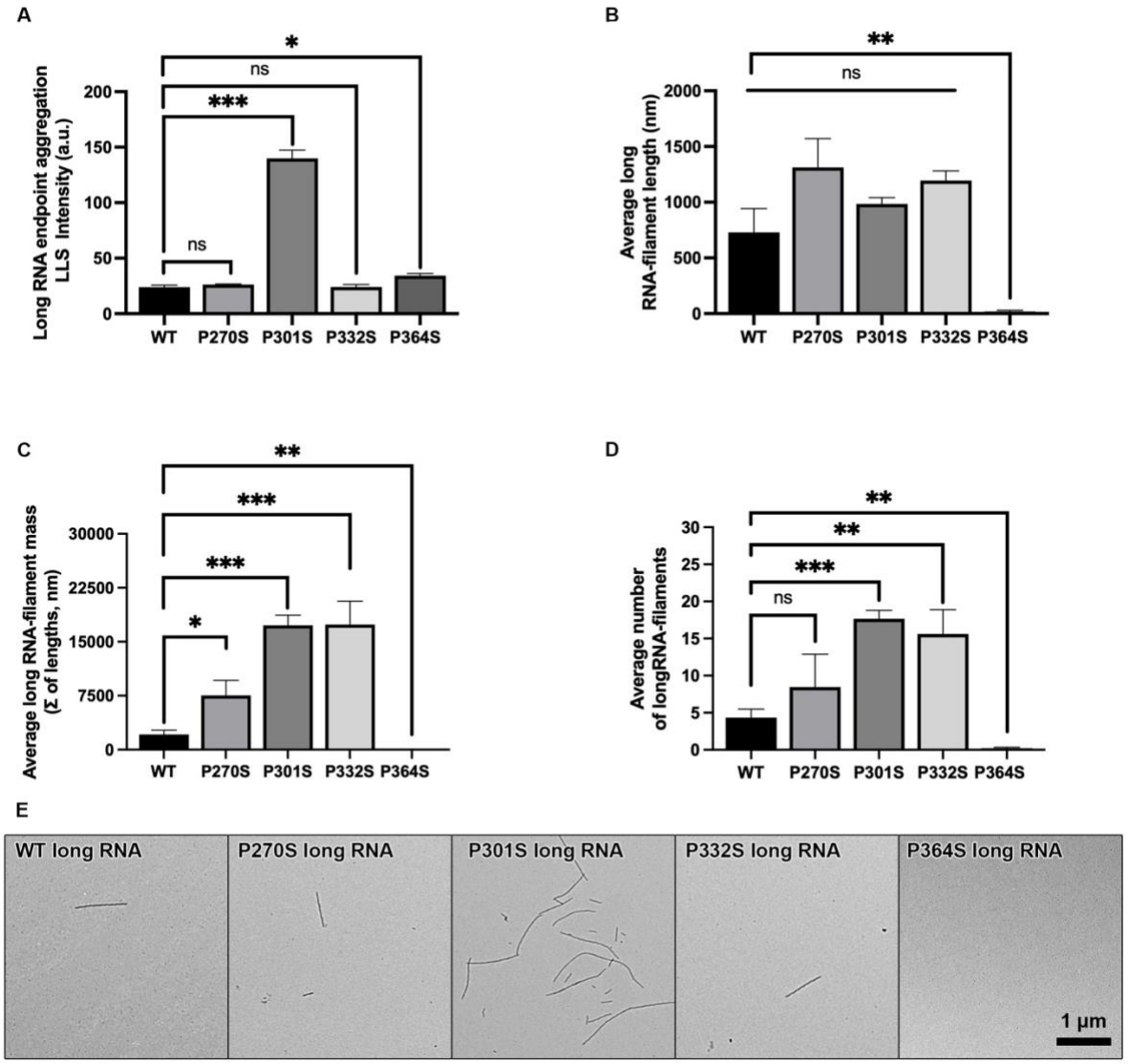

Figure 27: LLS and TEM measurements of long RNA endpoint aggregation reactions.
LLS measurement of endpoint total amount of aggregation of three independent experiments (A). B-D quantitative EM results, average filament length (B), average filament mass (C), average number of filaments (D). E) Representative TEM micrographs of WT and each of the four P to S mutations (see labeling in upper left corner of each micrograph). Scale bar in bottom right corner of P364S long RNA image represents 1 µm for each micrograph. Figures B-D represent averages of 15 different random micrographs taken from a single EM grid at a 5,000x magnification. LLS and TEM grid preparation was completed by Madison J. McGuire. Error bars on figures A-D represents SD of each data set. Each P to S mutation was compared to WT using an unpaired t-test.

$* \; p \leq 0.05; \; ** \; p \leq 0.01; \; *** \; p \leq 0.001.$

Small RNA endpoint aggregation experiments:

Although endpoint aggregation measured by LLS (figure 28A) showed the P270S mutation had no effect on aggregation when compared to WT tau, TEM analysis revealed a significant decrease in filament mass and number of filaments (figure 28 C and D, respectively). When comparing small RNA induced P301S and WT tau, the results were similar to the results when inducing with long RNA. However, the increase in aggregation caused by the P301S mutation was not as stark using small RNA (~3 fold) when compared to reactions induced with long RNA (>5 fold). Using small RNA as an inducer, the P332S mutation resulted in no significant difference in LLS, length of filaments, and filament mass, however there was a significant increase in the number filaments. In contrast to the TEM results of P364S induced with long RNA, using small RNA as an inducer did form filaments that were detected using TEM. However, total filament mass and number of filaments formed was significantly less than with WT tau.

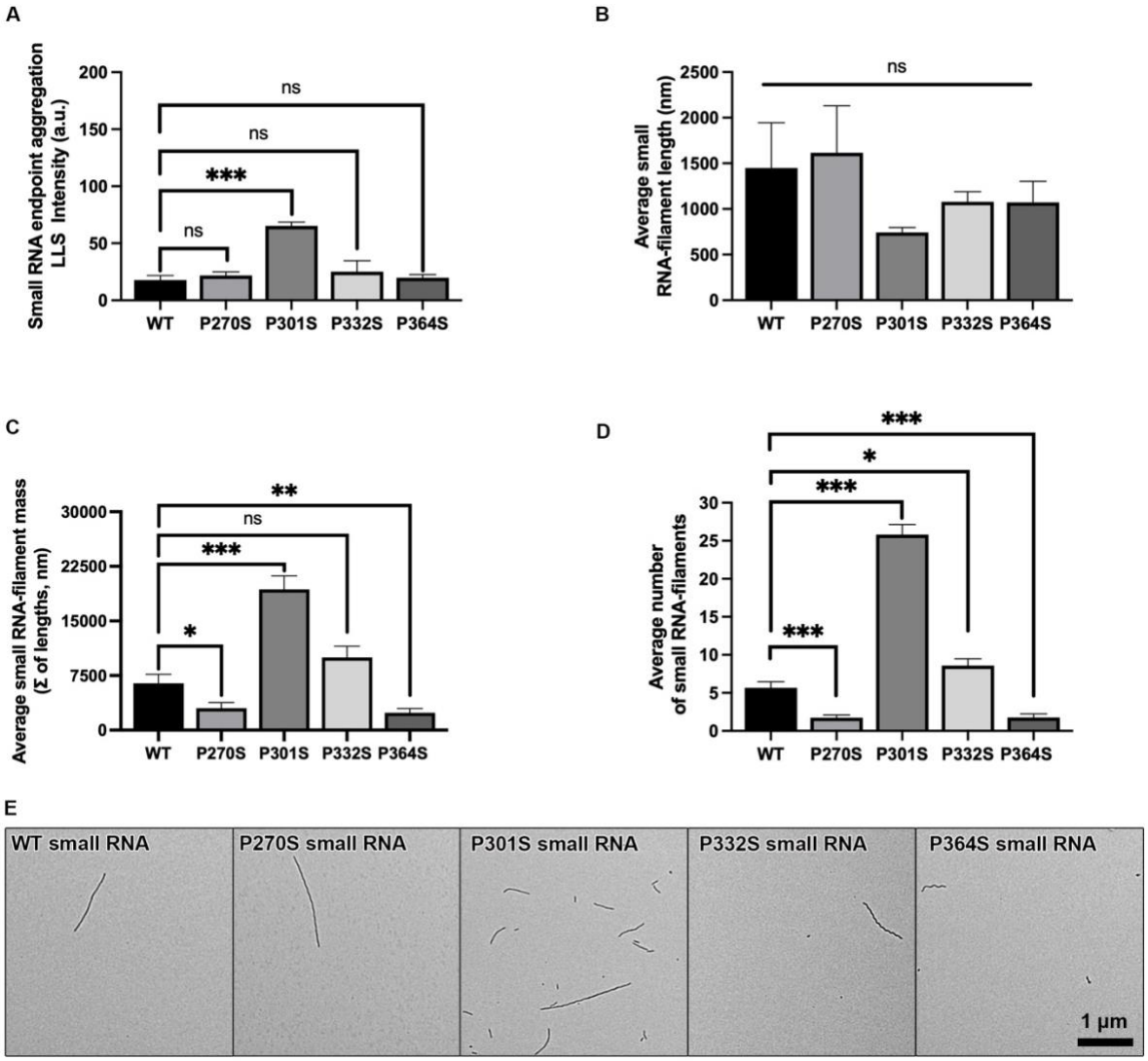

Figure 28: LLS and TEM measurement of small RNA induced endpoint aggregation reactions.
LLS measurement of endpoint total amount of aggregation of three independent experiments (A). B-D quantitative EM results, average filament length (B), average filament mass (C), average number of filaments (D). E) Representative TEM micrographs of WT and each of the four P to S mutations (see labeling in upper left corner of each micrograph). Scale bar in bottom right corner of P364S small RNA image represents 1 µm for each micrograph. Figures B-D represent averages of 15 different random micrographs taken from a single EM grid at a 5,000x magnification. LLS and TEM grid preparation was completed by Madison J. McGuire. Error bars on figures A-D represents SD of each data set. Each P to S mutation was compared to WT using an unpaired t-test.
$* \; p \leq 0.05; \; ** \; p \leq 0.01; \; *** \; p \leq 0.001.$

RNA induced aggregation measured by sandwich ELISA:

Despite a noticeable difference between P301S and WT tau as shown by TNT ELISA for long RNA, due to the variability in data this result did not reach statistical significance (figure 29). This was also the case for both long RNA and small RNA when comparing TOC1 ELISA results. However, small RNA induced P301S TNT1 reactivity was significantly higher than WT tau. None of the other mutations were significantly different than WT with regard to either the TNT1 and TOC1 ELISA using both long RNA and small RNA.

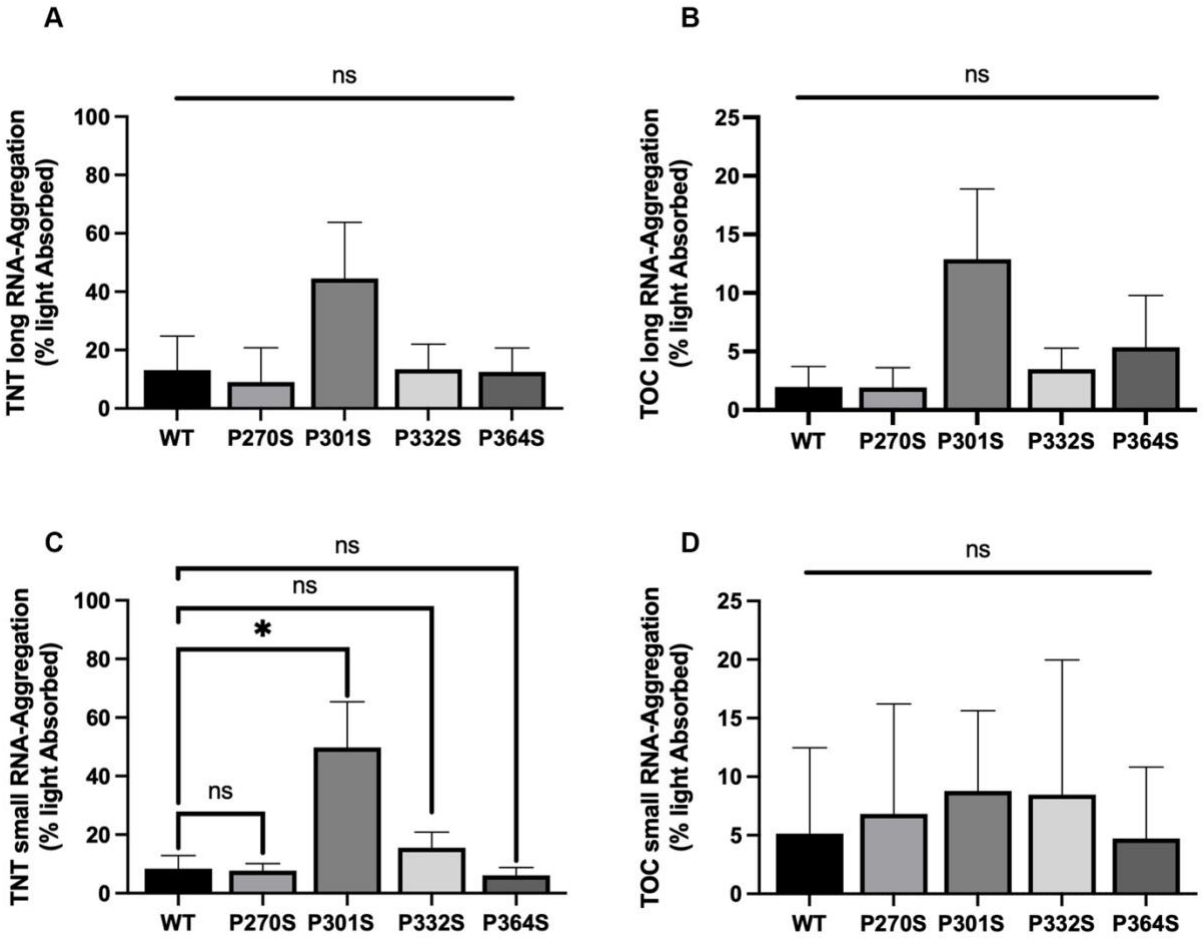

Figure 29: Immuno-reactivity of long RNA and small RNA reactions.
ELISA results using TNT (A & C) and TOC (B & D) capture antibodies against long RNA (A & B) and small RNA (C & D) induced filaments. Y-axis represents % light absorbed value (converted from A450 reading). Error bars represent SD of 3 independent experiments. Each P to S mutation was compared to WT using an unpaired t-test. $ns\ p > 0.05$, $* p \leq 0.05$; $** p \leq 0.01$; $*** p \leq 0.001$. *ns* = not significant.

RNA summary:

Using both long RNA and small RNA as an inducer molecule, we found differences in total polymerization, filament length, filament mass, number of filaments, and immuno-reactivity. The P270S mutation caused no change in total polymerization as determined by LLS for both long RNA and small RNA. However, when induced with small RNA there was a significant decrease in filament mass and number of filaments as determined by TEM. In contrast, P270S induced with long RNA caused a significant increase in filament mass, and an increase in the number of filaments and average filament length, although neither were statistically significant. There was also no significant difference in immuno-reactivity between P270S and WT using either TOC1 or TNT1 capture antibodies for either sizes of RNA.

When inducing P301S with both small and long RNA, there was a dramatic increase in total aggregation as determined by LLS (>5 fold for long RNA, and ~3 fold for small RNA). Interestingly, despite an increase in LLS, number of filaments, and total filament mass, using both RNA inducer molecules, the P301S mutation did not cause a significant difference in average filament length when compared to WT. Using long RNA to induce P301S aggregation caused an increase in TNT1 and TOC1 reactivity, however this increase did not reach the threshold to be statistically significant. Using small RNA, there was a significant increase in TNT1 reactive species, however no substantial change was seen when using the TOC1 capture antibody. The P332S mutation had no significant effect on total polymerization as determined by LLS, however, TEM analysis revealed an increase in number of filaments when induced with both RNA species, and a significant increase in filament mass when induced with long RNA. In initial endpoint aggregation experiments, there was a significant increase in LLS when induced

with long RNA, however, no filaments were present in the EM micrographs. When comparing P364S and WT induced with small RNA, there was no significant change in LLS and filaments were present as shown by TEM. Analysis of these images revealed a decrease in total filament mass and number of filaments, but no significant change to average filament length.

Comparison of each inducer molecule:

Table 5 summarizes the results of each experiment using each of the 5 inducer molecules: ARA, P100, P700, long RNA, and small RNA). It is clear from this summary that the choice of inducer molecule and method of aggregate detection can influence whether differences are detected and also the absolute extent of differences. It is also apparent that the P301S more consistently demonstrates differences from the wild type protein regardless of inducer and method of detection as compared to the other P to S mutations.

Table 5: Comparison of *in vitro* aggregation results by inducer, mutant, and method of detection.

Method	LLS	TEM			sELISA			Kinetics		
Parameter	Max	$\bar{L}$	Σ	#	TNT1	TOC1	T22	Max	Rate	Lag
				Arachidonic Acid						
P270S	≈	---	≈	+	≈	≈	≈	≈	≈	≈
P301S	++	++	≈	---	≈	≈	---	++	≈	++
P332S	-	≈	---	--	≈	≈	---	≈	≈	≈
P364S	≈	≈	≈	≈	≈	≈	-	≈	≈	≈
				Polyphosphate P100						
P270S	-	+	≈	≈	≈	≈	*n.a.*	≈	≈	≈
P301S	≈	≈	≈	--	≈	≈	*n.a.*	≈	+	≈
P332S	≈	++	---	---	≈	≈	*n.a.*	≈	-	≈
P364S	≈	+++	-	---	≈	≈	*n.a.*	-	≈	+
				Polyphosphate P700						
P270S	≈	++	-	---	≈	≈	*n.a.*	≈	-	≈
P301S	+	++	≈	-	≈	≈	*n.a.*	≈	+	≈
P332S	≈	+++	-	---	≈	≈	*n.a.*	--	≈	+++
P364S	≈	+++	≈	-	≈	≈	*n.a.*	≈	≈	≈
				Long RNA (> 200 nts)						
P270S	≈	≈	+	≈	≈	≈	*n.a.*	*n.a.*	*n.a.*	*n.a.*
P301S	+++	≈	+++	+++	≈	≈	*n.a.*	*n.a.*	*n.a.*	*n.a.*
P332S	≈	≈	+++	++	≈	≈	*n.a.*	*n.a.*	*n.a.*	*n.a.*
P364S	+	---	--	--	≈	≈	*n.a.*	*n.a.*	*n.a.*	*n.a.*
				Small RNA (<200 nts)						
P270S	≈	≈	-	---	≈	≈	*n.a.*	*n.a.*	*n.a.*	*n.a.*
P301S	+++	≈	+++	+++	+	≈	*n.a.*	*n.a.*	*n.a.*	*n.a.*
P332S	≈	≈	≈	+	≈	≈	*n.a.*	*n.a.*	*n.a.*	*n.a.*
P364S	≈	≈	--	---	≈	≈	*n.a.*	*n.a.*	*n.a.*	*n.a.*

This is a summary of the results from inducer aggregation experiments. $\bar{L}$ is average filament length; Σ is total filament mass; # is the number of filaments per micrograph; ≈ is no significant change; + indicates $p \leq 0.05$ significant increase from wt; ++ is $p \leq 0.01$; and +++ is $p \leq 0.001$; - indicates $p \leq 0.05$ significant decrease from wt; -- is $p \leq 0.01$; and --- is $p \leq 0.001$; n.a. (not applicable) indicates that the method could not be used for those conditions.

3.4 Discussion

It has been known for several decades that the term tauopathy includes a wide range of neurological disorders with diverse etiology, clinical presentation, and histopathology. Recent advances in structural biology techniques, primarily cryo-electron microscopy, have now shown that different tauopathies also include a range of structurally diverse tau aggregates[32, 39-41]. Previous studies have shown that missense mutations of the *MAPT* gene are associated with effects on tau pathology, neurodegeneration, and neurotoxicity[133-135]. Here, we examine how the use of different inducer molecules can have a profound effect on our understanding of the molecular characteristics of wild type tau and how it relates to missense mutations associated with a group of familial tauopathies known as frontotemporal dementia with parkinsonism linked to chromosome-17 (FTDP-17).

Previously, we, and others, have completed extensive *in vitro* aggregation studies using ARA as an inducer molecule of recombinantly expressed human tau. This has allowed for the development of optimized aggregation conditions and standard techniques to be able to complete characterization studies of *MAPT* mutations and other protein modifications. Comparisons of different fatty acids to induce tau aggregation have also shown that alkyl chain length and saturation of the fatty acid used can influence filament length, rate of polymerization, amount of polymerization, and filament density[136, 137]. In this study, we have used ARA as a fatty acid inducer of tau aggregation as it forms filaments that have similar morphology to straight filaments isolated from AD and has relatively higher stability when compared to fatty acids with a less saturated aliphatic tail[99].

Following ARA induced aggregation experiments, we sought to compare the P to S mutations using polyphosphate as an inducer molecule. Similar to fatty acids, chain lengths of polyphosphate can influence the amount and length of tau filaments[125]. However, there are fewer studies characterizing these differences. For the purpose of this study we chose to complete aggregation experiments using medium chain polyphosphate (P100) and long chain polyphosphate (P700). Similarly, few studies have characterized how RNA induces tau aggregation. To limit the scope of this study we chose to use two different RNA samples that were separated based on length. However, it is possible that differences in small and long RNA's primary and secondary structure may be the cause of the variance of observed effects on aggregation.

In this study we used three independent assays (LLS, TEM, and ELISA) for studying the effects of disease related mutations in the PGGG motif in order to understand how these effects relate to the inducer molecule used. Right-angle laser light scattering (LLS) is a standard tool used in the field of studying *in vitro* protein aggregation. However, this assay does have certain limitations when being used to compare different samples. For example; 1) samples with dissimilar size distributions will scatter light dis-proportionately to each other, 2) changes in filament flexibility could potentially affect the radius of gyration and therefore the total amount of light scattered, 3) formation of micelles or RNA droplets could interfere with measuring filament light scattering, and 4) particles less than $1/20^{th}$ the wavelength of the light source will not scatter light proportionately. In addition, when light scattering endpoint aggregation studies are completed the reactions take place in a closed plastic microcentrifuge tube, but when light scattering is used for measuring aggregation kinetics, the reactions are incubated in a 5 mm x 5 mm glass cuvette

sealed with parafilm. The differences in the material of these vessels and how each one affects surface area to volume ratio, may cause significant effects on total aggregation. For example, the P332S mutation when induced with P700 has no significant effect on total aggregation as measured by LLS during the endpoint aggregation reactions. However, during aggregation kinetic studies, the maximum polymerization of P332S was significantly reduced when compared to WT tau.

In addition to using electron microscopy to validate the results of the LLS aggregation assay, we were also interested in finding out more information such as the total filament mass, average length of filaments, and number of filaments using each inducer. Through the use of image analysis software, we are able to use transmission electron microscopy as a semi-quantitative tool, with the following limitations. 1) Only filaments that bind to the EM grid are detectable and it is possible that certain tau variants and/or inducer-specific polymorphs will have a different binding affinity toward the EM grid. 2) Filament length may be altered by filament breaking as they adhere to the grid. 3) The stain used to visualize the filaments may bind to different tau variants and/or inducer-specific polymorphs differently. 4) We are visualizing a relatively small sample size of filaments compared to the sample of those analyzed by LLS[93].

Sandwich ELISA assays can provide useful information about the species of tau aggregate being used and how these might relate to toxic species associated with disease. Similar to LLS and quantitation TEM, ELISA also has certain assay specific limitations when comparing multiple different samples. 1) The aggregates must form the corresponding epitope to the antibodies being used, and that epitope must be accessible, 2) inducer molecules may interfere with antibody

binding by blocking epitope recognition, 3) changes in filament flexibility may change epitope accessibility, 4) changes in length distribution may change the number of epitopes accessible (this is known to be the case with TOC1, as it is thought to bind to filament ends[103]), 5) may not appear to validate other methods due to different limits of detection (oligomers smaller than 1/20th LLS wavelength and 25 nm in length, may still bind to oligomer specific antibodies such as TOC1 and T22, and pro-aggregate monomer may still bind TNT1). Therefore, with these limitations in mind, it is important be cautious when basing conclusions on any single assay. In addition to actual changes to filaments caused by FTDP-17 mutations, we should also consider the disproportionate effect mutations may have on the method of detection.

Initial endpoint aggregation studies using ARA, P100, P700, long RNA, and small RNA, illustrates that the type of inducer used can have significant effects on the total amount of aggregation as well as the effect missense mutations can have on total aggregation relative to wild type tau (WT). Although the P301S mutation caused a significant increase in ARA-induced aggregation when compared to WT, there was no statistically significant difference when induced with P100 polyphosphate. Interestingly, using P100 as an inducer, the P270S mutation did result in a significant decrease in aggregation, however this result was not seen with any of the other inducers. When induced with the longer chain P700 polyphosphate, a significant difference was seen when comparing P301S to WT. Although these results were reproducible among independent experiments, they were relatively subtle with a difference of less than 20% when comparing WT to P301S (ARA and P700) or P270S (P100). In contrast, the effect of the P301S mutation on RNA induced aggregation was much more noticeable. In the case of small

RNA, P301S aggregated approximately 3-fold more when compared to WT tau. Similarly, when induced with long RNA, P301S caused over a 5-fold increase in aggregation.
In addition, LLS experiments showed the P332S mutation increased aggregation when induced with ARA. This was further supported by the significant increase in filament mass as shown by TEM. Interestingly, P364S induced with long RNA also showed a significant increase in light scattering, however TEM analysis did not reveal any filaments, suggesting the possibility that this mutation enhances tau's interaction with RNA, but not resulting in the formation of stable fibrils.

Transmission electron microscopy revealed that filaments induced with the shorter chain P100 polyphosphate had a much longer average filament length than those induced with long chain P700 polyphosphate (compare figure 22 B and E to figure 23 B and E). Further comparisons of P to S mutations on filament length show substantial differences between the different inducer classes. For example; the effect of the P364S mutation on total aggregation, average filament length, and number of filaments when induced with ARA is not significantly different from WT. However, in the case of both P100 and P700 there appears to be significantly fewer, but longer filaments.

The influence of polyphosphate chain length on average tau filament length has previously been studied from a biophysical perspective[125]. This finding is further supported by our TEM and kinetic studies. For example, in the case of P100 induced aggregates average polymerization rates of WT and each of the P to S mutants are slower than the rate of their respective P700

induced counterparts. This suggests that filaments induced with P100 form more slowly but result in longer filaments than those induced with P700.

The filaments induced with both P100 and P700 appear to follow a nucleation independent mechanism, or a fast nucleation step as shown by the extremely short lag time, especially in the case of WT and P301S tau. Although, further investigations would be required to fully elucidate the mechanism of polyphosphate aggregation. Interestingly, the P301S mutation causes an increase in maximum aggregation for ARA, a slight but not significant increase for P100, and no change to P700 induced filaments. However, in the case of ARA induced filaments P301S has a significantly longer lag time with a slightly slower rate of aggregation, when compared to WT. This increased lag time suggests the P301S mutation slows the nucleation step. Conversely, in the case of both P100 and P700, neither WT, nor P301S have a measurable lag time, but the P301S rate of aggregation is substantially faster. This shows a fundamental difference between polyphosphate and ARA induced filaments in regards to the effect of the P301S mutation on aggregation kinetics and therefore warrants further investigation.

When completing kinetic studies using long RNA (figure 34), and to a lesser extent small RNA (data not shown), as an inducer molecule we witnessed a strange phenomenon where initial addition of the inducer caused almost immediate light scattering that then faded over a period of approximately 28 hours. This was then followed by a steady increase of light scattering between 28 and 72 hours. Samples prepared for TEM imaging at time zero showed no filaments present. However, images of samples at the 72-hour time point showed a proportional amount of tau filaments to the amount of light scattering. Initial light scattering may be due to an immediate

interaction between RNA and monomeric tau that is then followed by a dissociation and subsequent filament formation. Alternatively, initial light scattering could be RNA acting as a crowding agent causing liquid-liquid phase separation that form highly concentrated droplets of monomeric tau that are able to scatter light. However, more extensive studies would be required to fully understand this process and was considered outside the scope of this initial investigation.

Of the 9 tau based therapeutics that are currently in clinical trials, 6 are either passive or active immunotherapies[61]. Understanding the effect of different disease related mutations and *in vitro* inducer molecules have on antibody affinity toward tau aggregates can therefore not only provide useful characterization information, but may also be useful in the development of future therapeutics. From our current study, the clearest example of how different inducer molecules can affect antibody reactivity is the ability of T22 to detect ARA induced filaments in an ELISA, but not filaments induced by either of the polyphosphate or RNA inducers. However, T22 was reactive against RNA and polyphosphate when used in a dot blot assay. This suggests that the polyanion inducer molecules block the T22 binding, but this interaction can be disrupted through thorough wash steps that occur prior to interaction between aggregate samples and the T22 antibody. In addition, the T22 ELISA experiments also revealed that the P301S, P332S, and P364S mutations significantly decreased T22 reactive species when induced with ARA. Although the affinity of TOC and TNT antibodies does not appear to be influenced by these specific mutations, TOC does appear to show a higher affinity towards ARA induced filaments compared to fibrils induced by P100 and P700 (although the difference is not significant for P700, figure 32). Although TOC reactivity is also significantly lower for RNA induced fibrils this is most likely due to an overall lesser amount of total aggregation.

Together, these findings suggest that both the inducer molecule and disease relevant mutations can play an important role in the affinity of conformationally sensitive antibodies. In addition, different inducer molecules can provide contrasting information regarding the effects of disease relation mutations on total aggregation, filament morphology, and aggregation kinetics. Based on the data we have collected, it appears the P301S mutations has the most consistent effect on tau aggregation when comparing P to S mutations within the PGGG motif. However, other P to S mutations can also have significant effects on aggregation depending on the inducer molecule used and/or the method of detection. Until we can identify *in vitro* models that have been proven to be disease relevant, an abundance of caution should be taken when using a single inducer molecule. In particular, multiple inducer systems may be required for studies that aim to identify potential therapeutics or characterize the effects of tau aggregation conditions, disease related mutations, or post-translational modifications.

Supplemental Information:

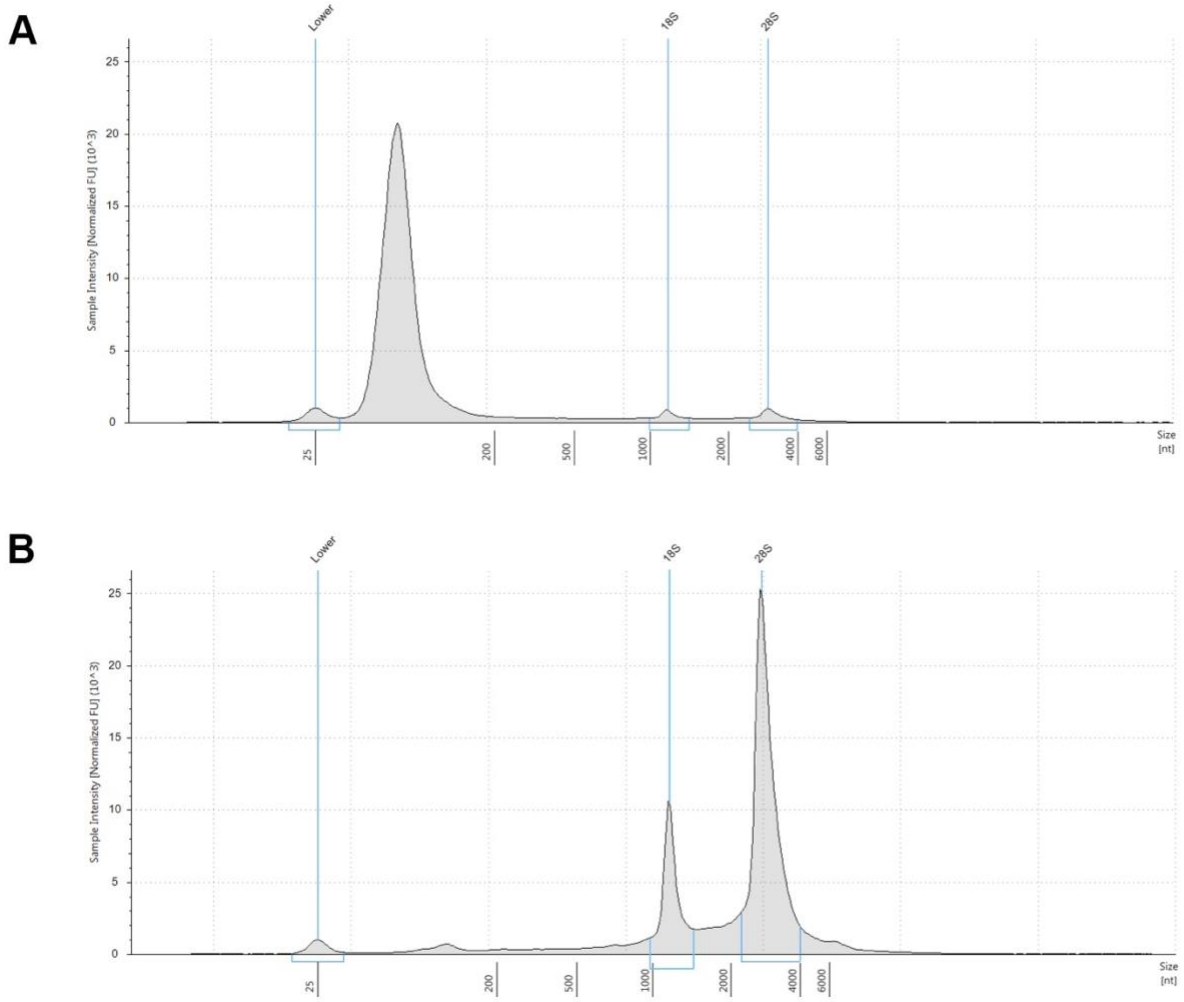

Figure 30: Tapestation results for A) small RNA (<200 nts), and B) long RNA (>200 nts).
Y-axis for each graph represents the band intensity based on tapestation gel image. X-axis represents the molecular weight of the band in number of nucleotides (nt). Vertical blue line labelled "Lower" at approximately 25 nt on the X-axis, represents the dye front and therefore masks any potential RNA species within the size range illustrated by the bracket on the X-axis. Vertical blue lines labelled "18S" (~900 nt -1,400 nt) and "28S" (~ 2,200 nt – 4,000 nt) indicate the expected location of 18S and 28S ribosomal RNA, respectively. Isolation of small and long RNA from total RNA was completed by Madison J. McGuire and myself.

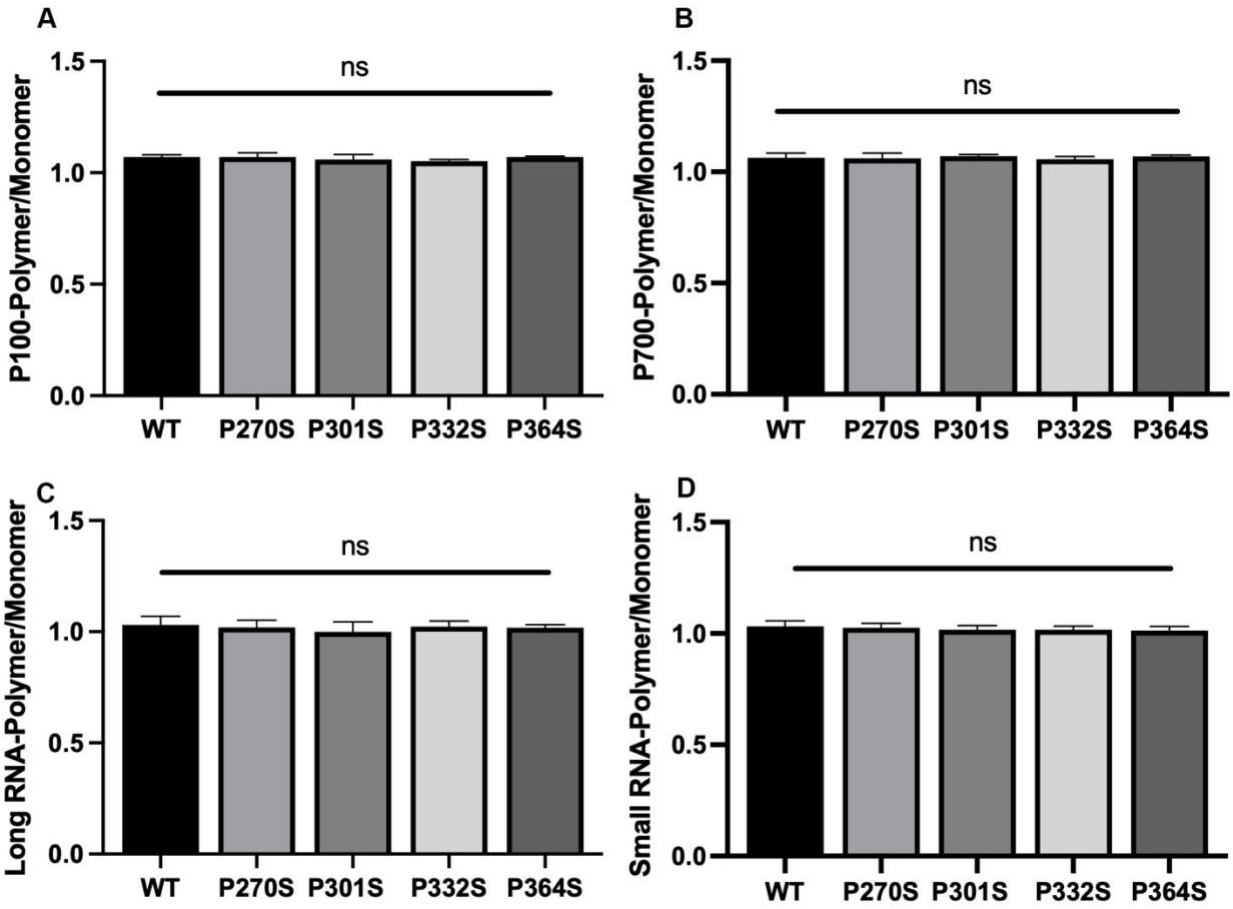

Figure 31: Polyphosphate and RNA 5,7,12 ELISA.
ELISA results using 5,7,12 monoclonal total-tau antibody mixture as a capture antibody. The signal for each aggregate was divided by the signal for monomeric tau (either WT or the respective P to S mutations). Y axis represents a fraction of monomeric tau signal (e.g. 1=100%). Data were analyzed using a Tukey's multiple comparison test and "ns" represents no significant difference.

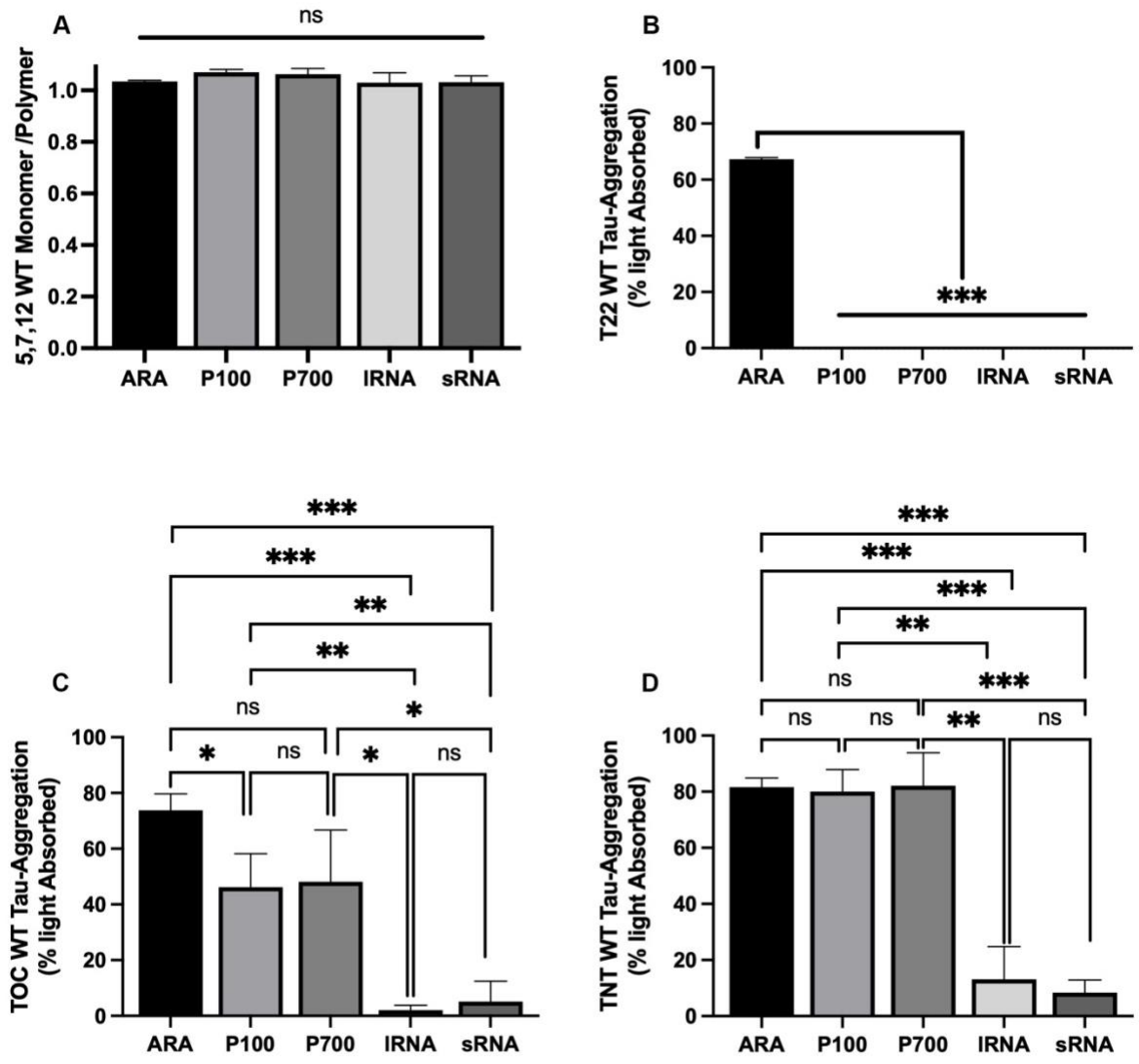

Figure 32: Immunoreactivity of WT HT40 using ARA, P100, P700, long RNA, and small RNA as inducer. ELISA results using 5,7,12 monoclonal total-tau antibody mixture as a capture antibody. The signal for each aggregate was divided by the signal for monomeric WT 2N4R tau. Y axis represents a fraction of monomeric tau signal (e.g. 1=100%). B-D, ELISA results of conformationally sensitive antibodies T22 (B), TOC1 (C), and TNT (D). Y-axis represents % light absorbed value (converted from A450 reading). Error bars represent SD of 3 independent experiments and data sets were compared using an un-paired t-test multiple comparison test.

$* p \leq 0.05;\ ** p \leq 0.01;\ *** p \leq 0.001.$

Reactivity of T22 antibody in dot-blot assay:

Similar to filaments induced by P100 and P700 polyphosphate, neither RNA species formed T22 reactive aggregates. To ensure this was not an assay specific result, we completed a dot blot assay detecting with T22 antibody against samples of WT and P301S induced aggregates (figure 33). In this assay, polyphosphate and RNA samples did form T22 reactive species, however, although repeated experiments showed positive reactivity, the values had a high amount of variability (~50%) and therefore, we were unable to complete meaningful comparison studies.

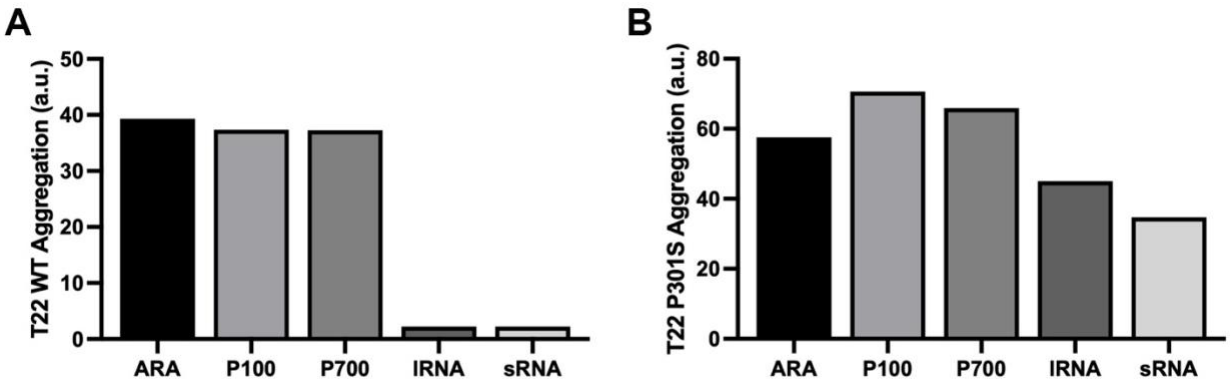

Figure 33: Dot-blot assay detecting endpoint aggregates using T22 antibody.
A) Comparison of WT tau induced with ARA, P100, P700, long RNA, and small RNA. B) Comparison of P301S tau induced with ARA, P100, P700, long RNA, and small RNA. Y-axis represent light intensity as measure using histogram function in Adobe Photoshop, and both data sets have been zeroed against a no inducer monomer control (n=1).

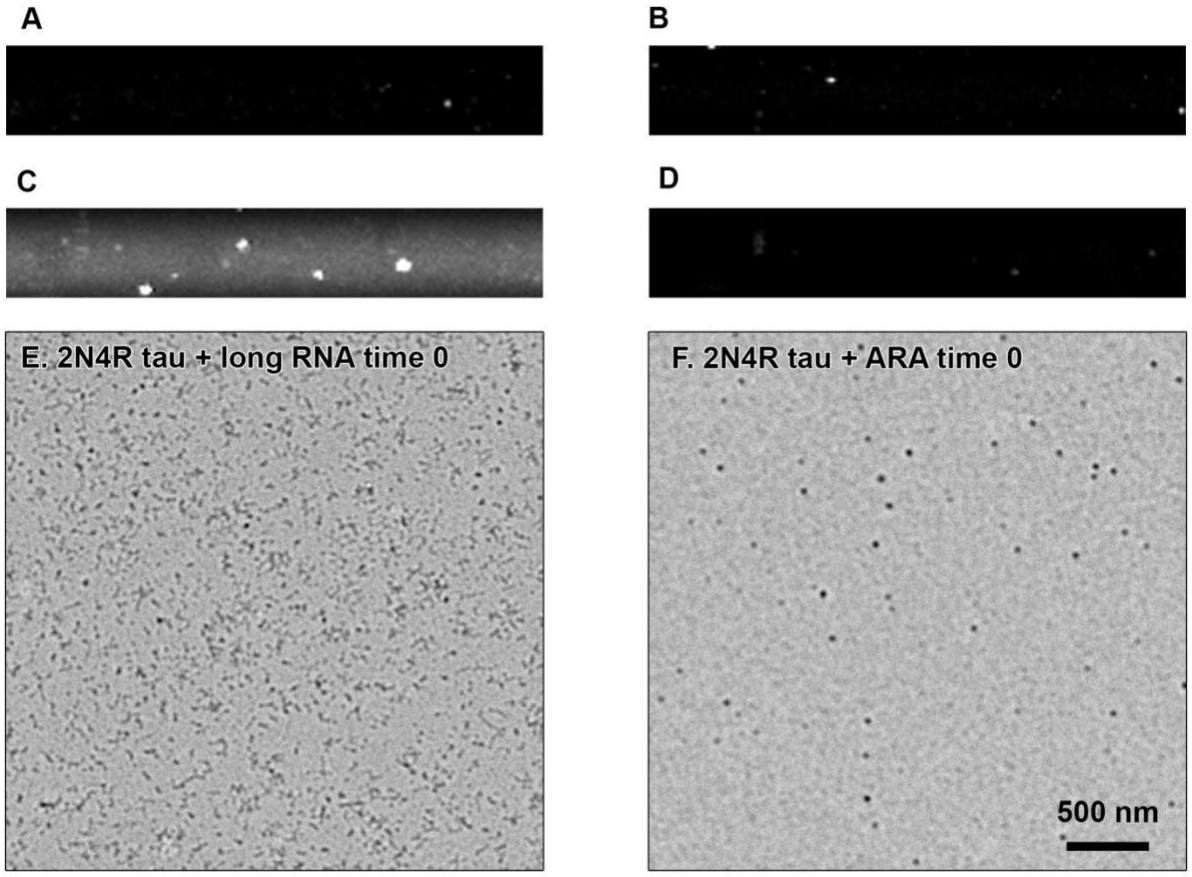

Figure 34: Laser light scattering and TEM upon the addition of long RNA, or ARA, to monomeric WT tau at time zero.
Right-angled laser light scattering images of rRNA only (A), 2N4R tau only (B), RNA + 2N4R tau at time zero (C) and the accompanying micrograph (E), ARA + 2N4R tau at time zero (D) and the accompanying micrograph (F). LLS images were taken at an aperture of f/5.6 and scale bar in figure F represents 500 nm for both EM micrographs.

Chapter 4: Techniques for forming *in vitro* tau aggregates

4.1: Introduction

Forming disease relevant *in vitro* tau aggregates will be a powerful tool in the identification of future therapeutics and our understanding of how tau aggregation relates to disease. Although high-resolution structural data would be useful for showing similarities of *in vitro* filaments to filaments isolated from tauopathies, understanding how different filaments interact with common assays used within the field is also necessary for future characterization studies. This chapter is a short guide and summary of what we have learned working with common tau aggregation inducer molecules and other aggregation inducing techniques. It is a collection of preliminary unpublished data and information highlighted from the literature that has been collated to identify methods, hints, and tips for working with these aggregation inducing techniques in the context of using them to model tau aggregation in disease, and therefore, be used for future drug screening and aggregation modeling studies. In addition, we have highlighted common techniques for studying protein aggregation and a brief discussion of the advantages and disadvantages of each technique. As well as how the limitations of these techniques pertain to aggregation inhibitor screening studies, studying molecular dynamics of tau aggregation, and their specific use in relation to the aggregation inducing techniques covered in this chapter.

It should be noted that there are other published studies and reviews that have also completed comparisons of different classes of inducer molecules[138] as well as more in depth studies of the interactions between tau and certain inducers[136, 139]. However, this work will focus specifically on the practical aspects of using inducer molecules to model tau aggregation in disease and why these inducers may, or may not, be forming disease relevant polymorphs. In addition to small

molecule inducers, the energy barrier for tau aggregation can also be overcome in the presence of other proteins, pro-aggregate mutations, and divalent metal cations such as Zn^{+2} [74, 132, 140]. In order to limit the scope of this study we will focus on using small molecules, authentic filament seeds isolated from tauopathies, and alternative incubation conditions in order to induce wild type recombinant human tau aggregation.

An alternative method to inducing tau aggregation *in vitro* is to use authentic tau fibrils isolated from disease as seeds to promote fibrilization of recombinant protein. Typically, studies using seeded aggregates use a pro-aggregate mutation (e.g. P301S) or low concentrations of heparin to promote seeding. Based the close proximity of the P301S mutation to the ordered fibril core of filaments isolated from disease[41] and the fact that heparin induced filaments are dissimilar to filaments from disease[59], it is likely that these methods result in fibrils that differ structurally from the original seed being used.

We have utilized a technique that allows for WT recombinant tau to aggregate using AD or PSP derived seeds without the presence of an inducer molecule. However, we do not yet know if these fibrils are propagating the original seed structure with high fidelity to the original seed structure. In addition, we have found that a similar technique will induce the aggregation of full length 3R tau without the presence of seeds. The resulting fibrils are thioflavin S positive, and share some morphological similarities to fibrils isolated from Pick's disease (a 3R tauopathy). These preliminary findings provide alternative methods for inducing aggregation *in vitro*. Further optimization and characterization studies would be required to identify if these techniques could be used to form disease relevant *in vitro* structures.

4.2: Techniques for studying *in vitro* induced tau aggregation

Common methods for studying *in vitro* induced tau filaments include transmission electron microscopy, thioflavin S or thioflavin T fluorescence, right-angle laser light scattering, ultracentrifugation, immunoassays such as filter trap or ELISA[93, 100, 106, 141].

Transmission electron microscopy:

Transmission electron microscopy (TEM) is a powerful tool in the study of tau aggregation. It can be used to study filament morphology, filament length, and number of filaments. In addition, techniques such as immuno-labelling can also provide crude structural information of tau fibrils based on the binding of monoclonal antibodies with high affinity toward specific regions of tau. For example, to validate cryo-EM findings that the ordered cores of AD filaments were made up of MTBRs 3 and 4, Falcon et. al. utilized four different monoclonal antibodies that bind to either MTBR 1, 2, 3, or 4 to complete gold nanoparticle immuno-EM[38]. Labelled tau filaments could then be visualized using TEM to identify which MTBR domains are accessible to the antibodies and which have been incorporated into the ordered fibril core.

Most studies utilize TEM as a qualitative secondary validation assay to support findings from other aggregation studies (light scattering and thioflavin fluorescence). Under well controlled conditions, TEM can be used as a semi-quantitative method for comparing different samples. However, this is a low throughput, time intensive technique due to only being able to image one sample at a time, the need for access to expensive core facilities, and the need of labor-intensive image analysis. In addition, as different inducer molecules, mutations, and post-translation modifications can greatly influence filament length, spatial distribution of filaments on the grid,

and number of filaments, quantitative TEM is not appropriate for all samples. For example; polyanionic inducers such as heparin, can form extremely long filaments when compared to those induced by ARA[123]. Also, using pseudophosphorylation (a Ser, Thr, or Tyr residue mutated to negatively charged Asp or Glu residue to mimic phosphorylation) as a proxy for studying post-translational modification can result in much longer filaments than WT tau (see figure 35 comparing WT 2N4R ARA induced fibrils to 11Phos 2N4R ARA induced fibrils). The longer filaments can greatly influence the distribution of protein on the grid and therefore reduce the statistical power of the assay. This can be partially mitigated by taking more images of each sample, however, this also results in more time and labor-intensive data collection and analysis. Other limitations of this assay include: difficulty in quantifying aggregates below 25 nm in length, potential filament breakage when being fixed to the grid may change measured filament length, addition of co-factors, small molecules, and post-translational modifications (PTMs) may result in poor filament staining or lower binding affinity to the EM grid, heterogenous samples may provide erroneous results due to the limited sample size.

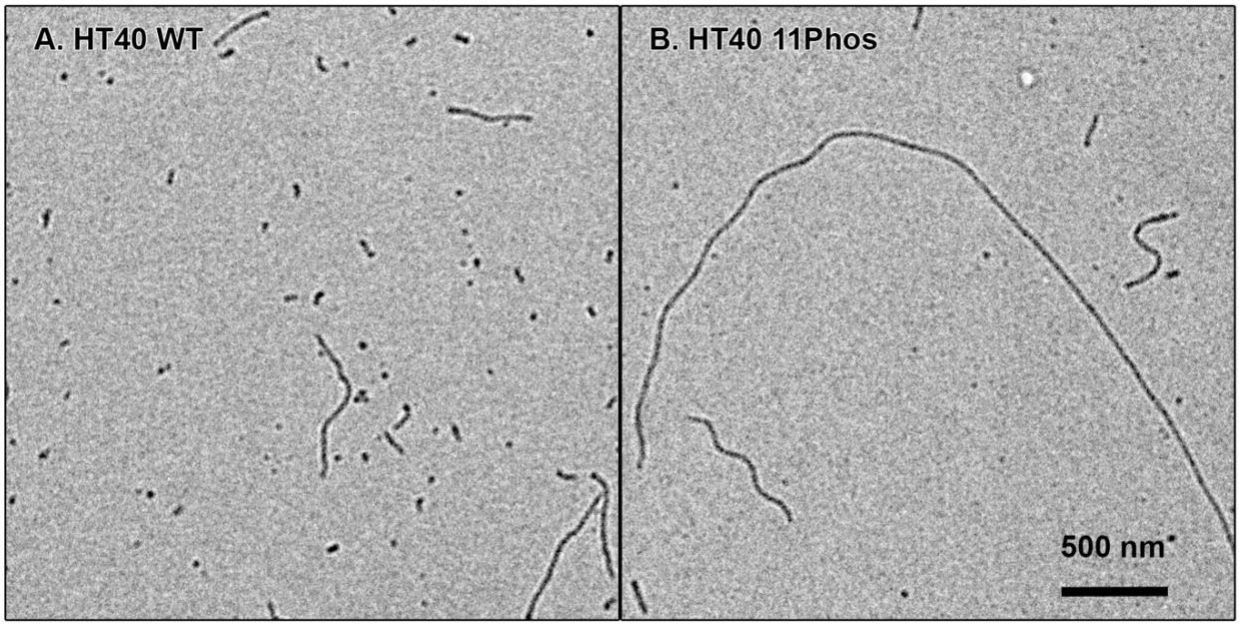

Figure 35: HT40 WT vs HT40 11Phos.
Representative TEM micrographs of WT HT40 (A), and the HT40 11Phos mutant with 11 pseudophosphorylated residues (B). Scale bar in B represents 500 nm for both images.

Thioflavin fluorescence:

Thioflavin S (ThS) and thioflavin T (ThT) fluorescence are useful tools for identifying endpoint total amounts of polymerization and identifying if aggregates form thioflavin positive inclusions, a common attribute of amyloids in disease. The assay relies on the principle that the fluorescent dye, ThS or ThT, will bind to amyloid folds between β-strands and this binding results in a shift of the fluorophore's emission spectra[142]. This spectral shift can then be detected using a fluorescence spectrometer and the intensity of emitted light can be measured as being proportional to amyloid fold formation. However, there are several instances in which thioflavin fluorescence is not a suitable assay. The use of other compounds such as small molecule inhibitors may give false positive or false negative results by increasing, quenching, or modulating the thioflavin fluorescence signal (figure 13, chapter 2). Certain inducer molecules

such as RNA will also have a false negative effect on thioflavin S fluorescence and provide false positive thioflavin T fluorescence. Commonly used fluorescent tags such as GFP can also quench thioflavin fluorescence. In addition, thioflavin based techniques, such as RT-Quik (real-time quaking induced conversion) are often used for studying aggregation kinetics, *in vitro* seeding, or prion-like mechanisms of action. However, it has previously been shown that at high concentrations thioflavin dyes will induce tau fibrilization[138]. In addition, thioflavin T is known to bind monomeric protein as well as amyloid aggregates, therefore, it is possible that it may influence the structure of the fibril fold being formed when used as a reporter for aggregation kinetic studies[138]. When comparing samples of tau aggregates, filament length distribution can also disproportionately affect the amount of measured aggregation. For example; at equimolar concentrations long fibrils may have more binding sites than small oligomers, filament flexibility may allow for steric hinderance of thioflavin dyes, thioflavin dyes may have higher affinity toward certain amyloid structures.

Right-Angle Laser light scattering:

Although there are several different light scattering techniques that can be used to quantify protein aggregation, such as dynamic light scattering (DLS) and multi-angle light scattering (MALS), this chapter will primarily refer to light scattering in the context right-angle laser light scattering (LLS). However, many of the limitations and issues faced using LLS will also apply to DLS and MALS. A significant advantage LLS has over TEM and thioflavin fluorescence, is that this assay is non-invasive and can be used on samples at any time throughout the aggregation process allowing for the collection of kinetic data and endpoint data without modifying buffer conditions of the filaments being formed. However, there are several limitations to the use of this

assay for studying *in vitro* aggregation. For example; small molecules often have light absorbing or light scattering properties, this can be due to specific chromophores within the molecule or the overall hydrophobicity of the compound causing poor solubility in aqueous solutions. In addition, certain inducer molecules can also interfere with light scattering, especially long chain polyanions at high concentrations, planar aromatic dyes, or fatty acids above their critical micelle concentration (CMC). As found with the RNA kinetic experiments in chapter 3, certain inducer molecules may interact with tau protein without forming stable filaments, while still scattering light. In addition, samples isolated from tissue or cell culture will also contain many large contaminants that scatter light even when diluted. This should be carefully considered when using LLS as a primary assay of seeding recombinant protein with tau fibrils isolated from brain tissue. Similar to ThS and TEM, samples with dissimilar size distributions will scatter light disproportionately, and longer more flexible fibrils may affect the radius of gyration and therefore the amount of light scattered. Samples that are smaller than $1/20^{th}$ of the wavelength of light being used will also scatter light disproportionately.

Ultracentrifugation:

Ultracentrifugation can be a useful technique to identify the presence of, and separate, different tau species based on size and solubility. For example, a sucrose step gradient will allow the isolation of oligomer enriched fractions from monomeric tau and larger tau fibrils[100]. However, these methods are less sensitive than those previously described, and relatively time intensive and low throughput. The effect of tau aggregate size and solubility on their sedimentation coefficient can greatly affect results from ultracentrifugation and therefore should be carefully considered when using as method for validation of aggregation, inhibition, and disassembly of

tau fibrils. In addition, it is not fully known what effect high speed centrifugation can have on monomeric tau and aggregated tau. Therefore, caution should be used when using isolated samples to complete assays further downstream. Addition of certain co-factors and small molecular probes may cause samples to adhere to centrifuge tubes and result in poor rates of sample recovery.

Immunoassays:

Immunoassays (IA) can include a range of techniques that utilize specific antibodies that either bind to particular regions of tau, post-translational modifications, conformations of either monomeric or aggregated tau species. The most common IA based techniques used to study *in vitro* tau aggregation are filter trap, dot-blot, and ELISA.

A filter trap assay requires the samples to be added to a pre-wetted membrane housed in a vacuum manifold and then pulled through the membrane to isolate large tau aggregates from monomeric protein. The membrane can then be blocked and subsequently probed using different antibodies. A dot-blot assay is similar, but typically the sample is allowed to air dry on a dry nitrocellulose membrane before being blocked and treated with detection antibodies. Both of these techniques utilize specific antibodies as an indirect reporter. Although there are many advantages and ways these techniques can be used, there are also several things that should be carefully considered. A filter trap assay relies on the electrostatic interactions between the highly charged nitrocellulose membrane and protein of interest. It is possible that these interactions could be disrupted by the addition of molecular probes, such as potential inhibitors. Also, small enough oligomers may be pulled through the membrane, providing false positive results.

Similarly, the binding of tau to a dry nitrocellulose membrane may cause conformational changes to the protein such as PAD exposure, or filament breakage.

ELISA assays can utilize the same antibody tools used in filter-trap and dot-blot assays, whilst relieving the mechanical stress on monomeric protein and filaments. This is beneficial for several reasons, the sample is allowed to directly interact with the antibody, rather than being 'fixed' to a membrane first, allowing heterogenous samples isolated from disease to be used. In addition, through the use of optimized sandwich ELISA conditions, this method can also be highly sensitive. Despite these advantages, ELISAs can be prone to false negative results due to inducer molecules or inhibitors blocking the epitope of the capture antibody. The interactions are often interrupted during dot-blot and filter-trap assays due to samples being "fixed" to a solid substrate and then washed prior to the addition of a primary antibody. In addition, both techniques require the epitope of the antibody to be accessible and this accessibility could be limited by increased filament flexibility. Therefore, it is often useful to characterize tau species through a range of different IA techniques and multiple different detection antibodies to ensure accuracy of the results.

4.3: Utilization of diverse *in vitro* tau aggregation inducer molecules

Below is a brief introduction to six commonly used *in vitro* tau aggregation inducer molecules. In addition, table 10 highlights buffer conditions, incubation times, and compatible assays for each of the different inducers.

Heparin:

Heparin induced filaments have long been used as a standard model for studying *in vitro* tau aggregation and is the most prevalent inducer used research studies. Heparin, not to be confused with haparan sulfate, is a heterogenous highly negatively charged biomolecule that is primarily found in mast cells. During periods of inflammation, heparin is released from mast cells and interacts with several different proteins and cofactors to influence coagulation and inflammation cascades, and can have many different functions and binding partners[143]. Due to tau filaments formed in the presence of heparin often having a PHF-like morphology, it has long been thought that heparin is an appropriate inducer for studying tau aggregation. Sonicated tau fibrils induced by heparin are known to seed tau aggregation in cell culture and mice, and also spread in a prion like fashion[91]. In addition, higher concentrations of heparin are known to competitively inhibit tau binding to cell surface heparan sulfate proteoglycans receptors (HSPGs) and therefore block prion-like spread of tau in cell culture[144]. Typically, conditions for heparin induced tau filaments require a 1:4 heparin to tau ratio, low ionic strength (15 mM-25 mM NaCl), incubation times of 48-96 hours at 37 °C. The resulting filaments are often extremely long when compared to typical fibrils isolated from disease, but will form twisted filaments that appear to have a gross morphology similar to fibrils isolated from disease. However, despite these similarities, both functionally and morphologically, recent high-resolution structural studies of heparin induced filaments and authentic filaments isolated from disease have shown that the structures formed by heparin are unique[41, 59, 114]. Although it is possible that changes to heparin, such as sulfation patterns, chain length, and buffer conditions may result in filaments with more biologically relevant morphologies[145]. Based on the structural data that is currently available, for the purposes

of studying aggregation dynamics, mutations, and screening for potential therapeutic agents, heparin is likely not an appropriate tool.

Arachidonic acid (ARA):

ARA is a polyunsaturated 20-carbon fatty acid with four cis double bonds positioned at carbons 5,8,11, and 14 and is ubiquitous in mammalian cells[146]. ARA is a precursor to a group of tightly regulated biomolecules known as eicosanoids that comprise of subgroups of inflammatory mediators including leukotrienes, prostaglandins, thromboxanes, and lipoxins[147]. Despite the tight regulation of ARA and its derivatives, during times of oxidative stress, the cellular concentration of ARA increases and therefore disrupts homeostasis within the cell[148]. The tau filaments formed in the presence of ARA are relatively short when compared to polyanions (heparin, RNA, polyphosphate), however the length distribution is more similar to the distribution of filaments isolated from disease. In addition, ARA-fibril's average width is similar to the straight filaments isolated from Alzheimer's disease. Fibrils formed after extended incubation with ARA (2-7 days at 37 °C) appear to form more PHF-like filaments[99]. However, to date we have no high-resolution structures of ARA induced fibrils and therefore we cannot draw a full comparison to fibril structures currently isolated from disease.

Ribonucleic acid (RNA):

RNA is a ubiquitous class of biomolecules that has a diverse range of functions including binding to and interacting with other biomolecules such as proteins, DNA, lipids, and other metabolites. RNA can be sub-categorized into three groups: 1) RNA involved with protein transcription and translation which primarily comprise of messenger RNA (mRNA), ribosomal

RNA (rRNA), and transfer RNA (tRNA). 2) RNAs that perform regulatory roles within the cell and extracellular environment such as micro RNA (miRNA), small interfering RNA (siRNA), short hairpin RNA (shRNA), short non-coding RNA (sncRNA), long non-coding RNA (lncRNA) and others. 3) RNAs that are thought to be parasitic including retrotransposons, RNA viruses, CRISPR RNAs as well as others[149]. Although this is not an exhaustive list, it is clear that the role of RNA molecules is extremely diverse. In regards to inducing tau aggregation, we do not yet fully understand how different classes of RNA can influence tau aggregation. For example; some studies have shown that tRNAs and rRNA can induce PHF-like filaments, and that tRNA is overwhelmingly the most abundant RNA type that is associated with tau isolated from mammalian cell culture[127, 128]. In our studies we have found that RNA isolated from HEK 293T cells can induce tau aggregation at concentrations 5- 25 ng/μL. Interestingly, we found that the size of RNA isolated, <200 nts and >200 nts, can have significantly different effects on the total amount of aggregation, average filaments length, average number of filaments, and immunoreactivity, as well as assembly of tau with single missense mutations (see chapter 3, table 5). However, it should be noted that we do not know if these differences are due to a difference in RNA chain length, sequence, or secondary structure. In addition to characterizing the filaments formed using RNA as an inducer, there may be novel molecular interactions that take place during the aggregation process. For example, some studies have shown that RNA can act as a crowding agent leading to liquid-liquid phase separation of tau in aqueous solution[128].

Polyphosphate (PP):

PP is thought to have a wide range of functions within eukaryotes and prokaryotes, many of which have not yet been fully understood. It has been shown to increase amyloidogenic

aggregation of a range of different proteins including those associated with neurodegenerative disease, alpha synuclein, Aβ-42, and tau[150]. We found PP was effective at inducing tau aggregation within a concentration range of 1 - 25 ng/μL, with an optimal concentration of 10 ng/μL. Interestingly, the optimal PP molar concentration is approximately 94 μM in terms of single Pi subunits, similar to concentration ranges detected in brain tissue of some mammals (~95 μM)[151]. PP chain lengths isolated from mammalian cells and brain tissue range from 50-800 units[151, 152]. We chose to use average chain lengths of 100 units (P100) and 700 units (P700) to stay within this this physiological range. Although the aggregation kinetics of PP induced tau filaments is relatively fast when compared to other polyanions, e.g heparin, we completed all reactions by incubating for 48 hours at 37 °C as differences in the PP chain length can have significant impacts on the rate of aggregation (see chapter 3).

Congo red (CR):

CR is a planar aromatic dye that has been used to stain amyloids for almost a century[153]. It can be used to stain β-sheet enriched structures both in vitro and in vivo. In addition to being able to stain amyloids formed by protein such as Aβ and tau, CR can also be used as an inducer molecules for tau aggregation[138]. It is thought that CR binds to amyloids through polar interactions with β-strand amyloid backbones, however, this has not been shown to be the case when CR is used as an inducer molecule[154]. In our experiments we found the optimal condition for 2N4R tau fibrilization with CR was a concentration of 12.5 μM (CR) and 2 μM (2N4R tau) in our standard polymerization buffer (100 mM NaCl, 10mM HEPES (pH 7.64), 5 mM DTT, 0.1mM EDTA, 1% DMSO) for 48 hours at 37 °C. The filaments formed under these conditions are much shorter and wider than the other inducer molecules discussed here, and they appear to

have a twisted ribbon-like morphology. Unlike heparin, polyphosphate, and arachidonic acid, due to absorbance properties CR induced aggregates cannot be monitored using standard fluorescent dye based aggregation assays, such as thioflavin T (ThT) and thioflavin S (ThS). Similarly, when used in laser light scattering assays, the concentration of CR needs to be kept relatively low to avoid high noise to signal ratios. Based on the gross morphological differences between CR fibrils and authentic fibrils isolated from disease, interactions with standard aggregation assays, the fact that CR is not present in mammals it is unlikely that CR would be a useful inducer to model disease-relevant tau filaments for *in vitro* study.

Thiazine red (TR):

Another aromatic dye that has traditionally been used to stain amyloids in tissue and *in vitro*, is TR. Despite thiazine red also being a planar aromatic dye, the tau filaments formed in its presence do not share the same morphological characteristics as CR filaments. In an attempt to optimize conditions for polymerizing tau in the presence of TR we found that it was extremely difficult to get consistent results. Therefore, we completed some preliminary kinetics study on TR induced aggregation and found that the LLS signal appeared to increase after approximately 24 hours, but then decreased between 24 hrs and 112 hrs. We found similar results when taking TEM images of the samples at different time points. This suggests that filaments induced with TR are either non-stable and spontaneously depolymerize, or over time TR induced filaments adhere to the reaction vessel used (1.7 mL microcentrifuge tubes or LLS cuvette). In either case,

TR induced filaments would likely not be a useful *in vitro* inducer model for the purposes of studying aggregation dynamics, compound library screening, or studying aggregation conditions.

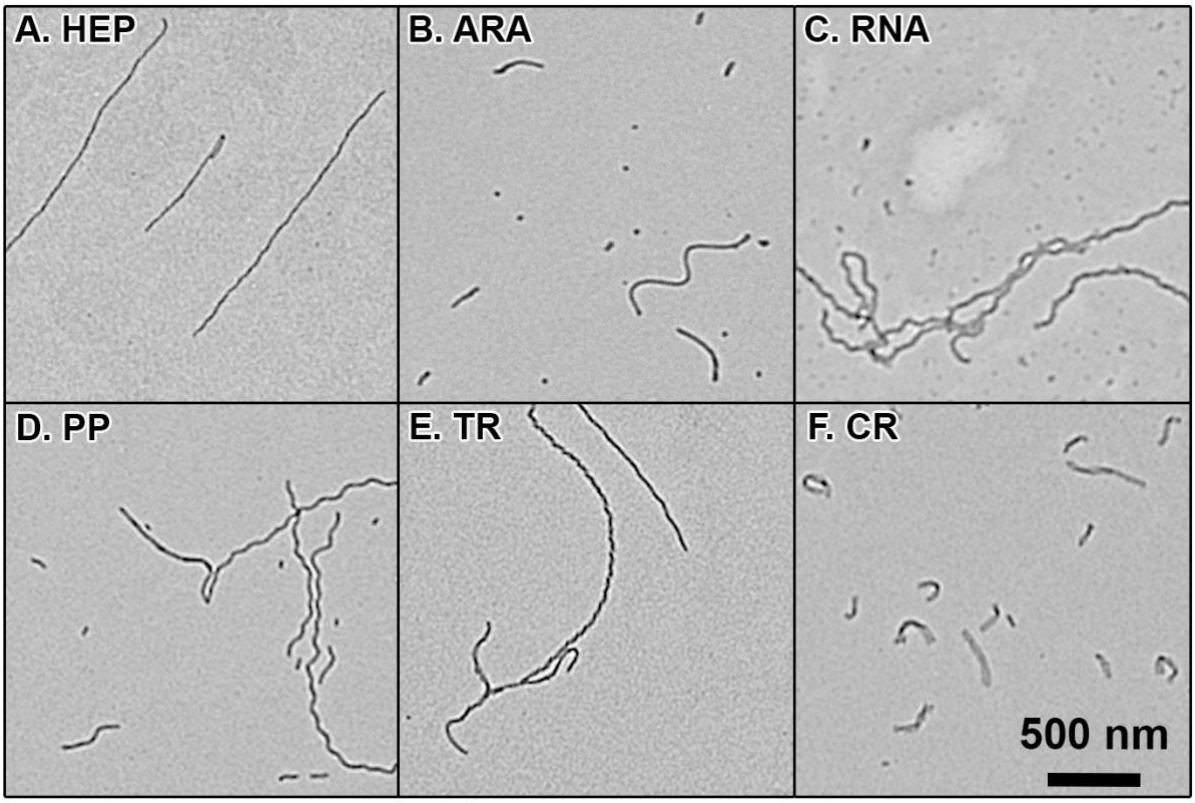

Figure 36: Representative TEM micrographs of different *in vitro* inducers of recombinant WT 2N4R tau. A) 2 µM tau in the presence of 0.5 µM heparin incubated at 37°C for 72 hours. B) 2 µM tau in the presence of 75 µM ARA incubated at 25°C for 20 hours. C) 2 µM tau in presence of 12.5 ng/µL total RNA isolated from Aspergillus nidulans for 72 hours at 37°C. D) 2 µM tau incubated with 10 ng/µL mixed length polyphosphate for 72 hours at 37°C. E) 2 µM tau incubated with 100 µM thiazine red for 72 hours at 37°C. F) 2 µM tau incubated with 50 µM Congo red for 72 hours at 37°C. All images were taken at 5,000X magnification and scale bar in figure F represents 500 nm for each micrograph.

Table 6: Summary of *in vitro* inducer conditions and assay compatibility.
*Denotes that inducer is not be fully compatible with the assay, either due to increased variability, or increase background signal. See section 4.2.2 for details.

Table 6: Summary of inducer conditions

(All inducer molecules form fibrils in a standard polymerization buffer containing 5 mM DTT, 10 mM HEPES, 0.1 mM EDTA, pH 7.64, 2 µM 2N4R recombinant tau, and NaCl concentration as indicated below)

Inducer	**Incubation temperature**	**Incubation time**	**NaCl concentration**	**Compatible assays**
Heparin	37°C	72 hours	15-25 µM	TEM, ThS, ThT, LLS, Immunoassays
ARA	25 °C or 37°C	20 hours	100 µM	TEM, ThS, ThT, LLS, Immunoassays
RNA	37°C	72 hours	25-100 µM	TEM, LLS*, Immunoassays*
Polyphosphate	37°C	48 hours	25 µM	TEM, ThS, ThT, LLS, Immunoassay*
Thiazine Red	37°C	72 hours	25 µM	TEM*, LLS*, Immunoassays*
Congo Red	37°C	72 hours	25 µM	TEM, LLS*, Immunoassays*

4.4: *In vitro* seeding using authentic tau filaments isolated from AD and PSP

As tau is thought to be a prion like protein, filaments isolated from disease have the ability to recruit inert monomeric recombinant tau to form new aggregates. Although this has been shown to occur in mice and cell culture, it is typically done *in vitro* in the presence of heparin, through an inducer templated seeding mechanism, or, by introducing a missense mutation that promotes aggregation (typically the P301S mutation)[44]. Below we describe preliminary findings using a seeding technique using authentic filaments isolated from two different tauopathies (AD and PSP) that does not require the presence of a co-factor such as heparin, any mutation, truncation, or post translation modification to WT recombinant tau.

In vitro AD-PHF seeding of recombinant 2N4R and 2N3R tau:

Based on previous studies by Carlogmagno et. al. and Guo et. al. we have found that by incubating sonicated AD-PHF seeds in the presence of recombinant tau with constant agitation (see materials and methods for details), we can induce seeding without the presence of inducer molecules (figure 37)[155, 156]. Although both 2N4R and 2N3R AD seeded fibrils mostly appear to have a SF morphology and no filaments with the stereotypical AD-PHF morphology defined as having a regular half periodicity of ~80 nm and widths between 8 nm and 20 nm, were observed (compare figures 31B-31D to 31E and 31F). However, when combining equimolar concentrations of 2N4R and 2N3R and adding AD-PHF seeds, occasional paired filaments with apparent regular twists begin to form (Figure 31G). Although, the majority of filaments still have a SF-like morphology. Interestingly, we found that this seeding process could be propagated across several seed generations by sonicating the resulting first generation fibrils (0.75% AD-PHF) and then adding them as seeds to recombinant monomeric protein (0.0375%

AD-PHF). The percentage of AD-PHF refers to the concentration of the original AD-PHF isolated from brain tissue. For example, first generation seeds were formed in the presence of 0.75% of original isolate. Second generation seeding experiments were completed by sonicating first generation fibrils and adding them at a final concentration of 5% to 2 μM monomeric recombinant protein. Therefore, the resulting estimated concentration of original AD-PHFs isolated from tissue in the second generation seeding experiments is 0.0375% of original isolate. At this concentration, sonicated AD-PHF only samples do not scatter light and are undetectable on TEM.

It should be noted, that although the occurrence of detectable first and second generation seeding was highly reproducible in terms of the formation of seeded fibrils, the total amount of monomeric protein converted into fibrils during first generation seeding experiments had a high amount of variability. The amount of monomeric seeding converted into fibrils during second generation experiments appear to be proportional to the total amount of first generation aggregates. For example; high conversion rates during first generation seeding led to higher conversion rates during second generation seeding. However, further studies would be required to understand this relationship between first and second generation seeds. Considering the variability in conversion rates, this would not be a useful *in vitro* model for studying tau aggregation under current conditions. Therefore extensive optimization would be required to ensure reproducible rates of conversion.

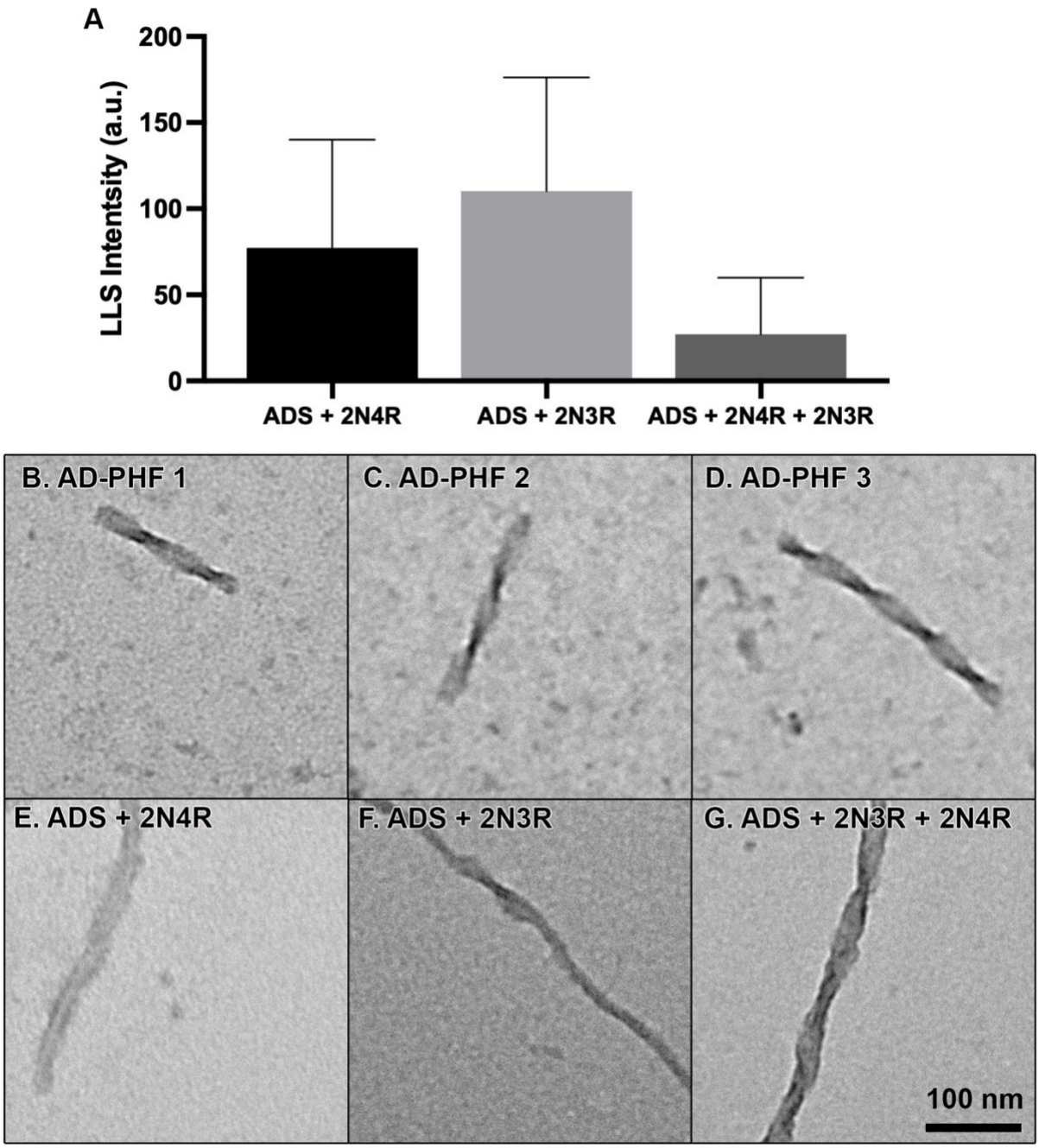

Figure 37: AD PHF seeding of recombinant 2N4R and 2N3R tau measured by LLS and validated with TEM.

A) Seeding as measured by LLS of second generation recombinant tau seeded reactions using sheared PHF seeds isolated from AD with 2N4R monomeric tau (ADS + 2N4R), 2N3R monomeric tau (ADS + 2N3R), and an equimolar mixture of both 2N4R and 2N3R (ADS + 2N4R + 2N3R). TEM micrographs B, C, and D, are representative AD-PHFs isolated from AD brain. A representative micrograph of the straight filaments that form when seeding 2N4R with ADS (E) and 2N3R with ADS (F) compared to the apparent PHF-like filaments formed when seeding a 2N4R and 2N3R mixture using AD-PHF (G). All images were taken at a 30,000X magnification, scale bar in image G represents 100 nm for each micrograph.

In vitro PSP-tau seeding of recombinant 2N4R and 2N3R tau:

Using the same method as described for AD-PHF seeds, we attempted to seed monomeric recombinant 2N3R and 2N4R using tau seeds isolated from another tauopathy, progressive supranuclear palsy, (PSP). The PSP filaments isolated from diseased brain tissue did not have the typical AD-PHF like morphology (figure 38 B-D). Although light scattering when attempting to seed 2N4R with PSP-tau seeds (figure 38A) was higher than typical background noise, no filaments were present when analyzed using TEM (figure 38E). To our surprise, PSP-tau seeds did convert 2N3R monomeric tau into fibrils (figure 38F). Although the majority of these fibrils had a SF morphology, some did appear to form PHF-like structures. Interestingly, aggregates formed when PSP-tau seeds to a mixture of both 2N4R and 2N3R were not filamentous (figure 38G). Similar to seeding experiments using AD-PHF seeds, PSP-tau seeding experiments had a high amount of variability. Further exploration of seeding conditions, and characterization of the resulting filaments would be required before considering this assay as a future *in vitro* model.

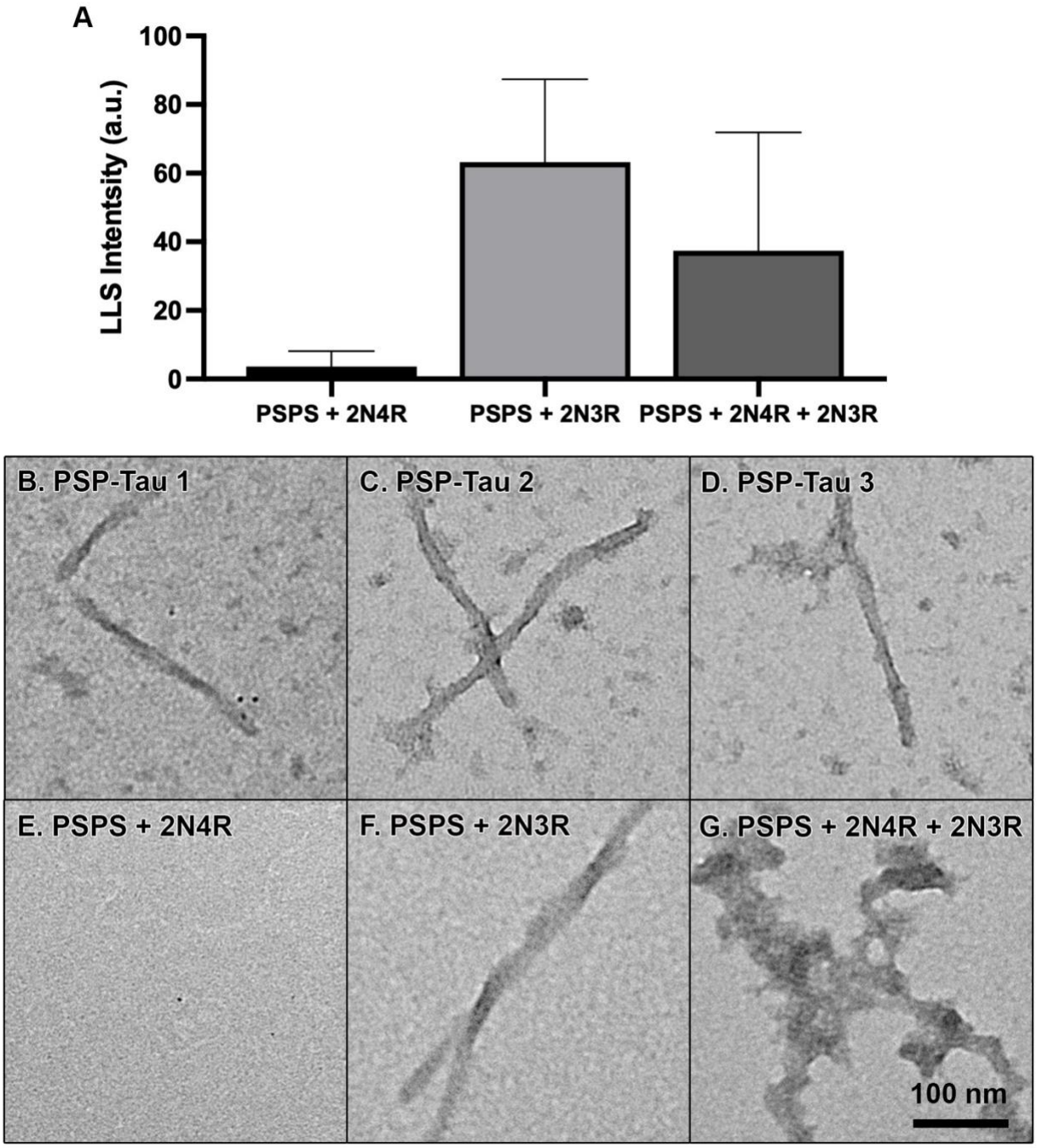

Figure 38: PSP-tau seeding of recombinant 2N3R and 2N4R tau measured by LLS and validated by TEM.
A) Seeding as measured by LLS of second generation recombinant tau seeded reactions using sheared PSP-tau seeds isolated from PSP diseased brain tissue with 2N4R monomeric tau (PSPS + 2N4R), 2N3R monomeric tau (PSPS + 2N3R), and an equimolar mixture of both 2N4R and 2N3R (PSPS + 2N4R + 2N3R). TEM micrographs B, C, and D, are representative PSP-tau isolated from PSP brain tissue. A representative micrograph showing lack of filaments formed when seeding 2N4R with PSPS (E) and representative PHF-like filaments when seeding 2N3R with PSPS (F) compared to the non-filamentous aggregates formed when seeding a 2N4R and 2N3R mixture using AD-PHF (G). All images were taken at a 30,000X magnification, scale bar in image G represents 100 nm for each micrograph.

LLS revealed that the addition of 2N3R tau appeared to greatly increase the amount of seeded aggregates. However, when completing non-seeded 2N3R only control experiments, we also found that there was a high amount of light scattering. We then prepared TEM grids of the 2N3R only samples and found that filaments were present (figure 39). Based on this finding it is difficult to know if the 2N3R only or 2N3R + 2N4R fibrils formed in the presence of AD-PHF seeds and PSP-tau seeds were indeed "seeded" by authentic filaments, or if they spontaneously aggregated.

4.5: Mechanically induced aggregation of recombinant 3R tau

To explore the apparent spontaneous aggregation of 2N3R tau, we completed a series of experiments using similar conditions to the seeding experiments, but without the presence of authentic disease isolated seeds. We initially completed a comparison study of two sets of monomeric samples, one in a static incubator and one in an orbital shaking incubator (330 rpm). We found that agitation, or quaking, was required for spontaneous 2N3R tau aggregation. We also found that spontaneous aggregation occurred in multiple different buffers and salt concentrations (data not shown), although the total amount of quaking induced conversion (QUIC) varied greatly among samples. Based on images taken using TEM, fibrils appear to be a mixture of straight filaments and paired filaments, and share similar morphological characteristics to the narrow Pick filaments (NPF) and wide Pick filaments (WPF) that have been isolated by other research groups from diseased tissue. We attempted the same technique using monomeric 2N4R, however the LLS and ThS was very low and had a high amount of variability between reactions, therefore, we did not analyze the sample using TEM.

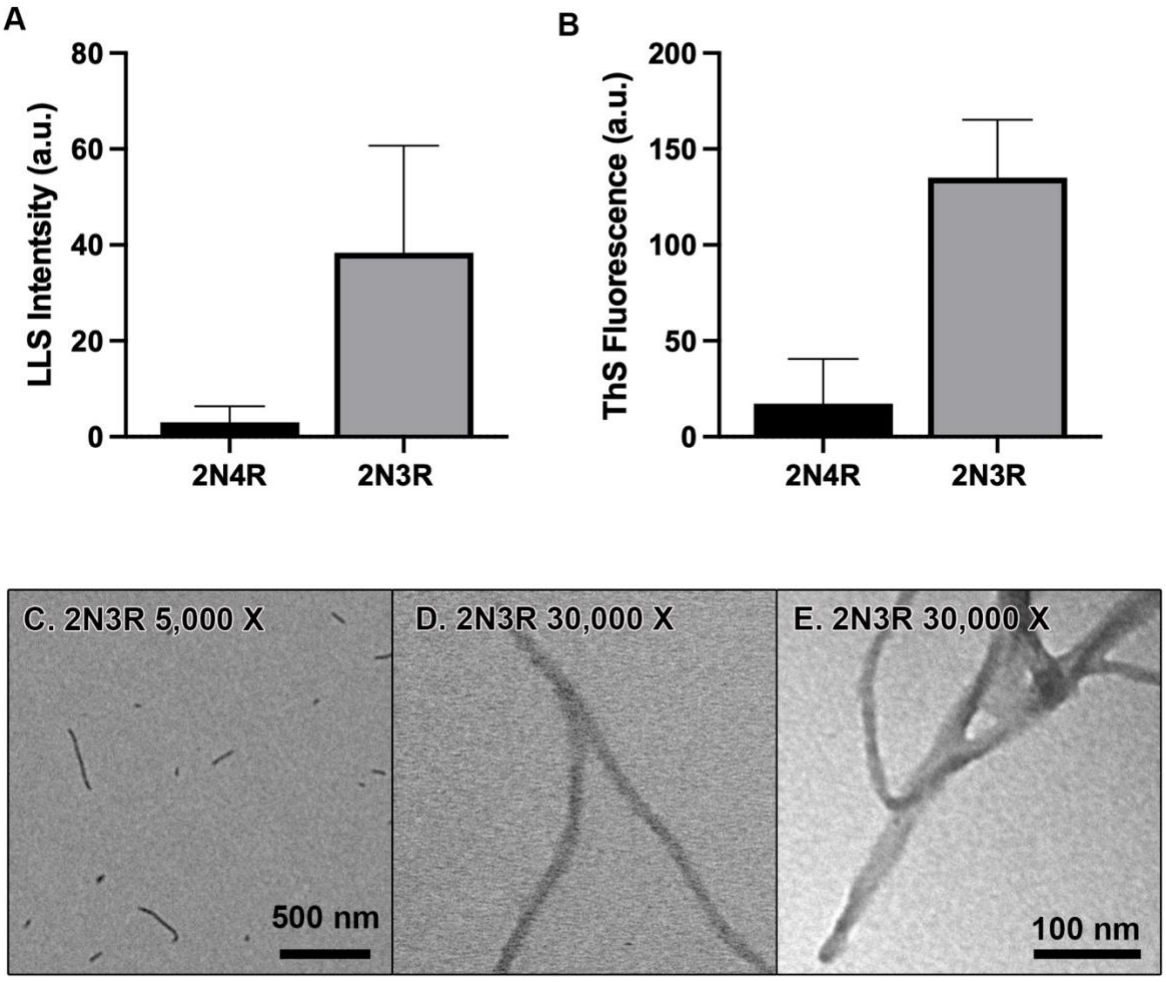

Figure 39: QUIC of 2N3R recombinant tau measured by LLS, ThS, and validated by TEM.
Average LLS (A) and ThS (B) readings of three independent reactions using both monomeric 2N4R and 2N3R recombinant tau. Low magnification (C) and high magnification (D and E) representative TEM micrograph of filaments formed by QUIC of monomeric 2N3R. Scale bar of 500 nm in figure C represents figure C only, scale bar of 100 nm in figure E represents figures D and E.

4.6 Materials and Methods:

Isolating authentic tau pathology from diseased brain tissue:

AD case information: Brain tissue from a single case of AD was provided by the KU Alzheimer's Disease Center Neuropathology Core. Tissue isolated from the frontal cortex of a confirmed case of AD, 84 year old female patient, ADC #4.

PSP case information: Brain tissue from a single case of PSP was provided by the Mayo Clinic Alzheimer's Disease Resource Center. Tissue isolated from the frontal cortex of a confirmed case of PSP, 68 year old male patient, Braak stage 2.5.

Equipment and reagents used: Homogenization was completed using a Wheaton USA, 15mL (A) glass dounce homogenizer. Ultracentrifugation was completed on a Beckman TL-100 ultracentrifuge using a TLA 100.3 rotor and 3.5 mL open top thick wall polycarbonate tube 13mm x 51mm, purchased from Beckman Coulter, Indianapolis, IN (#349622). Western blot samples were detected using Tau-5 mouse monoclonal antibody at a concentration of 1:5,000. Western blot was developed using Thermo Fisher Supersignal West Pico Plus chemiluminescent substrate (catalog number 34580). An image of the blot was taken using UVP Chemidoc IT_2 western blot imager.

1X Brain homogenization buffer (BHB): (50 mM Tris, pH 7.4, 275 mM NaCl, 5 mM KCl) with addition of fresh protease inhibitors: (10 µg/ml Pepstatin (Add 10 µl of 1 mg/ml stock per mL of Brain Homogenization Buffer), 10 µg/ml Leupeptin (Add 2 µl of 5 mg/ml stock per mL of Brain Homogenization Buffer), 10 µg/ml Aprotinin (Add 10 µl of 1 mg/ml stock per mL of Brain Homogenization Buffer), 1 mM PMSF (2 µl of 500 mM stock per mL of Brain Homogenization Buffer). 1X Brain Pellet Homogenization Buffer (BPHB): (0.8 M NaCl, 10%

Sucrose, 10 mM Tris pH 7.4, 1 mM EGTA. In separate bottle add 10% sarkosyl to 1X Brain Pellet Homogenization Buffer.

Tau pathology isolation protocol: Ultracentrifuge was pre-chilled to 4°C. While centrifuge was cooling fresh PMSF was prepared by dissolving 87.1 mg/mL PMSF in DMSO. Approximately 1 gram of brain tissue was thawed in 9 volumes of BPHB containing protease inhibitors and PMSF on ice. The brain pellet was then homogenized thoroughly using a dounce homogenizer. Approximately 100 µl of the resulting homogenate (H1) was stored at -80 °C. Sarkosyl was added to a final concentration 0.1% to the remaining homogenate and mixed thoroughly by inverting in a 15 mL conical tube several times. The remaining homogenate was then centrifuged at 10,580 x g for 10 minutes at 4°C (16,000 rpm in TLA 100.3). The supernatant (S1) was isolated and kept on ice (100 µl of S1 was stored at -80 °C) and the resulting pellet (P1) was re-extracted using the same buffer conditions (100 µl of P1 was stored at -80 °C). The second resulting supernatant (S2) was once again isolated from the pellet (P2) (100 µl of S2 was stored at -80 °C) and then S2 was then pooled with supernatant S1 (to form S1-2) and mixed by inverting in a 50 mL conical tube. Pellet P2 was once resuspended in the same BPHP buffer conditions as buffer and 100 µl of P2 was stored at -80 °C. Sarakosyl was added to pooled supernatant S1-2 to a final concentration of 1% and placed in a 50 mL conical tube at room temperature with gentle agitation. After incubation, S1-2 was centrifuged for 1 hour at 202,507 x g (70,000 rpm in TLA 100.3) at 4°C. The remaining supernatant from each tube was pooled and labelled S3 (100 µl of S3 was stored at -80 °C). The sarkosyl insoluble pellet (P3) was resuspended in Sup200 buffer (250 mM NaCl, 10 mM HEPES, 0.1 mM EGTA, pH 7.64) (100 µL/gram of original tissue used) using a 26 G 3/8 needle (~10 times) (collect and save 5 µl of P3 for western). Aliquot and freeze 20µL samples at -80°C. Frozen samples of H1, S1, S2,

S1-2, P1, P2, and P3 were used to complete a western blot to confirm isolation of tau by detecting with tau-5 antibody.

Preparation of seeds: Seeds were generated by thawing aliquots of tau isolated from diseased brain tissue on ice and then diluting to a final volume of 130 µL (either AD-PHF or PSP-tau). Samples were transferred to Covaris microtube-130 AFA fiber pre-slit snapcap tubes (PN 500514). Samples were then sheared for 450 seconds using a Covaris ME220 focused-ultrasonicator (Covaris Inc. Woburn MA) at 20 °C on settings of 50 W peak power, 20% duty factor, and 200 cycles per burst. The resulting sheared seeds were then transferred to a 650 µL microcentrifuge tube and kept on ice for later use.

Seeding of recombinant human tau: Monomeric recombinant tau was expressed and purified as previously described in chapter 2. A fresh aliquot of either tau was thawed on ice and diluted to a final concentration of 2 µM tau (either 2 µM 2N4R, 2 µM 2N3R, or a 1:1 mix of 1 µM 2N4R to 1 µM 2N3R) in polymerization buffer (PB) in a 1.7 mL microcentrifuge tube. PB final concentrations were 100 mM NaCl, 5 mM DTT, 10 mM HEPES (pH 7.64), 0.1 mM EDTA. Seeds were then added in 10 µL volumes to bring the final reaction volume to 200 µL and 0.75% original concentration of tau isolated from disease. Seeded reactions were then incubated at 37 °C for 72 hours with constant agitation of 330 rpm. A non-seeded negative control (2 µM recombinant tau only) and a seed only negative control (5% seed only) were also prepared and incubated in the same conditions. Second generation seeding experiments were completed by sonicating 130 µL of first generation seeded reactions by transferring the sample to a Covaris microtube-130 AFA fiber pre-slit snapcap tube and following the procedure outlined above.

Sonicated first generation seeded fibrils were than used as seeds following the same protocol as used for first generation reactions.

Quaking induced conversion of monomeric 2N3R tau: As previously described 2N3R aliquots were thawed on ice and then added to standard PB buffer at a final concentration of 2 µM protein in a 1.7 mL microcentrifuge tube. Sample were then incubated at 37 °C for 72 hours with constant agitation of 330 rpm in an orbital shaking incubator.

Right-angle laser light scattering: Seeded fibrils and non-seeded QUIC 2N3R fibrils were analyzed using right-angle laser light scattering as described in chapter 2. Briefly, 180 µL of sample were transferred to a 5 mm x 5 mm cuvette and placed in the path of a 532 nm wavelength 12 mW solid-state laser operating at 7.6 mW (B&W Tek Inc. Newark, DE) and images were captured using a Sony XC-ST270 digital camera with an aperture of f.s. 5.6. Images were analyzed using Adobe Photo Shop 2021 by taking histogram readings of the pixel intensity across the scattered light path.

Transmission Electron Microscopy: TEM grids were also prepared as previously described in chapter 2, at a 1:10 dilution. Briefly, 5 µL of sample was thoroughly mixed in 35 µL of polymerization buffer and then fixed by added 10 µL of 10% glutaraldehyde and incubating at room temperature for 5 minutes. A 300 mesh carbon coated copper formvar grid was then floated on top of a 10 µL droplet of the fixed sample for 1 minute, before being blotted on Whatman filter paper and washed by floating on top of 10 µL of H_2O, blotted, then floated on 10 µL of 2% uranyl acetated, then blotted, and stained by floating on a 10 µL droplet of 2% uranyl acetate for

1 minute, before a final blotting on Whatman filter paper. Selected images were capture at various magnifications between 5,000x and 30,000x using a JEOL JEM 1400 transmission electron microscope fitted with a LaB_6 electron source (Electron Microscopy Research Lab, University of Kansas Medical Center).

4.6: Discussion

Developing disease relevant *in vitro* induced strains will provide researchers the tools to complete targeted drug screening assays, studies of molecular dynamics involved in aggregation, and characterization of disease related mutations to further improve our understanding of tauopathies and how they can be treated. Using seeds isolated from disease brain tissue has the potential to form disease relevant strains that can be propagated indefinitely. Future directions should focus on improving the morphology of these fibrils in terms of disease similarity through a combination of techniques including; using multiple isoforms, seeding in the presence of different inducer molecules, use of tau variants with PTMs or pseudo-PTMs (e.g. pseudophosphorylation), and changes to buffer and incubation conditions.

In addition, further understanding and optimization of QUIC of monomeric 2N3R tau may provide a mechanism of inducing disease relevant structures without the need of inducer, or seed. It is unlikely that such a technique would result in the diverse range of structures seen in disease, however, it may be a useful tool for mimicking certain disease related tau species (e.g. NPFs and WPFs as seen in PiD).

Chapter 5: Summary and Future Directions

The recent advances made in the field of cryo-electron microscopy have revolutionized the way we think of tau aggregation and its role in different tauopathies. While there is still much unknown about the toxicity of certain tau species, mechanisms of prion-like spreading of tau, triggers of tau aggregation, and other functions of the tau protein, the structural diversity of fibrils isolated from tauopathies has opened up new possibilities as to how we think about identifying new treatments for this group of disorders.

The findings from chapter two of this work highlight the practical impacts of traditional therapeutic screening methods. We show that two different tau aggregation inhibitor molecules, LMTX and ANTC-15, have inducer-specific effects on tau aggregates. For example; filaments induced by ARA can be inhibited with ANTC-15, as well as partially disassembled. Whereas filaments induced by heparin can be inhibited by LMTX. However, neither compound is effective at inhibiting filaments formed by both inducer molecules. The implications of this finding could be far reaching. For example; it is highly likely that based on the diversity of structures isolated from disease that screening against a single aggregation inducer is insufficient for completing successful high throughput screening (HTS) assays. In addition, it also possible that we have missed potential hits in previous screenings due to using non-disease relevant tau filaments as ligands (e.g. heparin induced filaments). Similar to cancer biology, the complexity of AD and ADRDs will require a multipronged approach. Perhaps even precision based therapeutics that match potent and specific inhibitor molecules to specific “strains” of tau aggregates. Or by taking a wider approach to identify broad-spectrum tau aggregation inhibitors that are effective against multiple tau “strains”.

In addition to the effects of using only one tau aggregation inducer molecule on identifying potential therapeutics, chapter three highlights the implications of using only one inducer molecule for studying aggregation dynamics and potential changes caused by certain disease related mutations. In this study we found that different classes of tau aggregation inducers could fundamentally change the effects of certain disease related mutations. This was most clearly shown by comparing WT and P301S tau using ARA and polyphosphate as inducer molecules. For example; using ARA, P301S aggregates significantly slower than WT and forms longer filaments, with a higher total amount of aggregation. In contrast, using polyphosphate as an inducer molecule causes P301S to aggregate significantly faster than WT and the filament length is dependent on the length of the polyphosphate chain. In addition, the immunoreactivity studies highlighted a clear difference between how ARA induced fibrils and fibrils induced by either polyphosphate or RNA interact with antibodies that have been raised against oligomeric tau species, T22 and TOC1.

Together these data support the hypothesis that using different aggregation inducers can form different polymorphs that are functionally distinct when considering ligand interactions and aggregation dynamics. Therefore, in order to make progress in identifying tau based therapeutics for the treatment of AD and ADRDs, understanding the biological mechanisms of tau aggregation, and understanding the effects of missense mutations and post-translation modifications we must work towards identifying disease relevant tau aggregates to be utilized in laboratory studies. Ideally, *in vitro* findings should be confirmed using an array of different aggregation inducing techniques until we can identify robust disease-relevant model systems.

In addition to small molecule inducers, chapter 4 highlights some alternative techniques to inducing tau aggregation *in vitro*. Using seeds isolated from authentic cases of tauopathies is perhaps the most appealing technique for inducing disease relevant recombinant tau aggregation. However, in our experiments the filaments appeared to have different morphology from those isolated from disease and were thioflavin S negative. Interestingly, QUIC of monomeric 2N3R tau appears to form filaments with a similar morphology to those found in the 3R tauopathy, Pick's disease, as well as filaments that are thioflavin S positive. Both of these techniques require optimization of conditions to be able to be performed with high fidelity. However, optimization of conditions is not necessary until further characterization studies have shown that the fibrils induced by these methods are indeed disease relevant.

In addition, to high-resolution structural studies such as cryo-EM, low resolution techniques such as immunolabelled-EM, morphological characterization using quantitative EM, and the use of disease specific antibodies should also be used to further characterize and validate *in vitro* induced tau aggregates. Immunolabelled-EM and quantitative EM have already been discussed in section 4.2.1. In contrast, the use of disease specific antibodies is currently limited by the antibodies that are currently available. For example, Gibbons et. al. have shown that the GT-38 antibody specifically binds to fibrils isolated from AD, and not those isolated from other tauopathies, or heparin induced filaments. We have used this antibody in several dot-blot experiments and found that 2N4R filaments induced by ARA, HEP, PP, CR, TR, or RNA, are also not GT-38 reactive. It is possible that by copolymerizing isoforms, using a combination of techniques such as seeding in the presence of inducers, or the use of pseudophosphorylated tau

variants may result in GT-38 reactive species. The development of disease strain specific antibodies would be a valuable tool in the pursuit to identify and validate disease relevant inducer techniques.

Based on the findings presented in this body of work, we believe that identifying disease relevant *in vitro* inducing techniques should be a priority within the field of tau protein biochemistry. In order to accomplish this goal we must further explore the structures formed by current *in vitro* tau aggregation inducer molecules. Furthermore, alternative techniques such as seeding and QUIC should be characterized in the presence of different tau isoforms, potential co-factors, PTMs, and other tau variants. Until robust disease relevant *in vitro* models have been developed and validated, future studies characterizing tau aggregation and potential therapeutics must consider using multiple assays for validating findings. These assays should include the use of multiple inducer molecules, methods of detection, and comparison studies between authentic filament and *in vitro* formed filament characteristics.

References

1. Mandelkow, E.-M.; Mandelkow, E., Biochemistry and Cell Biology of Tau Protein in Neurofibrillary Degeneration. *Cold Spring Harbor Perspectives in Medicine* **2012,** *2* (7), a006247-a006247.
2. Wang, Y.; Mandelkow, E., Tau in physiology and pathology. *Nat Rev Neurosci* **2016,** *17* (1), 5-21.
3. Johnson, K. A.; Schultz, A.; Betensky, R. A.; Becker, J. A.; Sepulcre, J.; Rentz, D.; Mormino, E.; Chhatwal, J.; Amariglio, R.; Papp, K.; Marshall, G.; Albers, M.; Mauro, S.; Pepin, L.; Alverio, J.; Judge, K.; Philiossaint, M.; Shoup, T.; Yokell, D.; Dickerson, B.; Gomez-Isla, T.; Hyman, B.; Vasdev, N.; Sperling, R., Tau positron emission tomographic imaging in aging and early Alzheimer disease. *Annals of Neurology* **2016,** *79* (1), 110-119.
4. Schöll, M.; Lockhart, N., Samuel; Schonhaut, R., Daniel; O'Neil, P., James; Janabi, M.; Ossenkoppele, R.; Baker, L., Suzanne; Vogel, W., Jacob; Faria, J.; Schwimmer, D., Henry; Rabinovici, D., Gil; Jagust, J., William, PET Imaging of Tau Deposition in the Aging Human Brain. *Neuron* **2016,** *89* (5), 971-982.
5. Smith, R.; Wibom, M.; Pawlik, D.; Englund, E.; Hansson, O., Correlation of In Vivo [18F]Flortaucipir With Postmortem Alzheimer Disease Tau Pathology. *JAMA Neurology* **2019,** *76* (3), 310.
6. Ozcelik, S.; Sprenger, F.; Skachokova, Z.; Fraser, G.; Abramowski, D.; Clavaguera, F.; Probst, A.; Frank, S.; Muller, M.; Staufenbiel, M.; Goedert, M.; Tolnay, M.; Winkler, D. T., Co-expression of truncated and full-length tau induces severe neurotoxicity. *Mol Psychiatry* **2016,** *21* (12), 1790-1798.
7. Gibbons, G. S.; Lee, V. M. Y.; Trojanowski, J. Q., Mechanisms of Cell-to-Cell Transmission of Pathological Tau. *JAMA Neurology* **2019,** *76* (1), 101.
8. Terada, S.; Ishizu, H.; Ishiguro, K.; Tanabe, Y.; Itoh, N.; Yasutake, K.; Furubayashi, A.; Kitamura, Y.; Kuroda, S., Exon 3 insert of tau protein in neurodegenerative diseases. *Acta Neuropathologica* **2005,** *110* (1), 12-18.
9. Hovakimyan, A.; Antonyan, T.; Shabestari, S. K.; Svystun, O.; Chailyan, G.; Coburn, M. A.; Carlen-Jones, W.; Petrushina, I.; Chadarevian, J. P.; Zagorski, K.; Petrovsky, N.; Cribbs, D. H.; Agadjanyan, M. G.; Ghochikyan, A.; Davtyan, H., A MultiTEP platform-based epitope vaccine targeting the phosphatase activating domain (PAD) of tau: therapeutic efficacy in PS19 mice. *Scientific Reports* **2019,** *9* (1).
10. Kolarova, M.; García-Sierra, F.; Bartos, A.; Ricny, J.; Ripova, D., Structure and Pathology of Tau Protein in Alzheimer Disease. *International Journal of Alzheimer's Disease* **2012,** *2012*, 1-13.
11. Ward, M., Sarah; Himmelstein, S., Diana; Lancia, K., Jody; Binder, I., Lester, Tau oligomers and tau toxicity in neurodegenerative disease. *Biochemical Society Transactions* **2012,** *40* (4), 667-671.
12. Mirbaha, H.; Chen, D.; Morazova, O. A.; Ruff, K. M.; Sharma, A. M.; Liu, X.; Goodarzi, M.; Pappu, R. V.; Colby, D. W.; Mirzaei, H.; Joachimiak, L. A.; Diamond, M. I., Inert and seed-competent tau monomers suggest structural origins of aggregation. *eLife* **2018,** *7*.
13. Jeganathan, S.; von Bergen, M.; Brutlach, H.; Steinhoff, H.-J.; Mandelkow, E., Global Hairpin Folding of Tau in Solution. *Biochemistry* **2006,** *45* (7), 2283-2293.

14. Combs, B.; Hamel, C.; Kanaan, N. M., Pathological conformations involving the amino terminus of tau occur early in Alzheimer's disease and are differentially detected by monoclonal antibodies. *Neurobiol Dis* **2016,** *94*, 18-31.
15. Zhang, X.; Vigers, M.; Mccarty, J.; Rauch, J. N.; Fredrickson, G. H.; Wilson, M. Z.; Shea, J.-E.; Han, S.; Kosik, K. S., The proline-rich domain promotes Tau liquid–liquid phase separation in cells. *Journal of Cell Biology* **2020,** *219* (11).
16. Siegert, A.; Rankovic, M.; Favretto, F.; Ukmar-Godec, T.; Strohäker, T.; Becker, S.; Zweckstetter, M., Interplay between tau and α-synuclein liquid–liquid phase separation. *Protein Science* **2021**.
17. Mcmillan, P. J.; Kraemer, B. C.; Robinson, L.; Leverenz, J. B.; Raskind, M.; Schellenberg, G., Truncation of tau at E391 Promotes Early Pathologic Changes in Transgenic Mice. *Journal of Neuropathology & Experimental Neurology* **2011,** *70* (11), 1006-1019.
18. Al-Hilaly, Y. K.; Foster, B. E.; Biasetti, L.; Lutter, L.; Pollack, S. J.; Rickard, J. E.; Storey, J. M. D.; Harrington, C. R.; Xue, W. F.; Wischik, C. M.; Serpell, L. C., Tau (297-391) forms filaments that structurally mimic the core of paired helical filaments in Alzheimer's disease brain. *FEBS Letters* **2020,** *594* (5), 944-950.
19. Basurto-Islas, G.; Luna-Muñoz, J.; Guillozet-Bongaarts, A. L.; Binder, L. I.; Mena, R.; García-Sierra, F., Accumulation of aspartic acid421- and glutamic acid391-cleaved tau in neurofibrillary tangles correlates with progression in Alzheimer disease. *J Neuropathol Exp Neurol* **2008,** *67* (5), 470-83.
20. Abraha, A.; Ghoshal, N.; Gamblin, T. C.; Cryns, V.; Berry, R. W.; Kuret, J.; Binder, L. I., C-terminal inhibition of tau assembly in vitro and in Alzheimer's disease. *Journal of Cell Science* **2000,** *113* (21), 3737-3745.
21. Kanmert, D.; Cantlon, A.; Muratore, C. R.; Jin, M.; O'Malley, T. T.; Lee, G.; Young-Pearse, T. L.; Selkoe, D. J.; Walsh, D. M., C-Terminally Truncated Forms of Tau, But Not Full-Length Tau or Its C-Terminal Fragments, Are Released from Neurons Independently of Cell Death. *Journal of Neuroscience* **2015,** *35* (30), 10851-10865.
22. Geng, J.; Xia, L.; Li, W.; Dou, F., The C-Terminus of Tau Protein Plays an Important Role in Its Stability and Toxicity. *Journal of Molecular Neuroscience* **2015,** *55* (1), 251-259.
23. Sokolow, S.; Henkins, K. M.; Bilousova, T.; Gonzalez, B.; Vinters, H. V.; Miller, C. A.; Cornwell, L.; Poon, W. W.; Gylys, K. H., Pre-synaptic C-terminal truncated tau is released from cortical synapses in Alzheimer's disease. *Journal of Neurochemistry* **2015,** *133* (3), 368-379.
24. D'Souza, I.; Schellenberg, G. D., Regulation of tau isoform expression and dementia. *Biochimica et Biophysica Acta (BBA) - Molecular Basis of Disease* **2005,** *1739* (2-3), 104-115.
25. Trabzuni, D.; Wray, S.; Vandrovcova, J.; Ramasamy, A.; Walker, R.; Smith, C.; Luk, C.; Gibbs, J. R.; Dillman, A.; Hernandez, D. G.; Arepalli, S.; Singleton, A. B.; Cookson, M. R.; Pittman, A. M.; De Silva, R.; Weale, M. E.; Hardy, J.; Ryten, M., MAPT expression and splicing is differentially regulated by brain region: relation to genotype and implication for tauopathies. *Human Molecular Genetics* **2012,** *21* (18), 4094-4103.
26. Khatoon, S.; Grundke-Iqbal, I.; Iqbal, K., Brain levels of microtubule-associated protein tau are elevated in Alzheimer's disease: a radioimmuno-slot-blot assay for nanograms of the protein. *J Neurochem* **1992,** *59* (2), 750-3.
27. Lacovich, V.; Espindola, S. L.; Alloatti, M.; Pozo Devoto, V.; Cromberg, L. E.; Čarná, M. E.; Forte, G.; Gallo, J.-M.; Bruno, L.; Stokin, G. B.; Avale, M. E.; Falzone, T. L., Tau Isoforms Imbalance Impairs the Axonal Transport of the Amyloid Precursor Protein in Human Neurons. *The Journal of Neuroscience* **2017,** *37* (1), 58-69.

28. Dehmelt, L.; Halpain, S., *Genome Biology* **2004,** *6* (1), 204.
29. Arendt, T.; Stieler, J. T.; Holzer, M., Tau and tauopathies. *Brain research bulletin* **2016,** *126* (Pt 3), 238-292.
30. Alquezar, C.; Arya, S.; Kao, A. W., Tau Post-translational Modifications: Dynamic Transformers of Tau Function, Degradation, and Aggregation. *Frontiers in Neurology* **2021,** *11*.
31. Janning, D.; Igaev, M.; Sündermann, F.; Brühmann, J.; Beutel, O.; Heinisch, J. J.; Bakota, L.; Piehler, J.; Junge, W.; Brandt, R., Single-molecule tracking of tau reveals fast kiss-and-hop interaction with microtubules in living neurons. *Molecular Biology of the Cell* **2014,** *25* (22), 3541-3551.
32. Falcon, B.; Zivanov, J.; Zhang, W.; Murzin, A. G.; Garringer, H. J.; Vidal, R.; Crowther, R. A.; Newell, K. L.; Ghetti, B.; Goedert, M.; Scheres, S. H. W., Novel tau filament fold in chronic traumatic encephalopathy encloses hydrophobic molecules. *Nature* **2019,** *568* (7752), 420-423.
33. Cowan, C. M.; Mudher, A., Are Tau Aggregates Toxic or Protective in Tauopathies? *Frontiers in Neurology* **2013,** *4*.
34. Meraz-Ríos, M. A.; Lira-De León, K. I.; Campos-Peña, V.; De Anda-Hernández, M. A.; Mena-López, R., Tau oligomers and aggregation in Alzheimer's disease. *Journal of Neurochemistry* **2010,** *112* (6), 1353-1367.
35. Wegmann, S.; Eftekharzadeh, B.; Tepper, K.; Zoltowska, K. M.; Bennett, R. E.; Dujardin, S.; Laskowski, P. R.; Mackenzie, D.; Kamath, T.; Commins, C.; Vanderburg, C.; Roe, A. D.; Fan, Z.; Molliex, A. M.; Hernandez-Vega, A.; Muller, D.; Hyman, A. A.; Mandelkow, E.; Taylor, J. P.; Hyman, B. T., Tau protein liquid–liquid phase separation can initiate tau aggregation. *The EMBO Journal* **2018,** *37* (7), e98049.
36. Kanaan, N. M.; Hamel, C.; Grabinski, T.; Combs, B., Liquid-liquid phase separation induces pathogenic tau conformations in vitro. *Nature Communications* **2020,** *11* (1).
37. Singh, V.; Xu, L.; Boyko, S.; Surewicz, K.; Surewicz, W. K., Zinc promotes liquid–liquid phase separation of tau protein. *Journal of Biological Chemistry* **2020,** *295* (18), 5850-5856.
38. Falcon, B.; Zhang, W.; Schweighauser, M.; Murzin, A. G.; Vidal, R.; Garringer, H. J.; Ghetti, B.; Scheres, S. H. W.; Goedert, M., Tau filaments from multiple cases of sporadic and inherited Alzheimer's disease adopt a common fold. *Acta Neuropathol* **2018,** *136* (5), 699-708.
39. Goedert, M.; Falcon, B.; Zhang, W.; Ghetti, B.; Scheres, S. H. W., Distinct Conformers of Assembled Tau in Alzheimer's and Pick's Diseases. *Cold Spring Harb Symp Quant Biol* **2018,** *83*, 163-171.
40. Zhang, W.; Tarutani, A.; Newell, K. L.; Murzin, A. G.; Matsubara, T.; Falcon, B.; Vidal, R.; Garringer, H. J.; Shi, Y.; Ikeuchi, T.; Murayama, S.; Ghetti, B.; Hasegawa, M.; Goedert, M.; Scheres, S. H. W., Novel tau filament fold in corticobasal degeneration. *Nature* **2020**.
41. Shi, Y.; Zhang, W.; Yang, Y.; Murzin, A. G.; Falcon, B.; Kotecha, A.; Van Beers, M.; Tarutani, A.; Kametani, F.; Garringer, H. J.; Vidal, R.; Hallinan, G. I.; Lashley, T.; Saito, Y.; Murayama, S.; Yoshida, M.; Tanaka, H.; Kakita, A.; Ikeuchi, T.; Robinson, A. C.; Mann, D. M. A.; Kovacs, G. G.; Revesz, T.; Ghetti, B.; Hasegawa, M.; Goedert, M.; Scheres, S., Structure-based Classification of Tauopathies. Cold Spring Harbor Laboratory: 2021.
42. Olszewska, D. A.; Lonergan, R.; Fallon, E. M.; Lynch, T., Genetics of Frontotemporal Dementia. *Current Neurology and Neuroscience Reports* **2016,** *16* (12).
43. Forrest, S. L.; Kril, J. J.; Stevens, C. H.; Kwok, J. B.; Hallupp, M.; Kim, W. S.; Huang, Y.; McGinley, C. V.; Werka, H.; Kiernan, M. C.; Götz, J.; Spillantini, M. G.; Hodges, J. R.;

Ittner, L. M.; Halliday, G. M., Retiring the term FTDP-17 as MAPT mutations are genetic forms of sporadic frontotemporal tauopathies. *Brain* **2018,** *141* (2), 521-534.
44. Goedert, M.; Eisenberg, D. S.; Crowther, R. A., Propagation of Tau Aggregates and Neurodegeneration. *Annual Review of Neuroscience* **2017,** *40* (1), 189-210.
45. Šerý, O.; Povová, J.; Míšek, I.; Pešák, L.; Janout, V., Molecular mechanisms of neuropathological changes in Alzheimer's disease: a review. *Folia Neuropathologica* **2013,** *1*, 1-9.
46. Perl, D. P., Neuropathology of Alzheimer's Disease. *Mount Sinai Journal of Medicine: A Journal of Translational and Personalized Medicine* **2010,** *77* (1), 32-42.
47. Van Der Kant, R.; Goldstein, L. S. B.; Ossenkoppele, R., Amyloid-β-independent regulators of tau pathology in Alzheimer disease. *Nature Reviews Neuroscience* **2020,** *21* (1), 21-35.
48. Congdon, E. E.; Sigurdsson, E. M., Tau-targeting therapies for Alzheimer disease. *Nature Reviews Neurology* **2018,** *14* (7), 399-415.
49. Crowther, R. A., Straight and paired helical filaments in Alzheimer disease have a common structural unit. *Proceedings of the National Academy of Sciences* **1991,** *88* (6), 2288-2292.
50. Fitzpatrick, A. W. P.; Falcon, B.; He, S.; Murzin, A. G.; Murshudov, G.; Garringer, H. J.; Crowther, R. A.; Ghetti, B.; Goedert, M.; Scheres, S. H. W., Cryo-EM structures of tau filaments from Alzheimer's disease. *Nature* **2017,** *547* (7662), 185-190.
51. Taniguchi-Watanabe, S.; Arai, T.; Kametani, F.; Nonaka, T.; Masuda-Suzukake, M.; Tarutani, A.; Murayama, S.; Saito, Y.; Arima, K.; Yoshida, M.; Akiyama, H.; Robinson, A.; Mann, D. M. A.; Iwatsubo, T.; Hasegawa, M., Biochemical classification of tauopathies by immunoblot, protein sequence and mass spectrometric analyses of sarkosyl-insoluble and trypsin-resistant tau. *Acta Neuropathologica* **2016,** *131* (2), 267-280.
52. Deture, M. A.; Dickson, D. W., The neuropathological diagnosis of Alzheimer's disease. *Molecular Neurodegeneration* **2019,** *14* (1).
53. Katsumoto, A.; Takeuchi, H.; Tanaka, F., Tau Pathology in Chronic Traumatic Encephalopathy and Alzheimer's Disease: Similarities and Differences. *Frontiers in Neurology* **2019,** *10*.
54. Ali, F.; Josephs, K. A., Corticobasal degeneration: key emerging issues. *Journal of Neurology* **2018,** *265* (2), 439-445.
55. Lopez, G.; Bayulkem, K.; Hallett, M., Progressive supranuclear palsy (PSP): Richardson syndrome and other PSP variants. *Acta Neurologica Scandinavica* **2016,** *134* (4), 242-249.
56. Lamb, R.; Rohrer, J. D.; Lees, A. J.; Morris, H. R., Progressive Supranuclear Palsy and Corticobasal Degeneration: Pathophysiology and Treatment Options. *Curr Treat Options Neurol* **2016,** *18* (9), 42.
57. Xiang, X.; Arakhamia, T.; Carlomagno, Y.; Dhingra, S.; Thierry, M.; Deture, M.; Cook, C. N.; Dickson, D. W.; Petrucelli, L.; Fitzpatrick, A. W. P., Role of molecular polymorphism in defining tau filament structures in neurodegenerative diseases. Cold Spring Harbor Laboratory: 2021.
58. Frederick, J., Pick Disease: A Brief Overview. *Archives of Pathology & Laboratory Medicine* **2006,** *130* (7), 1063-1066.
59. Zhang, W.; Falcon, B.; Murzin, A. G.; Fan, J.; Crowther, R. A.; Goedert, M.; Scheres, S. H., Heparin-induced tau filaments are polymorphic and differ from those in Alzheimer's and Pick's diseases. *Elife* **2019,** *8*.

60. Ricciarelli, R.; Fedele, E., The Amyloid Cascade Hypothesis in Alzheimer's Disease: It's Time to Change Our Mind. *Current Neuropharmacology* **2017,** *15* (6).
61. Cummings, J., Lee, G , Zhong, K , et al., Alzheimer's disease drug development pipeline: 2021. *Alzheimer's dementia: Translational Research and Clinical Interventions* **2021,** *7* (1), 1-24.
62. Schneider, L., A resurrection of aducanumab for Alzheimer's disease. *The Lancet Neurology* **2020,** *19* (2), 111-112.
63. Vakilinezhad, M. A.; Amini, A.; Akbari Javar, H.; Baha'Addini Beigi Zarandi, B. F.; Montaseri, H.; Dinarvand, R., Nicotinamide loaded functionalized solid lipid nanoparticles improves cognition in Alzheimer's disease animal model by reducing Tau hyperphosphorylation. *DARU Journal of Pharmaceutical Sciences* **2018,** *26* (2), 165-177.
64. Hoskin, J. L.; Sabbagh, M. N.; Al-Hasan, Y.; Decourt, B., Tau immunotherapies for Alzheimer's disease. *Expert Opinion on Investigational Drugs* **2019,** *28* (6), 545-554.
65. Grüninger, F., Invited review: Drug development for tauopathies. *Neuropathology and Applied Neurobiology* **2015,** *41* (1), 81-96.
66. Devos, S. L.; Miller, R. L.; Schoch, K. M.; Holmes, B. B.; Kebodeaux, C. S.; Wegener, A. J.; Chen, G.; Shen, T.; Tran, H.; Nichols, B.; Zanardi, T. A.; Kordasiewicz, H. B.; Swayze, E. E.; Bennett, C. F.; Diamond, M. I.; Miller, T. M., Tau reduction prevents neuronal loss and reverses pathological tau deposition and seeding in mice with tauopathy. *Science Translational Medicine* **2017,** *9* (374), eaag0481.
67. Wilcock, G. K.; Gauthier, S.; Frisoni, G. B.; Jia, J.; Hardlund, J. H.; Moebius, H. J.; Bentham, P.; Kook, K. A.; Schelter, B. O.; Wischik, D. J.; Davis, C. S.; Staff, R. T.; Vuksanovic, V.; Ahearn, T.; Bracoud, L.; Shamsi, K.; Marek, K.; Seibyl, J.; Riedel, G.; Storey, J. M. D.; Harrington, C. R.; Wischik, C. M., Potential of Low Dose Leuco-Methylthioninium Bis(Hydromethanesulphonate) (LMTM) Monotherapy for Treatment of Mild Alzheimer's Disease: Cohort Analysis as Modified Primary Outcome in a Phase III Clinical Trial. *J Alzheimers Dis* **2018,** *61* (1), 435-457.
68. Ayalon, G.; Lee, S.-H.; Adolfsson, O.; Foo-Atkins, C.; Atwal, J. K.; Blendstrup, M.; Booler, H.; Bravo, J.; Brendza, R.; Brunstein, F.; Chan, R.; Chandra, P.; Couch, J. A.; Datwani, A.; Demeule, B.; Dicara, D.; Erickson, R.; Ernst, J. A.; Foreman, O.; He, D.; Hötzel, I.; Keeley, M.; Kwok, M. C. M.; Lafrance-Vanasse, J.; Lin, H.; Lu, Y.; Luk, W.; Manser, P.; Muhs, A.; Ngu, H.; Pfeifer, A.; Pihlgren, M.; Rao, G. K.; Scearce-Levie, K.; Schauer, S. P.; Smith, W. B.; Solanoy, H.; Teng, E.; Wildsmith, K. R.; Bumbaca Yadav, D.; Ying, Y.; Fuji, R. N.; Kerchner, G. A., Antibody semorinemab reduces tau pathology in a transgenic mouse model and engages tau in patients with Alzheimer's disease. *Science Translational Medicine* **2021,** *13* (593), eabb2639.
69. (U.S.), N. L. o. M. A Study of LY3303560 in participants with early symptomatic Alzheimer's disease. https://clinicaltrials.gov/ct2/show/study/NCT03518073 (accessed 31st May).
70. Höglinger, G. U.; Litvan, I.; Mendonca, N.; Wang, D.; Zheng, H.; Rendenbach-Mueller, B.; Lon, H.-K.; Jin, Z.; Fisseha, N.; Budur, K.; Gold, M.; Ryman, D.; Florian, H.; Ahmed, A.; Aiba, I.; Albanese, A.; Bertram, K.; Bordelon, Y.; Bower, J.; Brosch, J.; Claassen, D.; Colosimo, C.; Corvol, J.-C.; Cudia, P.; Daniele, A.; Defebvre, L.; Driver-Dunckley, E.; Duquette, A.; Eleopra, R.; Eusebio, A.; Fung, V.; Geldmacher, D.; Golbe, L.; Grandas, F.; Hall, D.; Hatano, T.; Höglinger, G. U.; Honig, L.; Hui, J.; Kerwin, D.; Kikuchi, A.; Kimber, T.; Kimura, T.; Kumar, R.; Litvan, I.; Ljubenkov, P.; Lorenzl, S.; Ludolph, A.; Mari, Z.; Mcfarland, N.; Meissner, W.; Mir Rivera, P.; Mochizuki, H.; Morgan, J.; Munhoz, R.; Nishikawa, N.; O`Sullivan, J.; Oeda, T.; Oizumi, H.; Onodera, O.; Ory-Magne, F.; Peckham,

E.; Postuma, R.; Quattrone, A.; Quinn, J.; Ruggieri, S.; Sarna, J.; Schulz, P. E.; Slevin, J.; Tagliati, M.; Wile, D.; Wszolek, Z.; Xie, T.; Zesiewicz, T., Safety and efficacy of tilavonemab in progressive supranuclear palsy: a phase 2, randomised, placebo-controlled trial. *The Lancet Neurology* **2021,** *20* (3), 182-192.
71. (U.S.), N. L. o. M. A study to evaluate the safety, tolerability and immunogenecity of tau targeted vaccines in participants with Alzheimer's disease. https://clinicaltrials.gov/ct2/show/NCT04445831 (accessed 31st May).
72. Galpern, W. R.; Mercken, M.; Van Kolen, K.; Timmers, M.; Haeverans, K.; Janssens, L.; Triana-Baltzer, G.; Kolb, H. C.; Jacobs, T.; Nandy, P.; Malia, T.; Sun, H.; Van Nueten, L., P1-052: A SINGLE ASCENDING DOSE STUDY TO EVALUATE THE SAFETY, TOLERABILITY, PHARMACOKINETICS, AND PHARMACODYNAMICS OF THE ANTI-PHOSPHO-TAU ANTIBODY JNJ-63733657 IN HEALTHY SUBJECTS. *Alzheimer's & Dementia* **2019,** *15*, P252-P253.
73. Rosenqvist, N.; Asuni, A. A.; Andersson, C. R.; Christensen, S.; Daechsel, J. A.; Egebjerg, J.; Falsig, J.; Helboe, L.; Jul, P.; Kartberg, F.; Pedersen, L. Ø.; Sigurdsson, E. M.; Sotty, F.; Skjødt, K.; Stavenhagen, J. B.; Volbracht, C.; Pedersen, J. T., Highly specific and selective anti-pS396-tau antibody C10.2 targets seeding-competent tau. *Alzheimer's & Dementia: Translational Research & Clinical Interventions* **2018,** *4* (1), 521-534.
74. Chang, E.; Honson, N. S.; Bandyopadhyay, B.; Funk, K. E.; Jensen, J. R.; Kim, S.; Naphade, S.; Kuret, J., Modulation and detection of tau aggregation with small-molecule ligands. *Curr Alzheimer Res* **2009,** *6* (5), 409-414.
75. Dubey, T.; Gorantla, N. V.; Chandrashekara, K. T.; Chinnathambi, S., Photoexcited Toluidine Blue Inhibits Tau Aggregation in Alzheimer's Disease. *ACS Omega* **2019,** *4* (20), 18793-18802.
76. Seidler, P. M.; Boyer, D. R.; Rodriguez, J. A.; Sawaya, M. R.; Cascio, D.; Murray, K.; Gonen, T.; Eisenberg, D. S., Structure-based inhibitors of tau aggregation. *Nature Chemistry* **2018,** *10* (2), 170-176.
77. Hitt, B. D.; Vaquer-Alicea, J.; Manon, V. A.; Beaver, J. D.; Kashmer, O. M.; Garcia, J. N.; Diamond, M. I., Ultrasensitive tau biosensor cells detect no seeding in Alzheimer's disease CSF. *Acta Neuropathologica Communications* **2021,** *9* (1).
78. Lim, S.; Haque, M. M.; Kim, D.; Kim, D. J.; Kim, Y. K., Cell-based Models To Investigate Tau Aggregation. *Comput Struct Biotechnol J* **2014,** *12* (20-21), 7-13.
79. Pickhardt, M.; Gazova, Z.; Von Bergen, M.; Khlistunova, I.; Wang, Y.; Hascher, A.; Mandelkow, E.-M.; Biernat, J.; Mandelkow, E., Anthraquinones Inhibit Tau Aggregation and Dissolve Alzheimer's Paired Helical Filaments in Vitro and in Cells. *Journal of Biological Chemistry* **2005,** *280* (5), 3628-3635.
80. Melis, V.; Magbagbeolu, M.; Rickard, J. E.; Horsley, D.; Davidson, K.; Harrington, K. A.; Goatman, K.; Goatman, E. A.; Deiana, S.; Close, S. P.; Zabke, C.; Stamer, K.; Dietze, S.; Schwab, K.; Storey, J. M. D.; Harrington, C. R.; Wischik, C. M.; Theuring, F.; Riedel, G., Effects of oxidized and reduced forms of methylthioninium in two transgenic mouse tauopathy models. *Behavioural Pharmacology* **2015,** *26* (4), 353-368.
81. Zhang, Y.-H.; Wang, D.-W.; Xu, S.-F.; Zhang, S.; Fan, Y.-G.; Yang, Y.-Y.; Guo, S.-Q.; Wang, S.; Guo, T.; Wang, Z.-Y.; Guo, C., α-Lipoic acid improves abnormal behavior by mitigation of oxidative stress, inflammation, ferroptosis, and tauopathy in P301S Tau transgenic mice. *Redox Biology* **2018,** *14*, 535-548.

82. Song, J. X.; Malampati, S.; Zeng, Y.; Durairajan, S. S. K.; Yang, C. B.; Tong, B. C. K.; Iyaswamy, A.; Shang, W. B.; Sreenivasmurthy, S. G.; Zhu, Z.; Cheung, K. H.; Lu, J. H.; Tang, C.; Xu, N.; Li, M., A small molecule transcription factor EB activator ameliorates beta-amyloid precursor protein and Tau pathology in Alzheimer's disease models. *Aging Cell* **2020,** *19* (2).
83. Jankowsky, J. L.; Zheng, H., Practical considerations for choosing a mouse model of Alzheimer's disease. *Molecular Neurodegeneration* **2017,** *12* (1).
84. 2021
Alzheimer's disease facts and figures. *Alzheimer's & Dementia* **2021,** *17* (3), 327-406.
85. La Joie, R.; Visani, A. V.; Baker, S. L.; Brown, J. A.; Bourakova, V.; Cha, J.; Chaudhary, K.; Edwards, L.; Iaccarino, L.; Janabi, M.; Lesman-Segev, O. H.; Miller, Z. A.; Perry, D. C.; O'Neil, J. P.; Pham, J.; Rojas, J. C.; Rosen, H. J.; Seeley, W. W.; Tsai, R. M.; Miller, B. L.; Jagust, W. J.; Rabinovici, G. D., Prospective longitudinal atrophy in Alzheimer's disease correlates with the intensity and topography of baseline tau-PET. *Science Translational Medicine* **2020,** *12* (524), eaau5732.
86. Cummings, J. L.; Tong, G.; Ballard, C., Treatment Combinations for Alzheimer's Disease: Current and Future Pharmacotherapy Options. *J Alzheimers Dis* **2019,** *67* (3), 779-794.
87. Bulic, B.; Pickhardt, M.; Mandelkow, E., Progress and Developments in Tau Aggregation Inhibitors for Alzheimer Disease. *Journal of medicinal chemistry* **2013,** *56* (11), 4135-4155.
88. Pickhardt, M.; Larbig, G.; Khlistunova, I.; Coksezen, A.; Meyer, B.; Mandelkow, E.-M.; Schmidt, B.; Mandelkow, E., Phenylthiazolyl-hydrazide and its derivatives are potent inhibitors of tau aggregation and toxicity in vitro and in cells. *Biochemistry* **2007,** *46* (35), 10016.
89. Gauthier, S.; Feldman, H. H.; Schneider, L. S.; Wilcock, G. K.; Frisoni, G. B.; Hardlund, J. H.; Moebius, H. J.; Bentham, P.; Kook, K. A.; Wischik, D. J.; Schelter, B. O.; Davis, C. S.; Staff, R. T.; Bracoud, L.; Shamsi, K.; Storey, J. M. D.; Harrington, C. R.; Wischik, C. M., Efficacy and safety of tau-aggregation inhibitor therapy in patients with mild or moderate Alzheimer's disease: a randomised, controlled, double-blind, parallel-arm, phase 3 trial. *Lancet (London, England)* **2016,** *388* (10062), 2873-2884.
90. Taniguchi, S.; Suzuki, N.; Masuda, M.; Hisanaga, S.-I.; Iwatsubo, T.; Goedert, M.; Hasegawa, M., Inhibition of heparin-induced tau filament formation by phenothiazines, polyphenols, and porphyrins. *The Journal of biological chemistry* **2005,** *280* (9), 7614-7623.
91. Sanders, D. W.; Kaufman, S. K.; DeVos, S. L.; Sharma, A. M.; Mirbaha, H.; Li, A.; Barker, S. J.; Foley, A. C.; Thorpe, J. R.; Serpell, L. C.; Miller, T. M.; Grinberg, L. T.; Seeley, W. W.; Diamond, M. I., Distinct tau prion strains propagate in cells and mice and define different tauopathies. *Neuron* **2014,** *82* (6), 1271-1288.
92. Fichou, Y.; Han, S., Protein shapes at the core of chronic traumatic encephalopathy. *Nat Struct Mol Biol* **2019,** *26* (5), 336-338.
93. Carlson, S. W.; Branden, M.; Voss, K.; Sun, Q.; Rankin, C. A.; Gamblin, T. C., A Complex Mechanism for Inducer Mediated Tau Polymerization. *Biochemistry* **2007,** *46* (30), 8838-8849.
94. Paranjape, S. R.; Chiang, Y. M.; Sanchez, J. F.; Entwistle, R.; Wang, C. C.; Oakley, B. R.; Gamblin, T. C., Inhibition of Tau Aggregation by Three Aspergillus nidulans Secondary Metabolites: 2,omega-Dihydroxyemodin, Asperthecin, and Asperbenzaldehyde. *Planta medica* **2014,** *80* (1), 77-85.
95. Paranjape, S. R.; Riley, A. P.; Somoza, A. D.; Oakley, C. E.; Wang, C. C.; Prisinzano, T. E.; Oakley, B. R.; Gamblin, T. C., Azaphilones inhibit tau aggregation and dissolve tau aggregates in vitro. *ACS Chem Neurosci* **2015,** *6* (5), 751-760.

96. Ahuja, M.; Chiang, Y. M.; Chang, S. L.; Praseuth, M. B.; Entwistle, R.; Sanchez, J. F.; Lo, H. C.; Yeh, H. H.; Oakley, B. R.; Wang, C. C., Illuminating the diversity of aromatic polyketide synthases in Aspergillus nidulans. *J Am Chem Soc* **2012,** *134* (19), 8212-8221.
97. Grandjean, J.-M. M.; Jiu, A. Y.; West, J. W.; Aoyagi, A.; Droege, D. G.; Elepano, M.; Hirasawa, M.; Hirouchi, M.; Murakami, R.; Lee, J.; Sasaki, K.; Hirano, S.; Ohyama, T.; Tang, B. C.; Vaz, R. J.; Inoue, M.; Olson, S. H.; Prusiner, S. B.; Conrad, J.; Paras, N. A., Discovery of 4-Piperazine Isoquinoline Derivatives as Potent and Brain-Permeable Tau Prion Inhibitors with CDK8 Activity. *ACS Medicinal Chemistry Letters* **2020,** *11* (2), 127-132.
98. Rankin, C. A.; Sun, Q.; Gamblin, T. C., Pseudo-phosphorylation of tau at Ser202 and Thr205 affects tau filament formation. *Brain Res Mol Brain Res* **2005,** *138* (1), 84-93.
99. King, M. E.; Gamblin, T. C.; Kuret, J.; Binder, L. I., Differential Assembly of Human Tau Isoforms in the Presence of Arachidonic Acid. *Journal of Neurochemistry* **2000,** *74* (4), 1749-1757.
100. Combs, B.; Tiernan, C. T.; Hamel, C.; Kanaan, N. M., Production of recombinant tau oligomers in vitro. *Methods Cell Biol* **2017,** *141*, 45-64.
101. Combs, B.; Voss, K.; Gamblin, T. C., Pseudohyperphosphorylation Has Differential Effects on Polymerization and Function of Tau Isoforms. *Biochemistry* **2011,** *50* (44), 9446-9456.
102. Mutreja, Y., Methods in Tau Cell Biology Optimization of in vitro conditions to study the arachidonic acid induction of 4R isoforms of the microtubule-associated protein tau. *Methods in cell biology* **2017,** *141*, 65-88.
103. Ward, S. M.; Himmelstein, D. S.; Ren, Y.; Fu, Y.; Yu, X. W.; Roberts, K.; Binder, L. I.; Sahara, N., TOC1: a valuable tool in assessing disease progression in the rTg4510 mouse model of tauopathy. *Neurobiology of disease* **2014,** *67*, 37-48.
104. Kanaan, N. M.; Cox, K.; Alvarez, V. E.; Stein, T. D.; Poncil, S.; McKee, A. C., Characterization of Early Pathological Tau Conformations and Phosphorylation in Chronic Traumatic Encephalopathy. *J Neuropathol Exp Neurol* **2016,** *75* (1), 19-34.
105. Mufson, E. J.; Ward, S.; Binder, L., Prefibrillar tau oligomers in mild cognitive impairment and Alzheimer's disease. *Neurodegener Dis* **2014,** *13* (2-3), 151-153.
106. Soeda, Y.; Saito, M.; Maeda, S.; Ishida, K.; Nakamura, A.; Kojima, S.; Takashima, A., Methylene Blue Inhibits Formation of Tau Fibrils but not of Granular Tau Oligomers: A Plausible Key to Understanding Failure of a Clinical Trial for Alzheimer's Disease. *J. Alzheimers Dis.* **2019,** *68* (4), 1677-1686.
107. Harrington, C. R.; Storey, J. M. D.; Clunas, S.; Harrington, K. A.; Horsley, D.; Ishaq, A.; Kemp, S. J.; Larch, C. P.; Marshall, C.; Nicoll, S. L.; Rickard, J. E.; Simpson, M.; Sinclair, J. P.; Storey, L. J.; Wischik, C. M., Cellular Models of Aggregation-dependent Template-directed Proteolysis to Characterize Tau Aggregation Inhibitors for Treatment of Alzheimer Disease. *The Journal of biological chemistry* **2015,** *290* (17), 10862.
108. Götz, J.; Ittner, A.; Ittner, L. M., Tau-targeted treatment strategies in Alzheimer's disease. Oxford, UK, 2012; Vol. 165, pp 1246-1259.
109. Spillantini, M. G.; Goedert, M., Tau pathology and neurodegeneration. *Lancet neurology* **2013,** *12* (6), 609-622.
110. Prinz, H., Hill coefficients, dose-response curves and allosteric mechanisms. *Journal of chemical biology* **2010,** *3* (1), 37-44.
111. Tiernan, C. T.; Mufson, E. J.; Kanaan, N. M.; Counts, S. E., Tau Oligomer Pathology in Nucleus Basalis Neurons During the Progression of Alzheimer Disease. *J Neuropathol Exp Neurol* **2018,** *77* (3), 246-259.

112. Castillo-Carranza, D. L.; Gerson, J. E.; Sengupta, U.; Guerrero-Munoz, M. J.; Lasagna-Reeves, C. A.; Kayed, R., Specific targeting of tau oligomers in Htau mice prevents cognitive impairment and tau toxicity following injection with brain-derived tau oligomeric seeds. *J Alzheimers Dis* **2014,** *40 Suppl 1*, S97-S111.
113. Shafiei, S. S.; Guerrero-Muñoz, M. J.; Castillo-Carranza, D. L., Tau Oligomers: Cytotoxicity, Propagation, and Mitochondrial Damage. *Frontiers in Aging Neuroscience* **2017,** *9*, 83.
114. Fichou, Y.; Vigers, M.; Goring, A. K.; Eschmann, N. A.; Han, S., Heparin-induced tau filaments are structurally heterogeneous and differ from Alzheimer's disease filaments. *Chem Commun (Camb)* **2018,** *54* (36), 4573-4576.
115. Cummings, J. L.; Morstorf, T.; Zhong, K., Alzheimer's disease drug-development pipeline: few candidates, frequent failures. *Alzheimer's research & therapy* **2014,** *6* (4), 37.
116. Kurtishi, A.; Rosen, B.; Patil, K. S.; Alves, G. W.; Møller, S. G., Cellular Proteostasis in Neurodegeneration. *Molecular Neurobiology* **2019,** *56* (5), 3676-3689.
117. Morris, H. R., The Genetic and Pathological Classification of Familial Frontotemporal Dementia. *Archives of Neurology* **2001,** *58* (11), 1813.
118. Deramecourt, V.; Lebert, F.; Maurage, C.-A.; Fernandez-Gomez, F.-J.; Dujardin, S.; Colin, M.; Sergeant, N.; Buée-Scherrer, V.; Clot, F.; Ber, I. L.; Brice, A.; Pasquier, F.; Buée, L., Clinical, Neuropathological, and Biochemical Characterization of the Novel Tau Mutation P332S. *Journal of Alzheimer's Disease* **2012,** *31* (4), 741-749.
119. Štrafela, P.; Pleško, J.; Magdič, J.; Koritnik, B.; Zupan, A.; Glavač, D.; Bresjanac, M.; Popović, M., Familial tauopathy with P364SMAPTmutation: clinical course, neuropathology and ultrastructure of neuronal tau inclusions. *Neuropathology and Applied Neurobiology* **2018,** *44* (6), 550-562.
120. Götz, J.; Bodea, L.-G.; Goedert, M., Rodent models for Alzheimer disease. *Nature Reviews Neuroscience* **2018,** *19* (10), 583-598.
121. Falcon, B.; Zhang, W.; Murzin, A. G.; Murshudov, G.; Garringer, H. J.; Vidal, R.; Crowther, R. A.; Ghetti, B.; Scheres, S. H. W.; Goedert, M., Structures of filaments from Pick's disease reveal a novel tau protein fold. *Nature* **2018,** *561* (7721), 137-140.
122. Mélanie H. Thomas, S. P., Nicolas Vitale and Jean Luc Olivier, Arachidonic Acid in Alzheimer's disease. Journal of Neurology Neuromedicine: Journal of Neurology Neuromedicine, 2016; Vol. 1(9), pp 1-6.
123. Ingham, D. J.; Blankenfeld, B. R.; Chacko, S.; Perera, C.; Oakley, B. R.; Gamblin, T. C., Fungally Derived Isoquinoline Demonstrates Inducer-Specific Tau Aggregation Inhibition. *Biochemistry* **2021**.
124. Cremers, C. M.; Knoefler, D.; Gates, S.; Martin, N.; Dahl, J. U.; Lempart, J.; Xie, L.; Chapman, M. R.; Galvan, V.; Southworth, D. R.; Jakob, U., Polyphosphate: A Conserved Modifier of Amyloidogenic Processes. *Mol Cell* **2016,** *63* (5), 768-80.
125. Wickramasinghe, S. P.; Lempart, J.; Merens, H. E.; Murphy, J.; Huettemann, P.; Jakob, U.; Rhoades, E., Polyphosphate Initiates Tau Aggregation through Intra- and Intermolecular Scaffolding. *Biophys J* **2019,** *117* (4), 717-728.
126. Dinkel, P. D.; Holden, M. R.; Matin, N.; Margittai, M., RNA Binds to Tau Fibrils and Sustains Template-Assisted Growth. *Biochemistry* **2015,** *54* (30), 4731-4740.
127. Kampers, T.; Friedhoff, P.; Biernat, J.; Mandelkow, E. M.; Mandelkow, E., RNA stimulates aggregation of microtubule-associated protein tau into Alzheimer-like paired helical filaments. *FEBS Lett* **1996,** *399* (3), 344-9.

128. Zhang, X.; Lin, Y.; Eschmann, N. A.; Zhou, H.; Rauch, J. N.; Hernandez, I.; Guzman, E.; Kosik, K. S.; Han, S., RNA stores tau reversibly in complex coacervates. *PLOS Biology* **2017,** *15* (7), e2002183.
129. Ginsberg, S. D.; Crino, P. B.; Lee, V. M.-Y.; Eberwine, J. H.; Trojanowski, J. Q., Sequestration of RNA in Alzheimer's disease neurofibrillary tangles and senile plaques. *Annals of Neurology* **1997,** *41* (2), 200-209.
130. Horowitz, P. M., Early N-Terminal Changes and Caspase-6 Cleavage of Tau in Alzheimer's Disease. *Journal of Neuroscience* **2004,** *24* (36), 7895-7902.
131. Kanaan, N. M.; Grabinski, T., Neuronal and Glial Distribution of Tau Protein in the Adult Rat and Monkey. *Frontiers in Molecular Neuroscience* **2021,** *14*.
132. Lasagna-Reeves, C. A.; Castillo-Carranza, D. L.; Sengupta, U.; Sarmiento, J.; Troncoso, J.; Jackson, G. R.; Kayed, R., Identification of oligomers at early stages of tau aggregation in Alzheimer's disease. *FASEB Journal* **2012,** *26* (5), 1946-1959.
133. Macdonald, J. A.; Bronner, I. F.; Drynan, L.; Fan, J.; Curry, A.; Fraser, G.; Lavenir, I.; Goedert, M., Assembly of transgenic human P301S Tau is necessary for neurodegeneration in murine spinal cord. *Acta Neuropathol Commun* **2019,** *7* (1), 44.
134. Mazzaro, N.; Barini, E.; Spillantini, M. G.; Goedert, M.; Medini, P.; Gasparini, L., Tau-Driven Neuronal and Neurotrophic Dysfunction in a Mouse Model of Early Tauopathy. *J Neurosci* **2016,** *36* (7), 2086-100.
135. Mutreja, Y.; Combs, B.; Gamblin, T. C., FTDP-17 Mutations Alter the Aggregation and Microtubule Stabilization Propensity of Tau in an Isoform-Specific Fashion. *Biochemistry* **2019,** *58* (6), 742-754.
136. Wilson, D. M.; Binder, L. I., Free fatty acids stimulate the polymerization of tau and amyloid beta peptides. In vitro evidence for a common effector of pathogenesis in Alzheimer's disease. *Am J Pathol* **1997,** *150* (6), 2181-95.
137. Gamblin, T. C.; King, M. E.; Kuret, J.; Berry, R. W.; Binder, L. I., Oxidative Regulation of Fatty Acid-Induced Tau Polymerization†. *Biochemistry* **2000,** *39* (46), 14203-14210.
138. Chirita, C. N.; Congdon, E. E.; Yin, H.; Kuret, J., Triggers of Full-Length Tau Aggregation: A Role for Partially Folded Intermediates†. *Biochemistry* **2005,** *44* (15), 5862-5872.
139. Fichou, Y.; Oberholtzer, Z. R.; Ngo, H.; Cheng, C.-Y.; Keller, T. J.; Eschmann, N. A.; Han, S., Tau-Cofactor Complexes as Building Blocks of Tau Fibrils. *Frontiers in Neuroscience* **2019,** *13*.
140. Roman, A. Y.; Devred, F.; Byrne, D.; La Rocca, R.; Ninkina, N. N.; Peyrot, V.; Tsvetkov, P. O., Zinc Induces Temperature-Dependent Reversible Self-Assembly of Tau. *Journal of Molecular Biology* **2019,** *431* (4), 687-695.
141. Chang, E.; Kuret, J., Detection and quantification of tau aggregation using a membrane filter assay. *Analytical Biochemistry* **2008,** *373* (2), 330-336.
142. Biancalana, M.; Koide, S., Molecular mechanism of Thioflavin-T binding to amyloid fibrils. *Biochimica et Biophysica Acta (BBA) - Proteins and Proteomics* **2010,** *1804* (7), 1405-1412.
143. Meneghetti, M. C. Z.; Hughes, A. J.; Rudd, T. R.; Nader, H. B.; Powell, A. K.; Yates, E. A.; Lima, M. A., Heparan sulfate and heparin interactions with proteins. *Journal of The Royal Society Interface* **2015,** *12* (110), 20150589.
144. Holmes, B. B.; Devos, S. L.; Kfoury, N.; Li, M.; Jacks, R.; Yanamandra, K.; Ouidja, M. O.; Brodsky, F. M.; Marasa, J.; Bagchi, D. P.; Kotzbauer, P. T.; Miller, T. M.; Papy-Garcia, D.; Diamond, M. I., Heparan sulfate proteoglycans mediate internalization and propagation of

specific proteopathic seeds. *Proceedings of the National Academy of Sciences* **2013,** *110* (33), E3138-E3147.
145. Townsend, D.; Fullwood, N. J.; Yates, E. A.; Middleton, D. A., Aggregation Kinetics and Filament Structure of a Tau Fragment Are Influenced by the Sulfation Pattern of the Cofactor Heparin. *Biochemistry* **2020,** *59* (41), 4003-4014.
146. Martin, S. A.; Brash, A. R.; Murphy, R. C., The discovery and early structural studies of arachidonic acid. *Journal of Lipid Research* **2016,** *57* (7), 1126-1132.
147. Astudillo, A. M.; Balgoma, D.; Balboa, M. A.; Balsinde, J., Dynamics of arachidonic acid mobilization by inflammatory cells. *Biochimica et Biophysica Acta (BBA) - Molecular and Cell Biology of Lipids* **2012,** *1821* (2), 249-256.
148. Balboa, M. A.; Balsinde, J., Oxidative stress and arachidonic acid mobilization. *Biochimica et Biophysica Acta (BBA) - Molecular and Cell Biology of Lipids* **2006,** *1761* (4), 385-391.
149. Dai, X.; Zhang, S.; Zaleta-Rivera, K., RNA: interactions drive functionalities. *Molecular Biology Reports* **2020,** *47* (2), 1413-1434.
150. Lempart, J.; Jakob, U., Role of Polyphosphate in Amyloidogenic Processes. *Cold Spring Harbor Perspectives in Biology* **2019,** *11* (5), a034041.
151. Kumble, K. D.; Kornberg, A., Inorganic Polyphosphate in Mammalian Cells and Tissues. *Journal of Biological Chemistry* **1995,** *270* (11), 5818-5822.
152. Stotz, S. C.; Scott, L. O.; Drummond-Main, C.; Avchalumov, Y.; Girotto, F.; Davidsen, J.; Gómez-Gárcia, M. R.; Rho, J. M.; Pavlov, E. V.; Colicos, M. A., Inorganic polyphosphate regulates neuronal excitability through modulation of voltage-gated channels. *Molecular Brain* **2014,** *7* (1), 42.
153. Yakupova, I., Elmira; Bobyleva, G., Liya; Vikhlyantsev, M., Ivan; Bobylev, G., Alexander, Congo Red and amyloids: history and relationship. *Bioscience Reports* **2019,** *39* (1), BSR20181415.
154. Reinke, A. A.; Gestwicki, J. E., Insight into Amyloid Structure Using Chemical Probes. *Chemical Biology & Drug Design* **2011,** *77* (6), 399-411.
155. Carlomagno, Y.; Manne, S.; Deture, M.; Prudencio, M.; Zhang, Y.-J.; Hanna Al-Shaikh, R.; Dunmore, J. A.; Daughrity, L. M.; Song, Y.; Castanedes-Casey, M.; Lewis-Tuffin, L. J.; Nicholson, K. A.; Wszolek, Z. K.; Dickson, D. W.; Fitzpatrick, A. W. P.; Petrucelli, L.; Cook, C. N., The AD tau core spontaneously self-assembles and recruits full-length tau to filaments. *Cell Reports* **2021,** *34* (11), 108843.
156. Guo, J. L.; Narasimhan, S.; Changolkar, L.; He, Z.; Stieber, A.; Zhang, B.; Gathagan, R. J.; Iba, M.; Mcbride, J. D.; Trojanowski, J. Q.; Lee, V. M. Y., Unique pathological tau conformers from Alzheimer's brains transmit tau pathology in nontransgenic mice. *Journal of Experimental Medicine* **2016,** *213* (12), 2635-2654.